System Design and Optimization of an Aerial Refueling System for Transcontinental Flights

by

Ir. Keran Rong

B.Eng., Tianjin University (2013)
M.Sc., Technische Universiteit Delft (2015)

Submitted to the System Design and Management Program
in partial fulfillment of the requirements for the degree of

Master of Science in Engineering and Management

at the

MASSACHUSETTS INSTITUTE OF TECHNOLOGY

May 2020

Author .....
System Design and Management Program
May 15, 2020

Certified by .....
Olivier de Weck
Professor of Aeronautics and Astronautics and Engineering Systems
Thesis Supervisor

Accepted by .....
Joan Rubin
Executive Director, System Design & Management Program

System Design and Optimization of an Aerial Refueling System for Transcontinental Flights

by

Ir. Keran Rong

Submitted to the System Design and Management Program
on May 15, 2020, in partial fulfillment of the
requirements for the degree of
Master of Science in Engineering and Management

Abstract

Currently, intercontinental flights are long-haul flights, and commercial aircraft are not refueled during the flight. As a result, the fuel consumption of intercontinental flights increases exponentially with the distance travelled, because these long-haul flights consume extra fuel due to their weight gain. Intercontinental aviation already accounts for a significant portion of global carbon emissions and this is expected to grow rapidly in the foreseeable future. Therefore, aircraft emissions from transcontinental flights have become a global challenge both socially and technologically.

In this study, we propose a floating air refueling system (FARS) to reduce fuel costs on intercontinental flights. In this system, we launch a tanker to refuel incoming intercontinental aircraft. Through the refueling process, intercontinental flights avoid the exponential fuel consumption caused by the additional fuel required, and can potentially reduce aircraft emissions.

This thesis presents the design of a floating aerial refueling system, including stakeholder analysis, system architecture design and economic feasibility analysis. In addition, we propose a method for mathematical simulation and optimization of FARS using different techniques. Finally we analyze FARS's feasibility and sensitivity based on case studies. The case study of Singapore Airlines SQ21 shows that our optimized design can save up to 39,415 tons of jet fuel annually over a 25-year life cycle, with a net present value of USD 266 million.

Thesis Supervisor: Olivier de Weck
Title: Professor of Aeronautics and Astronautics and Engineering Systems

Acknowledgments

First of all, I would like to express my gratitude to my supervisor Olivier de Weck for introducing me to this topic and his inspiration, wisdom and focus during the study of this masters thesis. Without your guidance, I would not have been able to complete this thesis.

I would also like to thank the SDM teaching team and staff, who gave me opportunities for personal and professional growth. I am particularly grateful to Bryan Moser, who provided me a fellowship to fund part of my studies.

I would like to thank the outstanding cohort including Katie, Beldon, Gautam and Tom for their support. I especially want to thank Roland de Filippi, who provided a safe and comfortable place for me to live and to complete my thesis during the COVID-19 pandemic.

Finally, I would like to thank my loved ones: my parents Shaofu Rong and Cuijun Wen, for their unconditional love, financial supports and inspiration in my life.

Contents

List of Figures

List of Tables

Chapter 1

Introduction

1.1 Motivation

Since the first heavier-than-air controlled aircraft made by the Wright brothers, the aviation industry has undergone a revolutionary change. Figure 1-1 shows the number of annual passengers served by airlines to and from the United States during the period 2003-2018. According to data from the U.S. Department of Transportation[37], domestic and international U.S. flights served 1 billion passengers in 2018, 4.8% above the previous record high (2017). As of 2020, 21 stocks Of U.S. Standard & Poor's 500 index are directly related to the aviation industry. With more than 100 years of development, the aviation industry has become a critical part of modern society.

Intercontinental flights are in great demand. For instance, in the first quarter of 2019, there were 35 million passengers and 3.7 million tons of freight between Europe and the United States [36], an increase of 7% and 2% respectively compared to 2018 (see Figure 1-2). With the growth of the emerging markets and further integration of the global supply chains, the market for the aviation industry will continue to grow for the foreseeable future.

However, the high demand of the aviation industry is also associated with high carbon emissions. According to an analysis by Atmosfair[4], a flight from Boston Logan to Amsterdam Schiphol generates approximately 1,726 lbs of CO_2, more than the annual emission per capita of 53 countries. Currently, the aviation industry

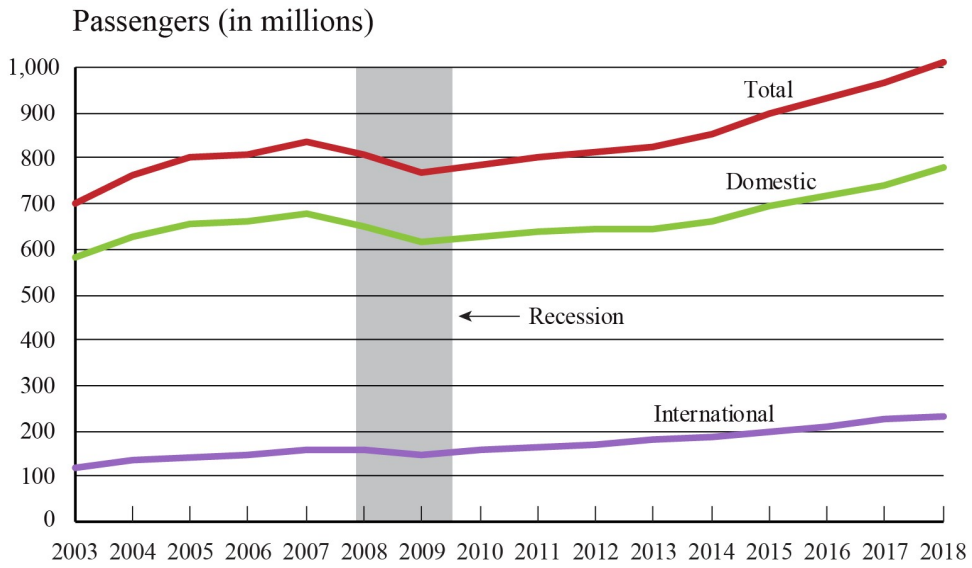

Figure 1-1: Annual passengers on all U.S. scheduled airline flights (domestic & international) and foreign airline flights to and from the United States, 2003-2018 [37]

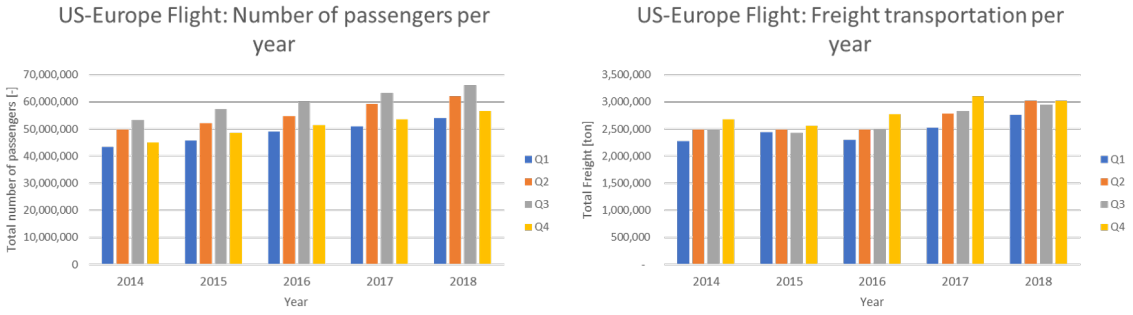

Figure 1-2: Statistics of freight and passengers' transportation between U.S. and Europe for 2014-2018 [36]

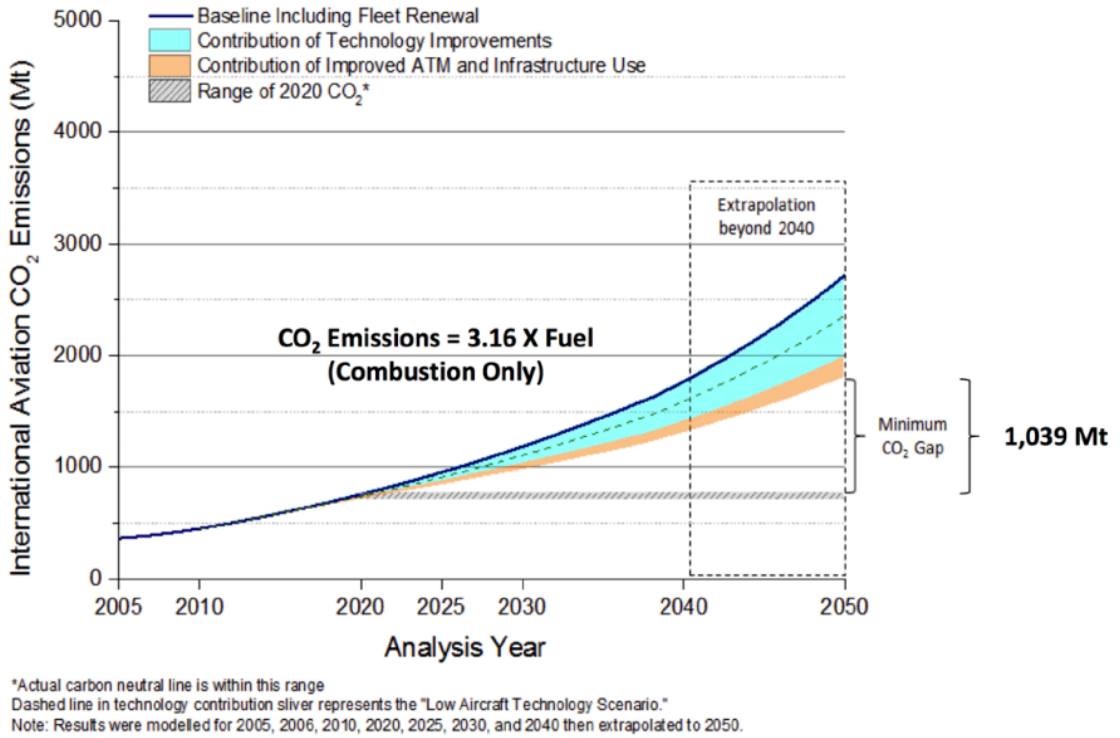

Figure 1-3: CO2 emissions Trends, international aviation, 2005 to 2050 [23]

accounts for approximately 2% of global emission and this is expected to triple by 2050[23] (see Figure 1-3). The aircraft emissions pose a global challenge both socially and technically.

In addition to carbon dioxide, aircraft emissions contain a series of other chemicals that will further damage the ecosystem and lead to social problems. Figure 1-4 shows a schematic diagram of the relationship between aircraft emissions and climate change. As shown in the figure, aircraft emissions contain NO_x and SO_x, which account for the formation of smog, acid rain and radiative pollution. As a result, aircraft emissions are responsible not only for contributing incrementally to global warming, but also indirectly for other serious social impacts.

The aircraft emissions are particularly significant for intercontinental flights. Under the current state of the practice, intercontinental airplanes take off from one continent and land on another without refueling either on the ground or in the air. Early aircraft in the 1930-1960s often had to land to refuel due to insufficient range.

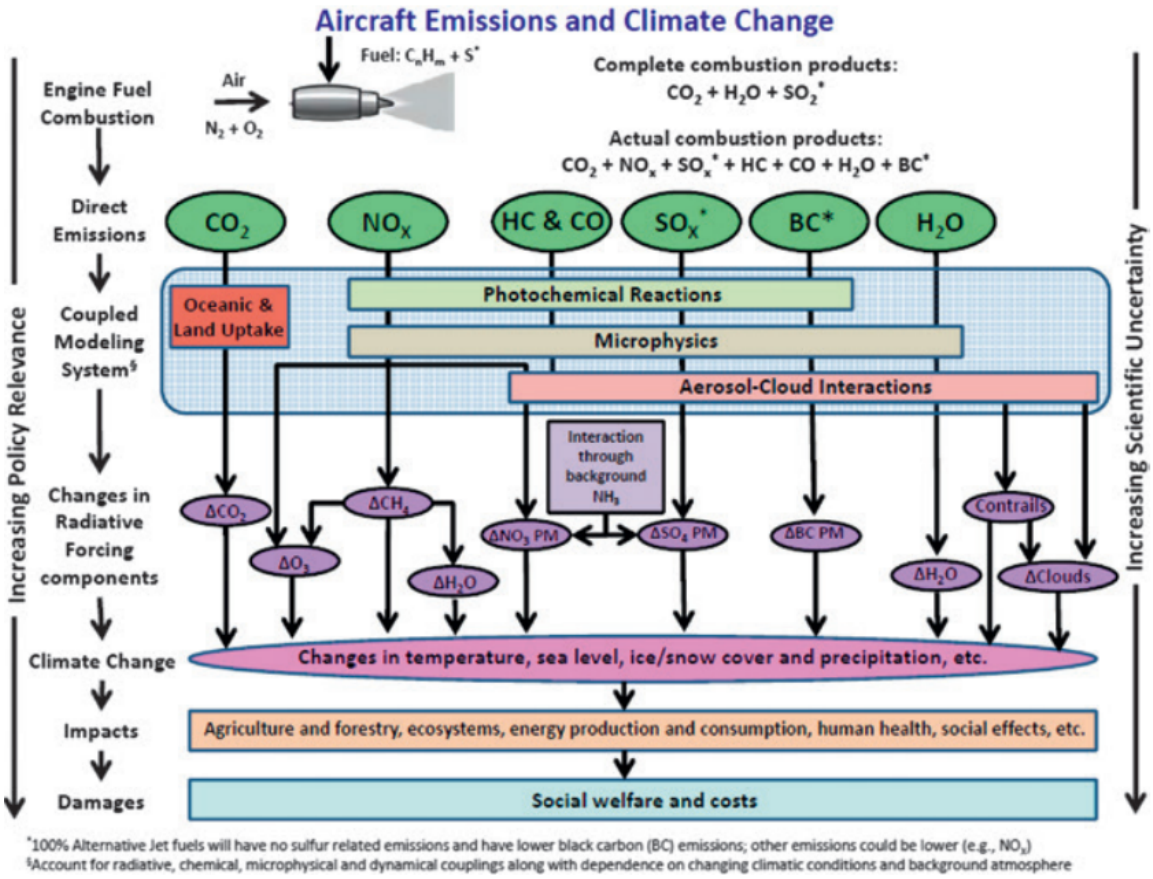

Figure 1-4: Schematic diagram of the relationship between aircraft emission and climate change, from Ref [9]

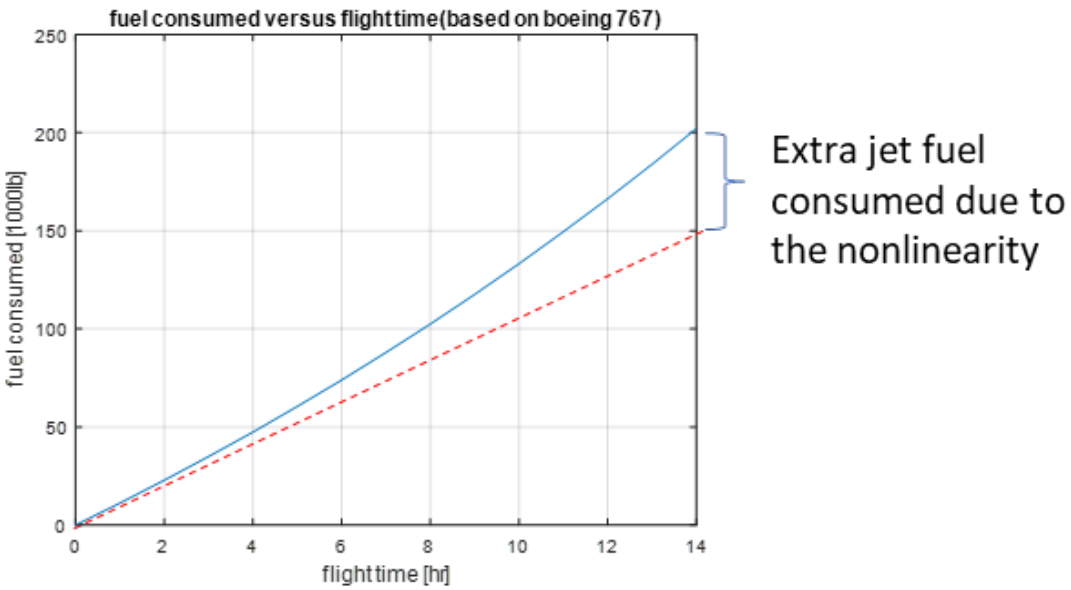

Figure 1-5: Jet fuel consumed versus flight time based on Boeing 767 (Breguet range equation, only considering the cruise phase)

Popular refueling stops on the North Atlantic route were Gander in Newfoundland, Shannon in Ireland or the Azores. Today, the aircraft need to carry enough fuel to complete the mission at the beginning of the journey. However, the increased mission range will lead to an increase in aircraft weight due to extra fuel, which will be consumed as even more fuel is needed to complete the mission. Figure 1-5 shows the fuel consumption of a Boeing 767 versus flight time calculated based on the famous Breguet range equation. As shown in the figure, a 14 hour flight (typical endurance of transpacific flights) will consume about 30% more fuel due to this non-linearity. Another way to say this in simple language is that long range aircraft burn a lot of fuel just to carry the fuel they will consume during the final hours of flight. This is particularly significant on ultra-long range flights of 18-20 hours flight time such as project "Sunrise" sponsored by Qantas, Australia's national airline. Therefore, if we can find a solution to reduce the non-linear fuel penalty of intercontinental flights, then both fuel burn and aircraft emissions will be greatly reduced.

Aerial refueling is a potential option to reduce the non-linear fuel consumption of transcontinental flights. Aerial refueling is the process of transferring jet fuel from one aircraft (the tanker) to another (the receiver) during flight. By aerial refueling, the

transcontinental flights do not need to carry fuel for the entire mission. As a result, we can greatly reduce the weight of the aircraft as well as the fuel consumption associated with it. In addition, aerial refueling has been widely used in military aviation and has proven to be reliable and feasible. Recent advances have been made, for example by Airbus, in the area of autonomous refueling[46].

In order to fully account for the total fuel consumed by the overall system (tanker plus long range aircraft) we must add the fuel consumed by the receiving long range aircraft, the fuel transferred during flight (potentially more than once) and the fuel consumed by the tanker aircraft itself. It is therefore important to shorten the tanker's flight distance as much as possible because it also consumes fuel. A large fraction of intercontinental flights are over the open ocean. Therefore, one option to shorten the tanker's flight distance is to launch the tanker from a floating platform (a large ship with a runway on the top deck), so that the tanker can be deployed onto the receivers' flight path, and thus the tanker can rendezvous with the receiver aircraft without having to execute a long-distance flight itself. An additional reason why this approach may work is because intercontinental flights often follow each other on specific flight corridors. It may therefore be possible for a tanker to refuel multiple receiving aircraft in turn without significant change in flight level.

Motivated by the high emissions of transcontinental flights and inspired by the already well established military application of aerial refueling, we propose the floating aerial refueling system (FARS) with primarily commercial applications in mind.

1.2 Stakeholders and Needs

To begin with, we present the potential stakeholders and their needs in the FARS design, shown as table 1.1. As shown in the table, the stakeholders of FARS mainly consist of:

1. The stakeholders that direct relate to values of FARS such as the aircraft producers, airliner operators, energy producers and passengers.

2. The stakeholders that support the operation of FARS such as researchers, local employees, government, NGOs and regulators.

3. The stakeholders that FARS has concerns about such as terrorists or pirates.

FARS shall be designed to meet or mitigate these stakeholders' needs.

Table 1.1: Stakeholders and Needs

TYPE	STAKEHOLDER	NEEDS
Beneficial	Aircraft producers	New market, More revenue, competitive advantage
	Commercial airliners	More revenue, Lower cost, More customers, Meet emission requirement, Better public relations, safety, Competitive advantage
	Passengers	Safe, Comfortable, Less time for travel, Better environmental awareness, Cheaper ticket, Convenience
	Government	More job opportunities, Safety, Regulations, Better public relations, More taxes, Meeting environmental standards
	Research Institute	R&D opportunities, More budgets, More social impact, Better public relations
	Energy suppliers	Stable supply chains, Customer diversification, Better public relations
	NGOs &	Lower Emissions, Better public relations, Higher social impact
	Local Community	More jobs opportunities, Local business opportunities
Other	Terrorists	Destroy & Attack, Higher social impact
	Thiefs & Pirates	Money
	Regulators	Meeting regulations

It is clear that FARS is not a simple but a complex system that may yield benefits for some stakeholders but not all.

1.3 System Problem Statement and Goals

The system problem statement of the floating aerial refueling system is to reduce overall fuel consumption from commercial transcontinental flights by aerial refueling using a floating aerial refueling system (FARS), while complying with safety standards and while being economically feasible.

In detail, we formulate goals and objectives of the FARS system as follow:

- **What FARS addresses:** Current challenge of further improving fuel consumption efficiency of transcontinental flights. FARS provides an aerial refueling process for incoming flights, thereby avoiding a steep exponential fuel consumption. In addition, FARS is also potentially a good business model: FARS can not only benefit from fuel saved, but also fill extra seats (or cargo) created by the aircraft weight reduction. In addition, FARS could serve as a local maritime energy production center and achieve zero emissions, once passenger jets update their jet fuel to hydrogen in the future. For example a FARS system could produce clean hydrogen using solar powered desalination followed by electrolysis.

- **Primary Goal**: Maximize fuel savings on intercontinental flights throughout the mission cycle. Specifically, reduce the fuel consumption of intercontinental flights with refueling compared to otherwise equivalent flights (same generation aircraft) without refueling under the same assumptions; reduce the fuel consumption of tanker airplanes for each operation; increase the capacity of refueling of tanker airplanes for each operation.

- **Secondary Goal**: Demonstrate that FARS can be an economically viable system and under what circumstances; Specifically, The FARS system shall

be profitable based on Net Present Value (NPV) analysis over a 25-year life span.

- **What system is not intended to address:** FARS does not intend to replace the existing R&D and R&T on airplane efficiency improvements such as research on new materials and engine designs. FARS does not address the fundamental changes needed in the aviation industry. FARS does not replace the functionality of existing airport and other aviation facilities.

1.4 Assumptions

In this study, we make the following assumptions:

- All technologies needed exist, are available and reliable
- Safety factors are not considered at present
- No political obstacles are considered in the analysis
- There will be no major socio-economic or policy changes in the foreseeable future. For example the longer term impact of the COVID-19 crisis is not taken into account.

1.5 Thesis Roadmap

Figure 1-6 shows the schematic diagram of the thesis roadmap.

First, we will introduce a literature review on aircraft efficiency, aerial refueling, and naval aviation. This is an important section since mid-air refueling is not new per se, but has been done for decades, particularly in the military. However the application of refueling to commercial aircraft and especially the use of ships as bases for tankers directly under or close to the flight path of trans-continental aircraft is new to our knowledge.

Then, we will discuss the system design of FARS, including its concept, main components and mode of operations.

After introducing the concept, we discussed the design and modeling of the main components of FARS, including the tanker, fueling strategy and the mothership.

Using the models and design variables introduced for FARS, we conducted multi-disciplinary optimization (MDO) of the FARS design. A series of optimized designs are proposed and the robustness of the design is discussed and examines through sensitivity analysis.

Finally, we conduct a trade-off analysis between the performance in terms of fuel savings and cost of FARS. We have applied the FARS design to several practical commercial flight case studies.

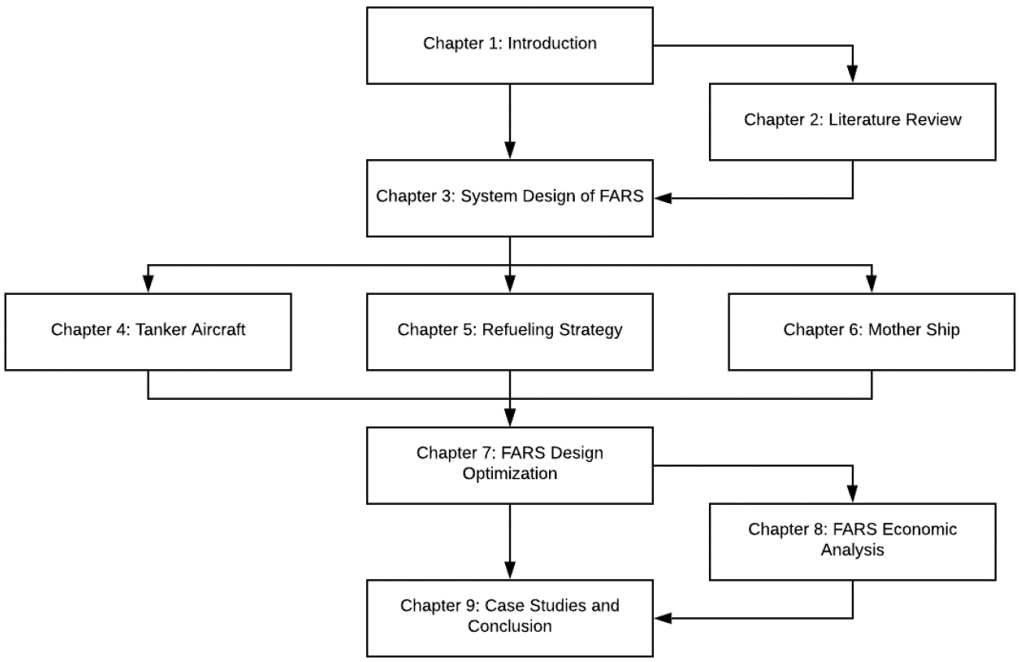

Figure 1-6: Thesis roadmap

Chapter 2

Literature Review

2.1 Flight Efficiency

Industry and academia have made significant progress in reducing fuel consumption for long-haul flights. This section is largely based on an aircraft case study written by Professor Olivier de Weck for the 16.887 technology roadmapping and development class at MIT. [14].

French aircraft designer and pilot Louis Bréguet proposed a mathematical formula to express the exponential relationship between the maximum range and weight of the aircraft, known as the Bréguet range equation, expressed as:

$$R = 3600 \frac{V}{SFC} \frac{L}{D} ln \frac{W_i}{W_f} \tag{2.1}$$

Where, R is the flight range of the aircraft (unit:ft). V is the aircraft's cruise speed (unit: ft/sec), $\frac{L}{D}$ is the lift to drag ratio (also known as Finesse), SFC is the specific fuel consumption of the engine (unit: lb/(h*lbf)), while W_i and W_f are the aircraft's initial and final flight weight, respectively.

Thus, the fuel consumption W_{fuel} for range R can be expressed as the difference of weight before and after flight, expressed as:

$$W_{fuel} = W_i - W_f \tag{2.2}$$

Note that this equation does not account for fuel burn during takeoff, climb, descent and landing and also ignores the wind. However for long range flight of > 6 hours it provides a good approximation to the actual fuel burn as long as the parameters that are plugged into the Bréguet range equation are close to reality. Traditionally, there are four strategies for reducing fuel consumption:

1. Optimize aircraft cruise speed V
2. Reduce the specific fuel consumption SFC of the aircraft engines by increasing their efficiency
3. Increase the maximum lift to drag ratio $max(\frac{L}{D})$
4. Reduce the empty weight of the aircraft W_f, for a given number of passengers (pax) and cargo

Thanks to technological advances in the past 80 years, the typical cruise speed of civilian aircraft has increased from 333km/h(DC-3A, 1936) to 903km/h(A350-900 ULR, 2018), an increase of 300%. However, further increasing cruise speed is not always a good thing. Once the cruise speed approaches or exceeds the speed of sound (Mach 1.0), the aircraft's lift-to-drag ratio will drop sharply due to shock waves, as shown in Figure 2-2. In addition, supersonic aircraft require turbojet engines, and their fuel consumption is much higher than that of turbofan engines (used for subsonic aircraft). Taking the supersonic aircraft *Concorde* as an example, the specific fuel consumption of the Rolls-Royce Olympus 593 (used by *Concorde*) is 1.195 $lb/(lbf{\cdot}h)$ [19], while the specific fuel consumption of the PW4000 engine (used by some Boeing 7-series aircraft) is 0.56 $lb/(lbf{\cdot}h)$ [34]. In addition, the aircraft's supersonic flight may also cause safety and maintenance issues. Therefore, modern commercial aircraft usually limit their cruise speed to the range Mach 0.7-0.9.

Reducing the specific fuel consumption of engines is one of the key points of aviation industry R&D and R&T (Note that R&D is the development of new or improved aircraft while R&T is the development and infusion of new technologies). Advances in engine technology play a key role in improving the aircraft's fuel consumption

efficiency: Engine improvements accounts for about 3.3% of aircraft fuel efficiency improvements annually, while all other technologies together account for about 2.5% [14]. Figure 2-1 shows some historical milestones of reducing specific fuel consumption versus normalized aircraft engine complexity. Since the first introduction of turbojet engines in the 1950s, the aviation industry has reduced unit fuel consumption by more than a factor of two through the following changes[14]:

1. Increase of the bypass ratio (BPR) of turbofan engines so that engines can accelerate larger amounts of cold but dense air to obtain a higher thrust with the same amount of the fuel consumption.

2. Change in the architecture of the engine to allow for two or more stages of engines with co-rotating spools. This change allows the engine to further optimize the pressure ratio of each stage.

3. New advances in materials, such as new alloys and ceramics, can increase the combustion temperature in the engine core while actively cooling turbine blades.

4. Advances in fan blade geometry optimization have resulted in higher aerodynamic efficiency and lighter engine weight.

5. P & W recently adopted a new fan drive gear system between the core and the fan to further increase the efficiency of the engine by 15%.

However, the increase in aircraft engine efficiency has led to an increase in aircraft engine complexity. The increased complexity of aircraft engines will increase the cost of engine development and introduce new failure modes for aircraft in the future.

In addition, another important factor in reducing aircraft fuel consumption is to increase the lift-to-drag ratio. The maximum lift-to-drag ratio is strongly affected by the cruise speed and the aspect ratio of the aircraft, as shown in Figure 2-2. Aspect ratio AR is defined as the ratio of the square of the wingspan b to the projected or reference wing area S. According to finite wing theory, the pressure difference between the top and bottom surfaces of an aircraft wing will cause the air to move

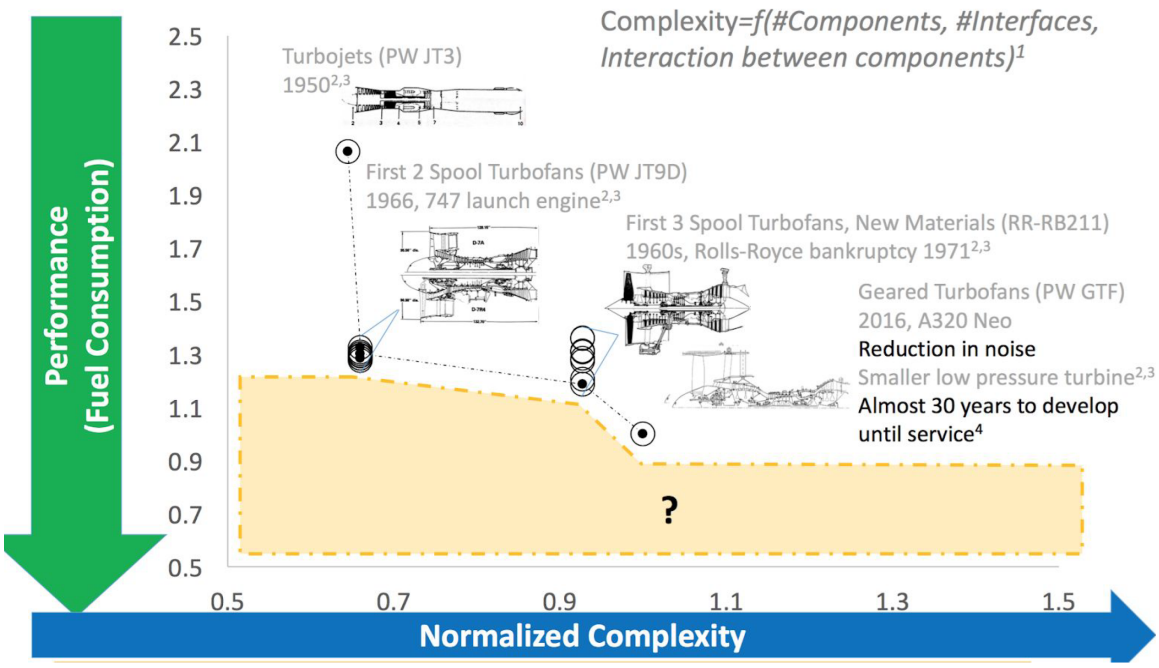

Figure 2-1: Normalized Performance (SFC) vs Complexity of Aircraft engines from Reference [14]

circularly around the tip of the wing, resulting in a trailing vortex or wake turbulence. Wake turbulence will reduce the effective angle of attack and cause drag. As shown in Figure 2-2, Increasing the aspect ratio will increase the maximum lift-to-drag ratio, thereby reducing the aircraft's fuel consumption.

Reducing the weight of the empty aircraft is also a good way to improve the fuel efficiency of the aircraft. Advances in computer-aided design and artificial intelligence have allowed aircraft engineers to further optimize aircraft structures. Figure 2-3 shows an example of the bionic optimization of Airbus A320's proposed cabin partition. The weight of the bionic cabin partition is 45% less than the current design, while providing similar structural strength[2]. With this new design, Airbus estimates that it could save up to 465,000 metric tons of CO2 emissions per year[2]. The increased application of composite materials in the aviation industry will also significantly reduce the empty weight of aircraft. Many researches indicate that the application of composite materials can decrease the weight of the aircraft's primary and secondary structural elements by 25% and 40% respectively[41].

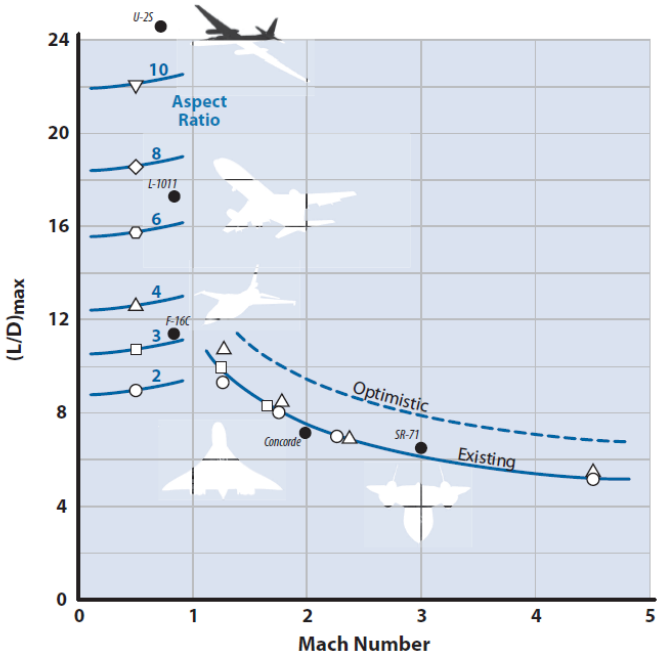

Figure 2-2: Max lift to drag ratio versus Mach number with different aspect ratio ref [34]

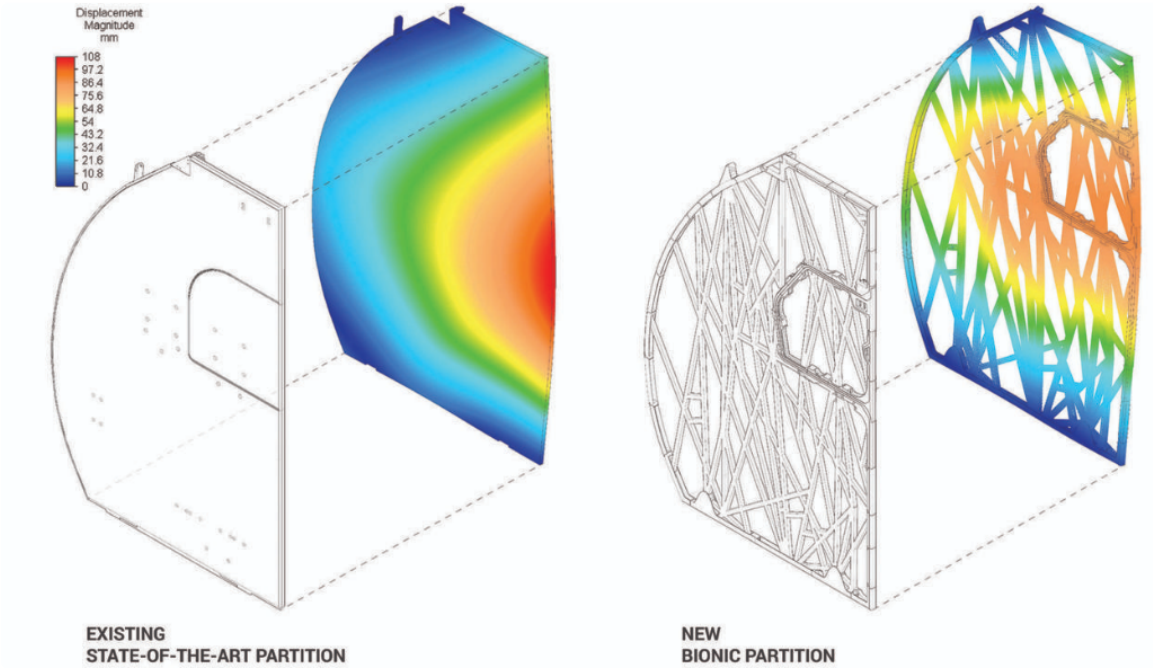

Figure 2-3: Bionic optimization of Airbus A320 cabin partition from ref [2]

2.2 Aerial Refueling

In this section, we will briefly discuss the history of aerial refueling. Due to the limited material on this topic, the history of aerial refueling is mainly based on the books by E. Wallwork et al[17].

The first documented air-to-air refueling occurred in 1923. On the 27th June 1923, the U.S. Army air service successfully performed air to air refueling between two De Haviland DH-4B aircraft. The receiver aircraft flew for 6-hours and 38 minutes after two air refueling operations. However, due to budget restrictions and application restrictions, the aerial refueling experiment progressed slowly and eventually stopped after an accident.

The first time that refueling in the air attracted public attention was the "question mark" flight. Inspired by a rescue operation, Captain Ira Eaker of the US Army Aviation demonstrated a long-term refueling technique: the *Question Mark* aircraft (Figure 2-4). The Question Mark is a variation of a Fokker C-2 with refueling capability. In their first experiment, the Question Mark was refueled by a Douglas C-1 with two 150 gallon tanks for offloading and a refueling hose through the hatch cut in the floor. The first flight of the Question Mark lasted for 150 hours and 60 minutes. During the flight, they performed 43 aerial refueling operations, and each contact lasted for 7 mins. The Question Mark was a huge success with tremendous public attention, though its mission yielded little military interest. Although the Question Mark was not of interest to the United States military, the aircraft stimulated British interest in aerial refueling. Based on the refueling technique demonstrated by the Question Mark, flight lieutenant Richard Atcherly invented the looped-host aerial refueling system, one of the first formal air refueling technologies invented. The British Royal Air Force (RAF) conducted a series of experiments until 1937, after which even the Royal Air Force concluded that air refueling technology provided only limited benefits. At the same time, nevertheless, the British commercial aviation industry showed their interest in air refueling. Flight Refueling Limited further improved the refueling technology invented by Richard Atchterly. The intention of commercial refueling was

Figure 2-4: Question Mark airplane from ref [17]

to reduce an airplanes' take-off weight, rather than to extend the flights' endurance. Before Britain was involved in World War II, there were 15 transatlantic missions carried out by Imperial Airline with aerial refueling.

The real turning point for aerial refueling technology was World War II. The US Army Air Force started to work on aerial refueling techniques in their struggle against Japan after the Pearl Harbor attack. The study of aerial refueling focused on extending U.S. bomber's capacity to attack Japan and return safely. During the famous Doolittle raid in 1942 the B-25 aircraft that were used did not have sufficient range to return and had to be sacrificed. The tests conducted in Florida during the war successfully extended the B-24 bomber's range from 1,000 to 1,500 miles. Although air refueling technology was not used operationally in WWII, the U.S. Army and later the Air Force examined and bought into the potential of aerial refueling technology and thus led its further development during the Cold War.

To prepare for a potential nuclear war with the Soviet Union, the U.S developed

Figure 2-5: Flying boom, from ref[33]

the B-47 and B-52. Both types of aircraft need to be aerial refueled in order to extend their range to Soviet' territory. The old British looped-host aerial refueling system did not satisfy the refueling requirements set by U.S Air Force. Therefore, Boeing developed a 'flying boom', which is a rigid, telescoping tube with movable flight control surfaces, as shown in Figure 2-5. The boom operator on the tanker aircraft can see both the boom and the receiving aircraft and extend and insert the tube into a receptacle on the receiving aircraft. Military airplanes with aerial refueling capability were first deployed in the Korean War and in most U.S. military operations afterwards.

Air refueling technology also imposes requirements on tankers. After a series of research and DoD contracts, the U.S. Air Force selected the KC-10A as the standard aircraft for U.S. military refueling, because the KC-10A, compared with its competitor the Boeing 747, was cheaper and provided the ability to take-off with maximum payload from a short run way.

2.3 Refueling and Naval Aviation

Naval aviation has recently entered another 100 years of history [16]. In 1910, Eugene Ely made the first successful launch of an aircraft from a ship, marking the birth of naval aviation. The breakout of World War I greatly accelerated the progress of Naval aviation. By the end of WWI, the U.S. Navy had 1865 aircraft, while there were only 56 before the war. However, naval aircraft before and during WWI were mainly seaplanes, a powered fixed wing aircraft capable of take-off and landing on water. Although, naval aviation has shown its strength in military operations, the majority of naval battles still relied on battleships at that moment.

Naval aviation truly showed its decisive power during World War II, especially in the Pacific war between the U.S. and Japan. The battle of the Coral Sea in 1942 was the first major battle without opposing ships making direct contact. At the battle of Midway, the turning point of WWII in the Pacific, four Japanese and three American aircraft carriers participated in the battle. It was the aircraft carriers that decided the final victory of the United States against Imperialist Japan.

U.S. aircraft carriers experienced further significant developments during the Cold War. With the invention and massive application of supersonic jet fighters, U.S. aircraft carriers were modified to host the landing and take-off of jet fighters. However, to host take-off and landing of modern aircraft is a great challenge. Modern aircraft usually have a higher weight to carry more complicated weapons systems. Besides, to obtain superior supersonic aerodynamic performance, modern jet fighters usually sacrifice their subsonic performance. Both factors resulted in a longer take-off distance for modern jet fighters. Therefore, the modification of the aircraft carriers to allow modern aircraft to take-off from a very short runway became necessary.

In general, there are two types of architectures for aircraft carriers to meet modern aircraft's take-off requirement: ski-jump and catapult. Figure 2-6 shows the ski jump of an aircraft carrier. The upward-curved of the ski-jump will allow aircraft to take – off at a lower airspeed than required because the aircraft will accelerate into the air at a positive angle of attack rather than on the horizontal runway.

Figure 2-6: Ski-jump, from ref[47]

Another way of launching modern aircraft is a catapult, as shown in Figure 2-7. Modern catapults are driven by high-pressure steam, and the mechanism is explained below[16]. Before launching, steam is collected in a high-pressure accumulator located below the catapult. After the accumulator reaches the required pressure, the catapult operator will close the flow control valve. After the accumulator is pressurized, crews will place the aircraft at the beginning of the catapult's stroke and raise the shot blasting deflector(figure2-8) to protect personnel and equipment from shot blasting. The front gear of the aircraft will be set into a shuttle. Once the aircraft is ready to take-off, the catapult will open the launching value to allow the high-pressure steam to flow into the stroke cylinder and to push the shaft connected with the shuttle. In such a way, the aircraft is rapidly accelerated.

Aircraft catapults are more powerful than ski-jumps, so they can launch heavier aircraft from aircraft carriers. For instance, a C-13-1 catapult is capable of accelerating a 80,000 pound aircraft to 140 knots within the stroke of 310 feet [16]. A newer generation of electromagnetic catapults is currently under development since steam catapults require a significant amount of maintenance and their thrust profile is difficult to tune to the particular aircraft to be launched.

In addition, in order to successfully land the aircraft on the carrier, an arresting gear system is required (see Figure 2-9). The arresting gear system consists of multiple wire ropes that cross the landing zone of the aircraft and these are intended to be caught by the tail hook of the aircraft. During the normal arresting process, the

tail hook engages the cable, and the kinetic energy of the aircraft is transferred to the hydraulic damping system installed below the carrier deck. Arresting gears are powerful, for example a Mark 7 Mod3 arresting gear can decelerate a 50,000-lb aircraft incoming at a speed of 130 knot within a stroke of 344 ft [16].

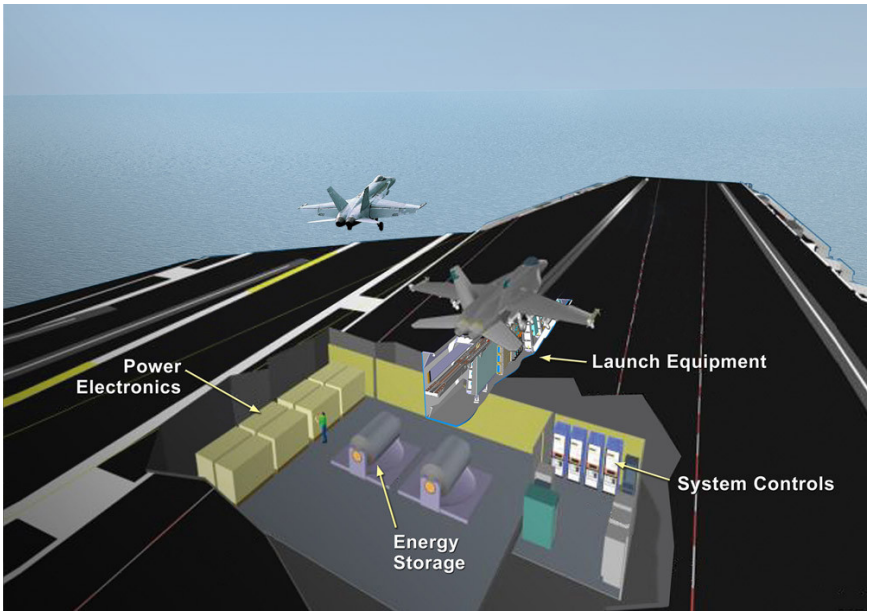

Figure 2-7: Aircraft Catapult from ref[3]

Figure 2-8: Jet blast deflectors, from ref[50]

Figure 2-9: Arresting Gear System, from ref[53]

2.4 Chapter Summary

In this chapter, we review the historical progress in improving flight efficiency, aerial refueling and naval aviation. Modern aircraft is constantly optimized in terms of aerodynamic performance, propulsion system and structural design, and the industry has made considerable progress. Aerial refueling has evolved from an abandoned experiment to a standard procedure in the modern air force. Naval aviation technology is the backbone of US military superiority. Modern aircraft design, aerial refueling and naval aviation technology form the technical basis for the system design of FARS.

Chapter 3

System Design of FARS

3.1 Concept Overview

In this thesis, we propose a floating aerial refueling system (FARS) to reduce the exponential fuel cost of intercontinental flights. Figure 3-1 shows a schematic diagram of FARS. This diagram shows the so-called Concept of Operations (CONOPS). We denote the airplane to be refueled as *Receiver aircraft* and the airplane to refuel as *Tanker aircraft*. As shown, we will deploy a ship (e.g. *Mother Ship* in the figure) near the receiver's flight path. Ideally the mother ship is directly under the flight path but some lateral distance is allowed. In this system, the receiver aircraft will not carry fuel for the entire mission at the beginning of the flight. Instead, the receiver will carry enough fuel to safely enter the FARS's service area. Once the receiver enters the service area, a tanker will take off from the mother ship and refuel the receiver aircraft. Through the FARS refueling process, the receiver avoids the exponential fuel consumption, and thus greatly reduces the operation cost and emissions of the flight.

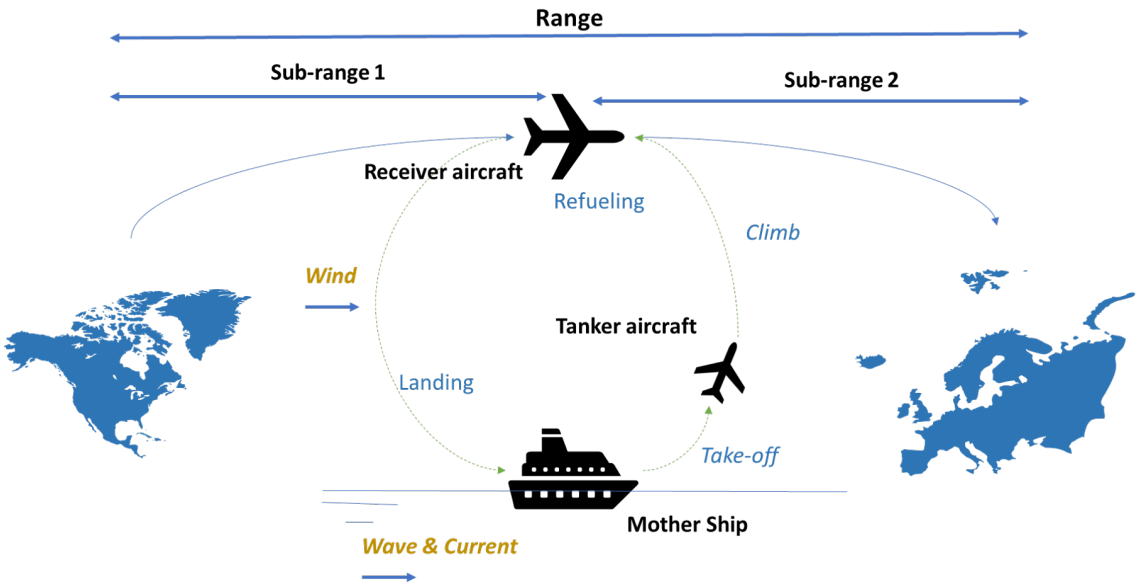

Figure 3-1: Schematic diagram of FARS CONOPS

The FARS system also includes an island-based or land-based airport as a backup landing location in case of the refueling operation fail, and all mother ships will be deployed within the service area of the island-based airport, as shown in Figure 3-2. We denote this island with airport as '*Base Island*'. One base island can be connected with several mother ships. The airport on the base island has a standard runway and thus allows the take-off and landing of large airplanes such as Boeing's 767 or Airbus A330. In general, there are three concerns for the base island:

1. The tankers can take-off or land from the base island to enhance the service-ability of the FARS, because the airport on the island has longer runways and better take-off and landing conditions.

2. In case of emergencies such as refueling failure, the receiver airplanes can land, refuel and take off from the base island.

3. The base island can also be used as a fuel storage and distribution center. Fuel for refueling can be stored on the base island in a central place, and distributed to the mother ship through pipelines when needed. Under this arrangement, due to economies of scale, fuel transportation and storage costs will be reduced.

Furthermore, we can establish a maintenance center on the base island. The on-board maintenance of tankers can be very expensive. Therefore, tankers can be maintained (particularly for scheduled maintenance) on the base island to reduce costs.

In addition, the costs can be further reduced as personnel does not need to live on the mother ship on a regular basis. The mother ship may be partially automated. In the future, fuels used for aircraft may be upgraded to hydrogen. Hydrogen can produced locally on the base island and thus achieve zero-emissions. Technologies such as solar-powered desalination followed by solar or wind-powered electrolysis may be used to produce clean hydrogen. The design of the larger island-based FARS infrastructure is outside the scope of this thesis.

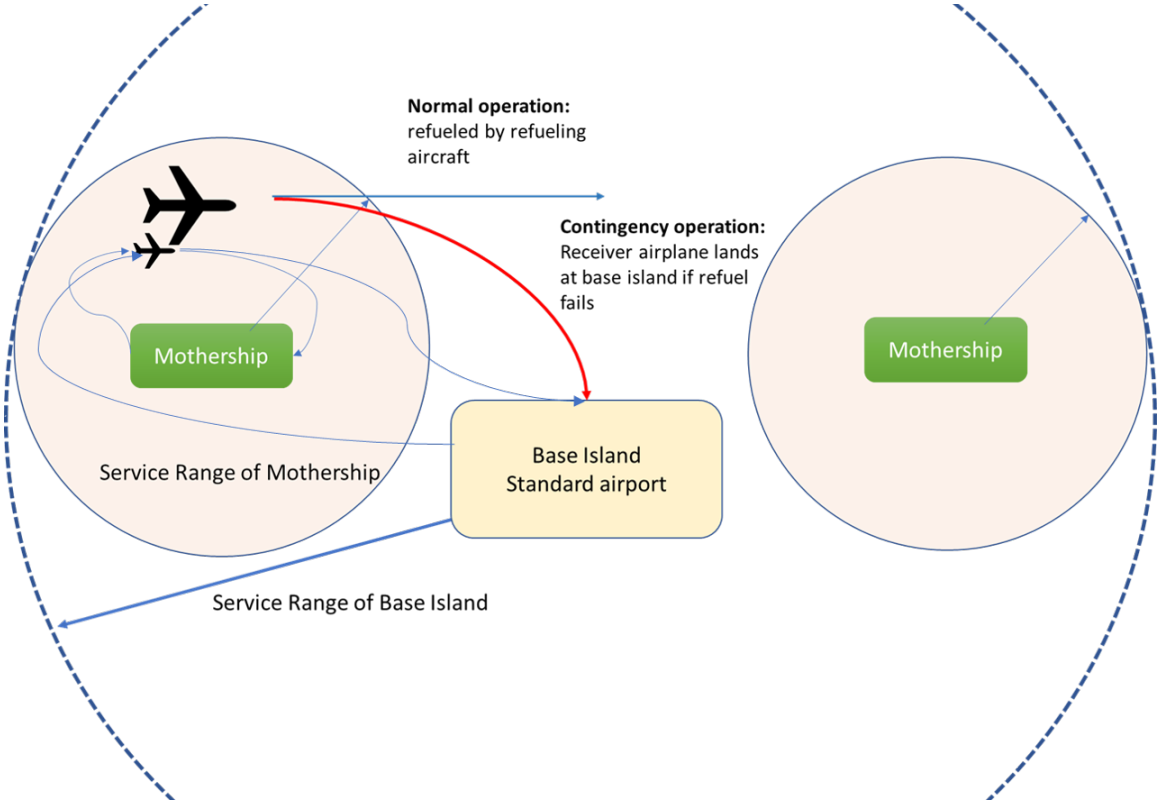

Figure 3-2: Horizontal arrangement of the FARS including overall service range

3.2 System Context

This section explains in some detail the architecture of the FARS system, including its decomposition into constituent subsystems and components. Figure 3-3 shows the physical decomposition of FARS.

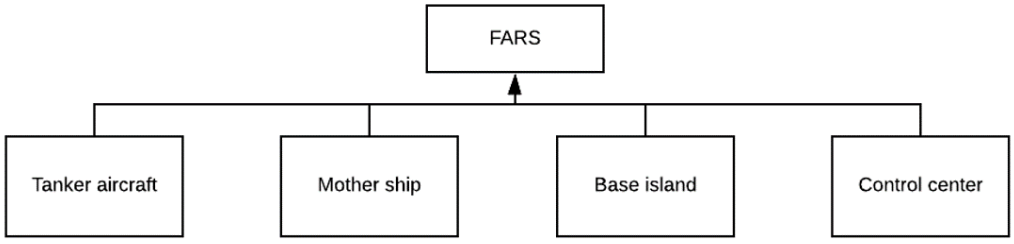

Figure 3-3: Physical decomposition of the FARS system

As shown in the figure, the physical decomposition of FARS consists of four major components:

Tanker aircraft: The tanker is an aircraft used to refuel the receiver aircraft. The tanker aircraft will take off from the mother ship or base island, refuel one or more receiver aircraft and return to be refueled.

The tanker has a large fuel tank, and an automatic flying boom system used for refueling. In addition, the tanker will be equipped with a hook for landing on the ship. The design of the tanker is crucial: FARS's fueling capacity depends on the fueling capacity of the tanker. We select the turbofan engine for the tanker aircraft since turbofan engines can provide large thrust at relatively low fuel consumption.

The tanker is designed to be autonomous and we will designate it as an unmanned aerial vehicle (UAV) for the following reasons:

- Autonomous landing and takeoff and refueling technologies have become more and more mature in the military field, so these technologies will be feasible in the commercial world in the foreseeable future.

- Compared with manned aircraft, the performance of drones is more stable and will not change due to pilots' experience and condition. This is particularly true

during nighttime operations. As a result, UAV systems make tankers downtime shorter and easier to expand.

- Drones have higher storage capacity and lower operating costs because pilots occupy space and are expensive, especially pilots with naval landing experience.

Mother ship: The mother ship is a large ship anchored near the receiver's flight path and it has the following functions:

- Storing jet fuel at economic of scale; refueling the tankers
- Provide airport systems for the autonomous take-off and landing of tankers, which may include short runways, catapult systems, arresting systems and traffic management systems.
- Provide space for temporary storage and maintenance of tankers
- Adjust the ship's forward direction to suit the take-off / landing direction of the tankers. The favorable heading takes into account the weather and flight direction of the receivers. Typically both landing and takeoff should be into the wind.
- Provide extra services other than FARS

The mother ships can be converted from existing oil tankers to reduce cost and increase reliability.

Base island: The base island is an island that is located at the center of several mother ships and is modified to be part of FARS. The base island provides the following services:

- The base island can be used as a storage and distribution center for jet fuel. By transporting jet fuel directly to the base island instead of the mother ship, due to economies of scale, we can reduce jet fuel transportation cost and reduce emissions during fuel transportation. Potentially the base island could even contain a refinery, specialized in Jet A (kerosene) or later hydrogen.

- The base island can provide a standard runway that allows take-off and landing of tankers and receivers in emergency situations.
- The base island can accommodate the refueling control center. The refueling control center is used to manage the refueling strategy and coordination between tankers, receivers and mother ships.
- The base island can serve as the storage and maintenance center for tankers.
- In the absence of mother ships, the base island itself can serve as an airport for refueling operations.
- Once the fuel used on the aircraft is updated to hydrogen in the future, the base island can be updated to a local hydrogen production system to achieve zero emissions.

Control center: The control center is a mixed system of human team, software and data management that is used for coordinating and controlling the refueling operations. The control center may be located on the base island. The control center has the following functions:

- Communicating with tankers, receivers and mother ships.
- Optimizing the refueling strategy to minimize overall fuel consumption while meeting safety requirements
- Assess system status and monitor system safety and performance
- Management operations in an emergency

The design of these four components is explained in detail in the next chapters.

3.3 System Diagram and System Boundary

The system diagram of the FARS is shown in Figure 3-4.

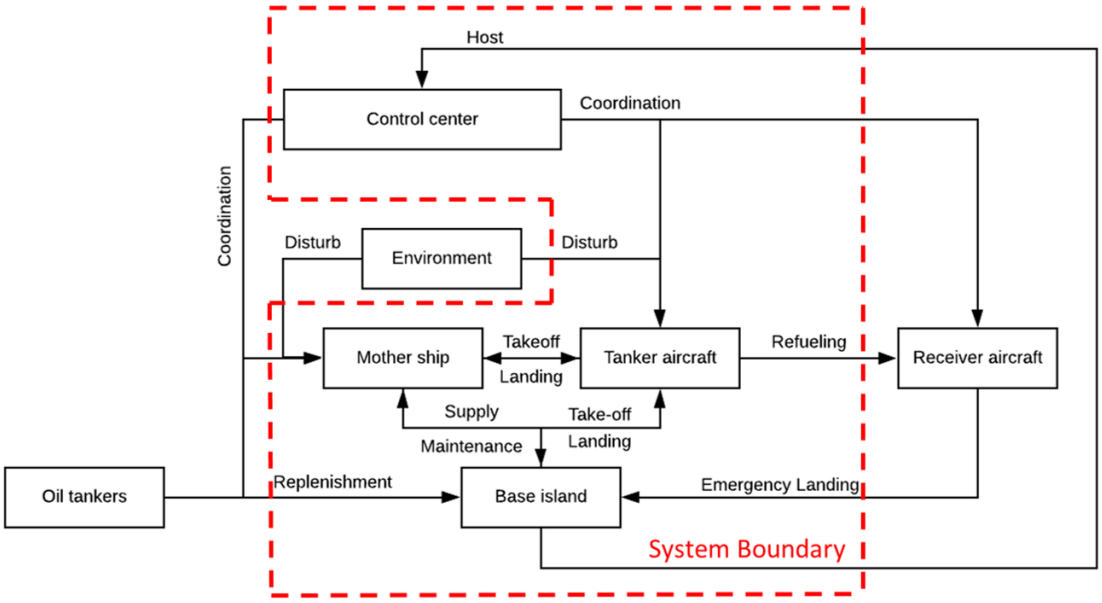

Figure 3-4: System diagram of the Floating Aerial Refueling System (FARS)

As depicted in the figure, there are three major interfaces between the FARS and external systems:

1. **The environment**: Environmental conditions include ocean waves, wind and ocean currents. The ocean currents can be regarded as a constant value, thus causing a static translation offset of the mother ship. The waves and wind will generate dynamic forces, which will interfere with the movement of the mother ship and aircraft, thus limiting their operations.

2. **Oil tankers**: Oil tankers will transport fuel used to replenish the base island's fuel stocks.

3. **Receiver aircraft**: The receivers are intercontinental commercial airplanes that will be refueled by FARS as a service. The total amount of fuel saved by receivers compared to carrying all the fuel onboard is the ultimate value of FARS, and is determined by system fueling capacity and fueling location. In addition, FARS can also be used as an airport for receiver aircraft to land in an emergency or when refueling operations are not possible.

3.4 Scalability

Scalability is the ability of the system to increase its capacity or serve higher levels of demand without fundamental changes in its underlying architecture. The need for FARS scalability comes from three aspects:

- Increasing demand of transcontinental flights
- The demand of reducing the operation and construction cost by leveraging the economies of scale
- The demand of increasing FARS availability, especially when multiple receivers enter the service range at the same time.

To match these demands, the FARS system is designed to be scalable. The scalability of FARS is enabled by four aspects:

- Each mother ship can host multiple tankers for take-off and landing in order to meet refueling demand and to share a mother ship's operation and construction cost.
- Each base island can meet the needs of multiple mother ships, thereby meeting fueling needs and reducing maintenance and logistics costs by leveraging economies of scale.
- Each tanker can refuel multiple receivers per operation to maximize the fuel saving utility
- Each receiver can be refueled multiple times during one mission to maximize the fuel saving margin.

3.5 Nominal & Off-Nominal Operating Modes

The nominal & off-nominal operating modes of FARS are designed as shown in Table 3.1. For each potential off-nominal condition there has to be at least one backup mode.

Table 3.1: Operations Mode of FARS

Nominal operation mode	**Off-nominal operation mode**
Tankers take off from Mother ship or Base Island, refuel the receiver aircraft and return	Refueling failed, receiver aircraft lands on base island
External oil tanker periodically replenishes the jet fuels storage center at base island	The landing of tanker aircraft on mother ship failed, the tanker aircraft will climb and land again.
Base island distributes the jet fuel to mother ships	The mother ship is temporarily unavailable for landing, the tanker aircraft lands on the base island.
Tanker aircraft flies from mother ship to base island for repair	

3.6 Key Attributes

We define key attributes of FARS as shown in Table 3.2. It turns out that even with the overall FARS architecture clearly defined there are many detailed design decisions to still be made. This is a very multi-disciplinary problem.

Table 3.2: Key Attributes of FARS

Key attribute (focused on value delivery)	**Performance metric**	**Rationale**
Minimum number of available tankers at any given time	% of tanker aircraft fleet in operation	Provide system availability at peak demand hours
Waiting time between two sequential tanker aircraft take-offs	Minutes	Influences the refueling strategy and reliability of the system
Capacity of each refueling operation	Weight [lb]	Determines the amount of fuel that can be saved for each operation
Take-off/landing success rate	%	Influences the reliability and availability of the system
The amount of fuel that the base island can store at any one time	Weight [lb]	Influences the availability and cost of the system operations

3.7 Chapter Summary

In this chapter, we present the system design of FARS. To begin with, we briefly describe the CONOPS of FARS, including its basic operation mechanism and general arrangement. Then, we introduce four major components of FARS: tanker, mother ship, base island and control center. The interaction between these four components have been discussed along with their boundaries and scalability considerations. Finally, we define the operational modes and key attributes for FARS. We will discuss the design and optimization of each component in details from next chapter.

Chapter 4

Tanker Aircraft

4.1 Design Reference

We select several existing types of aircraft as reference for tanker design. There are three types of aircraft selected as the baselines: Lockheed Martin S-3 Viking, Lockheed Martin C-130 Hercules and Boeing 737. In addition, we include three current mainstream military tankers for reference as well: KC-135, KC-46 and A330 MRTT. We select these references for the following reasons:

Lockheed Martin S-3 Viking is a carrier-based jet aircraft that has been used for military refueling. S-3 Viking has demonstrated its good carrier take-off/landing performance and thus is selected as reference.

Lockheed Martin C-130 Hercules may be the most well-known military transport aircraft in the world. KC-130, the modified version of the C-130 for naval refueling has demonstrated excellent performance. In Nov 1963, the U.S Navy successfully demonstrated the landing of a C-130 on USS Forrestal aircraft without arrest, making the C-130 a feasible candidate for FARS's tanker selection. Thus, we select the C-130 as reference for our tanker design. Unlike the C-130, our tanker design uses turbofan engines instead of turboprop engines to keep the flight envelope consistent with receiver aircraft such as the Boeing 767.

Boeing 737 is one of the most successful commercial airplanes in aviation history. First produced in 1967, Boeing has developed a branch of 737 variants and is still one

of the best-selling aircraft today. The capacity and performance of the Boeing 737 is similar to the C-130, but the design/aerodynamic properties of the Boeing 737 are more accessible to the public.

Boeing KC-135 Stratotanker, Boeing KC-46 Pegasus and Airbus A330 MRTT are the current mainstream tanker aircraft used in the U.S or E.U military and thus we include them here for comparison. Boeing's KC-135 Stratotanker is the first jet tanker for the U.S. Military. The KC-135 was developed from the Boeing 367-80 prototype and used for refueling U.S. strategic bombers in the Vietnam War and Operation Desert Storm. Boeing's KC-46 Pegasus is used by the U.S. Military to replace older KC-135 airplanes. The KC-46 is developed from Boeing's 767 jet airliner. The Airbus A330 MRTT is a military tanker derived from the civilian Airbus A330.

The image of each reference aircraft is shown in table 4.1.

Table 4.1: Image of reference airplanes [12][57][1][51][44]

Lockheed S-3 Viking	Lockheed C-130 Hercules	Boeing 737-200
		
KC-135 Stratotanker	Boeing KC-46 Pegasus	Airbus A330 MRTT
		

The specifications of each aircraft are shown in Table 4.2.

Table 4.2: Reference aircraft specifications [1][57][51][44][12]

	Lockheed S-3 Viking	**Lockheed C-130**	**Boeing 737-200**	**Boeing KC-135**	**Boeing KC-46**	**Airbus A330-MRTT**
Wing-span	68 ft 8 in	132 ft 7 in	93 ft	130 ft	157 ft	198 ft
Airfoil	root: NACA 0016.3-1.03 32.7/100 mod; tip: NACA 0012-1.10 40/1.00 mod	root: NACA 64A318; tip: NACA 64A412	Wing root- BAC 449/450/451; Wing tip- BAC 442	∼ Kc135a	unknown	unknown
Aspect ratio	7.73	10.1	9.45	7.1	8	9.26
Sweep Angle	15 deg	0 deg	25 deg	35 deg	31.5 deg	30 deg
Operations empty weight	26,581 lb	75,562 lb	93,680 lb	105,476 lb	204,000 lb	285,300 lb
Max take-off weight	52,539 lb	155,000 lb	181,200 lb	322,500 lb	415,000 lb	533,519 lb
Powerplant	2xGeneral Electric TF34-GE-2 turbofan engines	4xAllison T56-A-15 turboprop engines	Pratt & Whitney JT8D-7/-9/-5/-17	CFM – 56 turbofan	2xPW4062	2xPW4170
Max thrust	18,550 lbf	29,648 lbf	58,634 lbf	86,400 lbf	124,000 lbf	144,00 lbf

4.2 Inputs and Parameters

Refueling capacity and fuel consumption are the most important design criteria for tanker aircraft. They also have to be able to match the flight envelope of the receiver

aircraft in terms of altitude and speed. These factors are affected by the aircraft's propulsion, weight and aerodynamics. Heavier aircraft can carry more fuel, but require more power to take off, climb and cruise. The aerodynamic performance of an aircraft depends mainly on the characteristics of the wing, such as wing cross-section, wing span, aspect ratio and sweep angle. Aircraft with better lift performance usually have higher drag. The appendix provides more discussion on aerodynamics. Taking into account the importance and design flexibility of each factor, we define the design input variables of the tanker, as shown in Table 4.3. This table is setup to help define the design space for later multidisciplinary design optimization (MDO).

Table 4.3: Design variables of tanker aircraft

Input variables	Unit	Initial values	Lower bound	Higher bound	Basis for initial value estimation
Wing-span	[ft]	132	65	135	Based on Lockheed C-130[12]
Aspect Ratio	[-]	10.1	5.5	10.1	Based on Lockheed C-130[12]
Sweep angle	[deg]	25	0	25	Based on Lockheed S-3 Viking[1]
Max take-off weight	[lb]	42,000	40,000	250,000	Based on Lockheed Martin C-130[12]
Thrust to Weight Ratio	[-]	0.353	0.2	0.35	Based on Lockheed S-3[1]

The parameters are design features assumed to be constant in this study. We set the parameters based on the reference aircraft. The S-3 Viking and C-130 are military aircraft, so their detailed design / performance is confidential. The Boeing 737-200 has more public information available, but the available information is not enough to fully replicate its performance. Therefore, in order to overcome our accessibility limitations, we created a model with parameters based on similar aircraft arrangements

(such as the Boeing 747).

Table 4.4: Design parameters (fixed) of tanker aircraft

Parameters	Unit	Value	Note
Airplane height	[ft]	22	Based on S-3 Viking[1]
Airfoil type	[-]	BOEING BACXXX AIRFOIL	Airfoil used for Boeing 747[21]
Wing position	[-]	Middle of the aircraft	Similar to S-3 Viking
SFC at sea level	lb/(h· lbf)	0.32	Based on engine LEAP-1C used in COMAC C919[25]
SFC at cruise	lb/(h· lbf)	0.53	Based on engine LEAP-1C used in COMAC C919[25]
High-lift device	[-]	Full-flap	
Weight distribution	[-]	Scaled based on empirical data[34], see Appendix	
Drag at zero lift	[-]	0.0751 at 0.198 Mach, 0.0164 at 0.65 Mach, 0.0305 at 0.9 Mach	Based on Boeing 747-200 data[32]. Spline interpolation for different values.
Refueling ratio	[lb/min]	6000	Based on the military report to U.S. Congress[6]
Service range	[km]	500 km for mother-ship; 1000 km for island	

Once the tanker model is established and used for design optimization these parameters can be changed and refined, as well as subjected to sensitivity analysis.

4.3 Mission Profile and Numerical Modelling

To design the mission profile, we will first review the operations concept of FARS. As shown in Figure 4-1, the mother ship will be deployed around the flight path of

the receivers and next to the base island. Once a receiver aircraft enter the service region (determined by the service range of the tankers), the tankers will refuel the receivers (The refueling will only take a few minutes and thus the refueling time can be ignored in system level design and essentially treated as an instantaneous event). If the refueling operation fails, the receiver will execute the emergency plan, e.g. land at the base island for refueling on the ground.

This arrangement has two advantages: (1) less fuel is consumed when the tanker approaches the receiver (2) emergency landing on the base island can ensure the safety of the tanker and receiver.

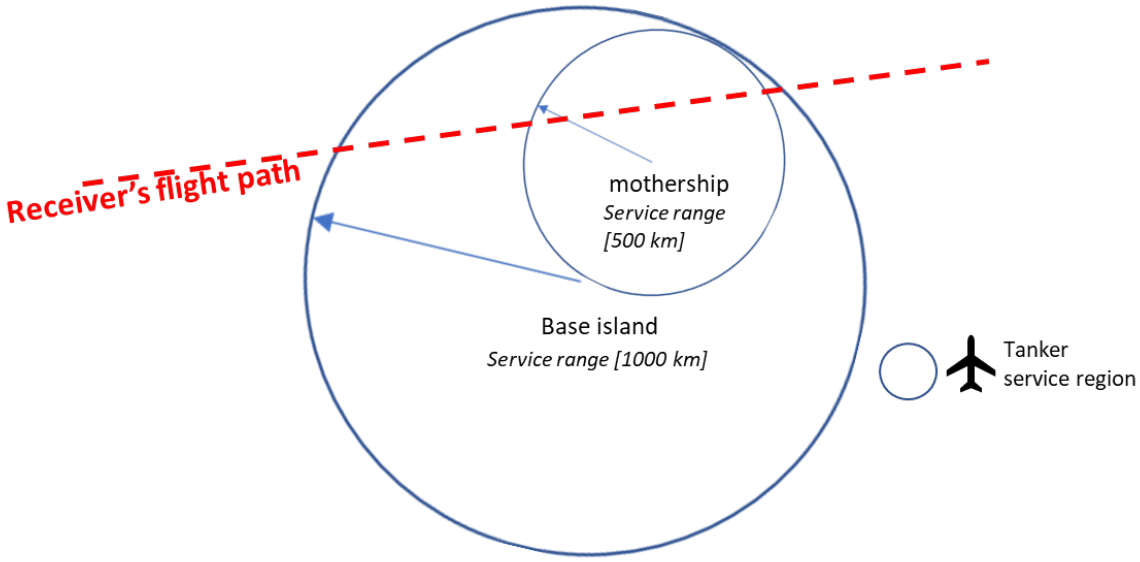

Figure 4-1: Concept of Operations of FARS

With the operations concept defined, Figure 4-2 shows the mission profile of tankers. As shown in the figure, we decompose the flight mission into 6 segments: take-off, climb, approach, refueling, return and landing. For each segment, the aircraft weight is accounted for carefully.

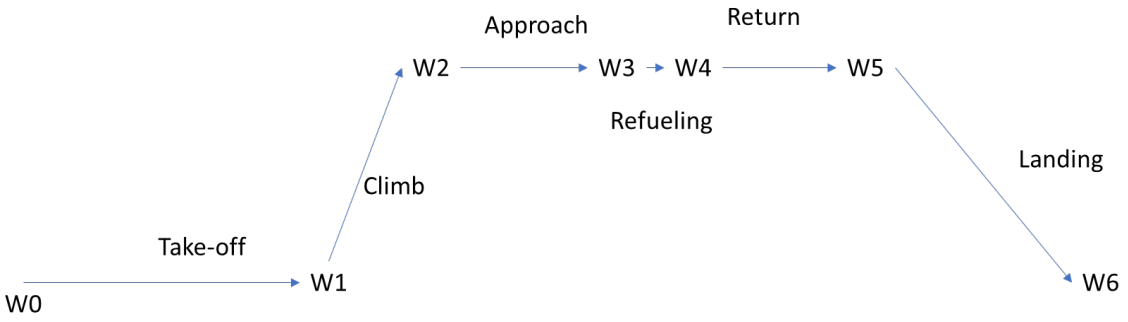

Figure 4-2: Mission profile of tanker aircraft

The maximum refueling capacity depends on service range. The larger the service range, the greater the amount of fuel consumed by the tanker aircraft refueling and the lower the refueling capacity. A too-large service area may cause the tanker aircraft to consume more fuel than it saves. Figure 4-3 shows the calculation procedure. For the segment before the refueling, we use a forward calculation approach and the initial weight W_0 is set to be equal to the maximum take-off weight. We use forward Euler method to calculate weight W_3 , the airplane weight just before the refueling begins. For the segment after refueling, we use backward calculation by assuming the landing weight equals the operation empty weight(OEW) of the tanker airplane, we can thus backtrack the weight just after refueling: W_4. The maximum refueling capacity equals the difference between weight W_3 and weight W_4 which should always be a positive number.

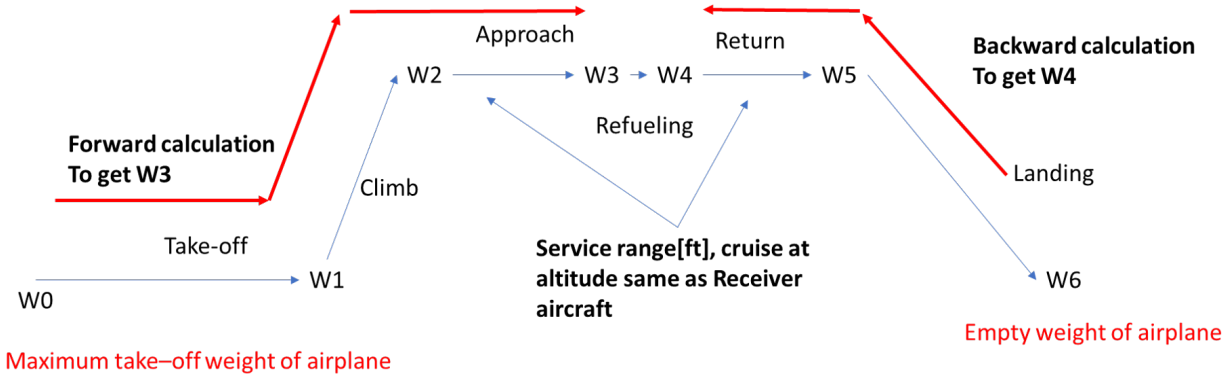

Figure 4-3: The determination of maximum refueling capacity $W_3 - W_4$

The maximum refueling strategy involving multiple refueling is slightly different

from our vanilla tasks and will be discussed further in the next chapter.

The take-off phase is calculated based on aircraft force equilibrium[30]. The horizontal acceleration of the aircraft can be expressed as

$$\frac{dV}{dt} = g\left(\frac{T}{W} - \mu\right) - \frac{g}{W}\frac{1}{2}\rho S V^2\left(C_{D_g} - \mu C_{Lg}\right) \tag{4.1}$$

Where T is the thrust [lbf], W is the weight of the aircraft [lbf], μ is ground friction of the landing gear (set to be 0.25 based on ref[34]), S is the projected wing area [ft^2], V is the horizontal velocity.

C_{D_g} and C_{Lg} are the ground drag and lift coefficients, explained in the Appendix. The value of C_{D_g} and C_{Lg} depends on the wing's angle of attack and we selected the angle that gives the maximum acceleration.

The take-off velocity V_{tf} is set to be 120% of stall velocity V_{stall}[34], where the stall velocity is calculated as:

$$V_{stall} = \sqrt{\frac{2W_0}{S\rho C_{lmax}}} \tag{4.2}$$

Therefore, the take-off distance $x_{takeoff}$ of the tanker aircraft is calculated as:

$$x_{takeoff} = \int_0^{V_{tf}} \frac{dV}{dt}\, dt \tag{4.3}$$

If the aircraft is taking-off from a mother ship, a catapult may be used. In this study, we treat the catapult as an extra externally provided thrust within the catapult stroke distance x_{stroke} , expressed as

$$T = \begin{cases} T_{thr} & if x > x_{stroke} \\ T_{thr} + T_{catapult} & if x \leq x_{stroke} \end{cases} \tag{4.4}$$

However, the fuel consumption for the take-off phase also contains start-up fuel (similar to taxi fuel at a fixed airport). We will underestimate the fuel consumption if we only account for the fuel burned for speed acceleration. Empirical data shows that the aircraft weight after the take-off phase usually equals 97%-97.5% of the aircraft's take-off weight [41]. Therefore, in this study, if the fuel consumed based on simulation

is less than 3% of the aircraft's take-off weight, we manually set the fuel consumption in the take-off phase to 3% of aircraft's take-off weight to obtain a conservative result.

During the climb phase, the climb rate is calculated based on force equilibrium and drag polar theory[30], expressed as:

$$\dot{h} = \sin\gamma V = \frac{T-D}{W}V = \sqrt{\frac{2W}{\rho S C_L}}\left(\frac{T}{W} - \frac{C_D}{C_L}\right) \tag{4.5}$$

The thrust of the aircraft varies with the altitude. In this study, we calculated the thrust T at altitude h as

$$\frac{T}{\rho_h} = \frac{Thr}{\rho_{h=0}} \tag{4.6}$$

Where ρ is the air density at h. Therefore, the altitude h is calculated as:

$$h = \int_0^t \dot{h}\ dt \tag{4.7}$$

We can see that the thrust required at altitude is less than at sea level. The approach and return phases are calculated based on the Breguet range equation[34], expressed as

$$R = V I_{sp}\left(\frac{L}{D}\right)_{\max} \ln\left[\frac{W_{i+1}}{W_i}\right] \tag{4.8}$$

Where $I_{sp} = \frac{3600}{SFC}$, $\left(\frac{L}{D}\right)_{\max}$ is the maximum lift to drag ratio determined by the best angle of attack sing drag polar theory.

The landing is the inverse process of the take-off phase. Therefore, the landing distance is calculated based on the same formula for the take-off distance with zero thrust and extra drag due to the braking and aircraft arresting system. Landing also consumes fuel. In this research, we use historical data to obtain a conservative estimation: we assume that the landing consumes 0.5% of aircraft weight.[41]

Landing on an ship is a complicated procedure and will be further discussed in the mother ship design section.

Therefore, the refueling capacity of a tanker aircraft is defined as,

$$\Delta W_c = W_3 - W_4 \tag{4.9}$$

The fuel consumed by the tanker aircraft during the mission itself is defined as,

$$\Delta W_{consumed} = (W_0 - W_3) + (W_4 - W_6) \tag{4.10}$$

4.4 Benchmark Validations

We perform numerical simulations on the tanker baseline configurations to check the validity of our tanker model and the results are shown in Table 4.5. As shown in the results, the refueling capacity is generally aligned with the refueling capacity based on the references. The take-off distances based on simulations are aligned with take-off distance from reference, stating the validation of take-off simulations. The fuel consumption in climbing phase is around 97% -98% of the aircraft weight, aligned with historical data(98.5%)[41].

Table 4.5: Benchmark performance of reference tanker aircraft

Aircraft type	S-3 Viking	C-130J Hercules	Boeing 737-200	KC-135	KC-46	A330-300
(refuel capacity - fuel cost) @ ship (Range: 500km)	16,484	49,568	66,571	73,953	174,030	208,126
(refuel capacity - fuel cost) @ ship (Range: 1000km)	13,015	40,095	56,849	70,899	163,245	178,636
Take-off distance[ft](model)	4,197	9,837	10,661	9,121	6,801	8,250
Take-off distance[ft](From reference)	Unknown	4,700	9,700	7,000	Unknown	7,280
Weight ratio burned by climb	97.73%	95.47%	98.04%	98.48%	98.26%	97.58%

Therefore, it can be concluded that our simulation is validate.

4.5 Chapter Summary

In this chapter, we introduce the design of tanker aircraft. The most important utility of the tanker aircraft is its refueling capacity. The refueling operation of tankers also consumes fuel, which will counter-balance the benefits of refueling. Besides, the take-off and landing of refueling aircraft are constrained by the limited runway length of the mother ship. These utilities of tanker aircraft are dominated by its aerodynamic, propulsion and weight properties, which can be determined by the tankers' design variables: wing-span, aspect ratio, sweep angle, max take-off weight and thrust to weight ratio. By establishing the relationship between utilities and design variables, we can formulate the model of tanker aircraft.

The optimal design of tanker aircraft does reply not only on the tanker aircraft itself, but also on other components of FARS, which will be discussed in following chapter.

Chapter 5

Refueling Strategy

5.1 Overview

In this chapter, we will discuss different refueling strategies. The refueling strategy is crucial to FARS design because it determines the amount of fuel we can potentially save overall.

There are two main players in the refueling strategy: tankers and receivers. The fuel capacity of tankers determines the amount of fuel available to receivers, and the receivers determine fuel saved since the FARS operation is based on the exponential fuel consumption of both tankers and receivers, since both are subject to the Breguet range equation.

In this study, we propose to examine four strategies for refueling:

1. One to One refueling strategy In this refueling strategy, there are only one tanker and one receiver. The tanker will take-off, approach, refuel the receiver and return, as shown in Figure 5-1. The tanker will refuel the receiver at its maximum capacity.

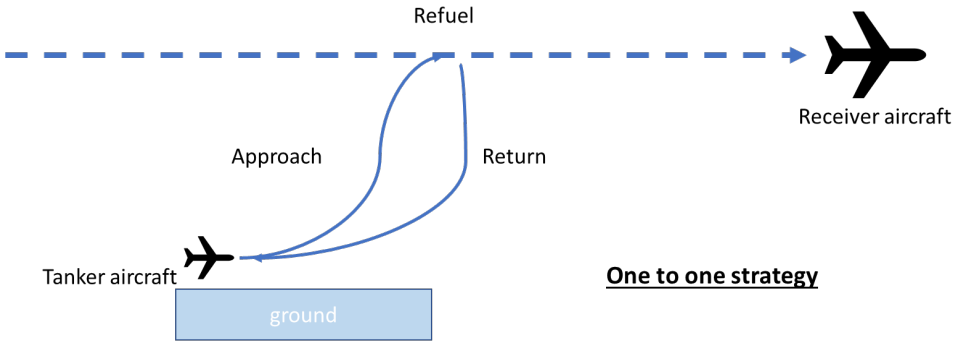

Figure 5-1: One to One refueling strategy

2. One to Multiple refueling strategy. In this strategy, there are one tanker and several receivers. The tanker will refuel multiple receivers during its flight, as shown in Figure 5-2. To simplify the strategy, the amount of fuel that each receiver gets is set to be equal.

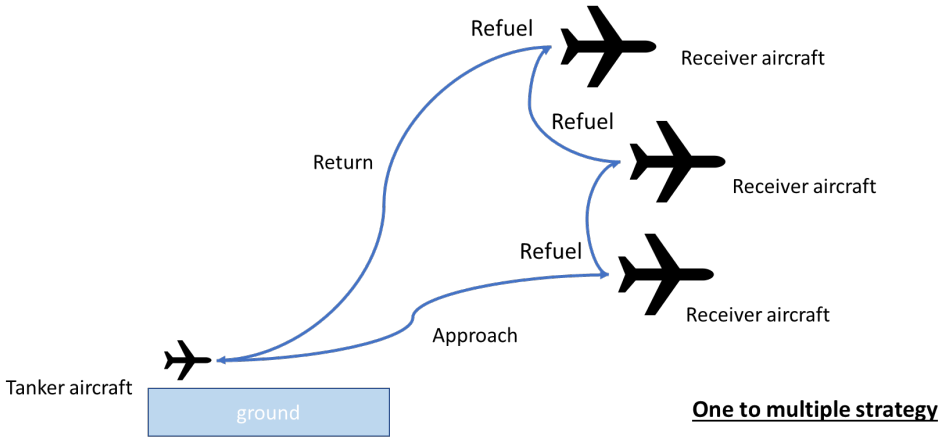

Figure 5-2: One to Multiple refueling strategy

3. Multiple to one refueling strategy. In this strategy, there are multiple tankers and one receiver. The receiver will be refueled at different stages of flight, as shown in Figure 5-3. This strategy may make sense especially for ultra-long-range flights.

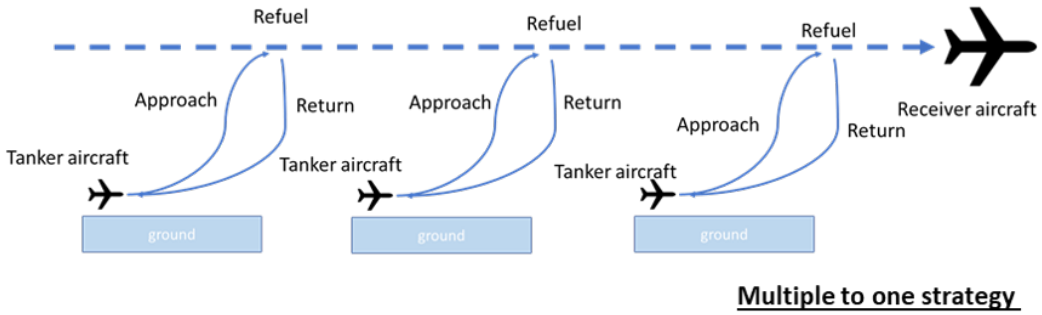

Figure 5-3: Multiple to One refueling strategy

4. The Multiple to Multiple refueling strategy. The Multiple to Multiple refueling strategy is a mixture of the strategies mentioned above. In this strategy, each receiver will be refueled at the different stages of the flight, while each tanker will refuel multiple receivers, as shown in Figure 5-4. This is the most complex strategy to analyze but also the one that may come closest to real life operations.

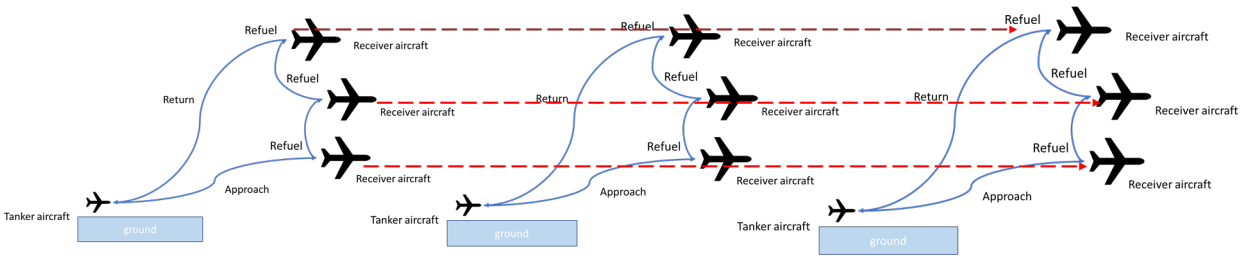

Figure 5-4: Mixed refueling strategy

In this chapter, we will first present an analytical study based on the one to one strategy and then extend this strategy to more complex strategies.

For the refueling analysis, we select a Boeing 767-200ER as the receiver aircraft baseline. To emphasize the fuel saved from aerial refueling, we select a 13.5 hour flight (typical flight duration from Tokyo to New York). The tanker will fly with the same cruising altitude and speed as the receiver to reduce extra movement of the receiver for fuel savings and safety considerations.

Table 5.1: The specification of Boeing 767-200ER from ref[54][31]

Parameter	Value
Max take-off weight	395,000 lb
Max L/D	16.1
Max payload	78,390 lb
Operating empty weight (OEW)	181,610 lb
Cruise speed	0.8 Mach
Cruise altitude	35,000 ft
Mission endurance	13.5hrs
SFC	0.6 $lb/(lbf{\cdot}h)$

5.2 One to One Refueling Strategy

In the one-to-one refueling strategy, the mission profile of the receiver airplane is estimated as follows. Figure 5-5 shows the simplified mission profile of the receiver airplane. In this strategy, we only have one refueling point for each receiver and each tanker will only serve one receiver aircraft.

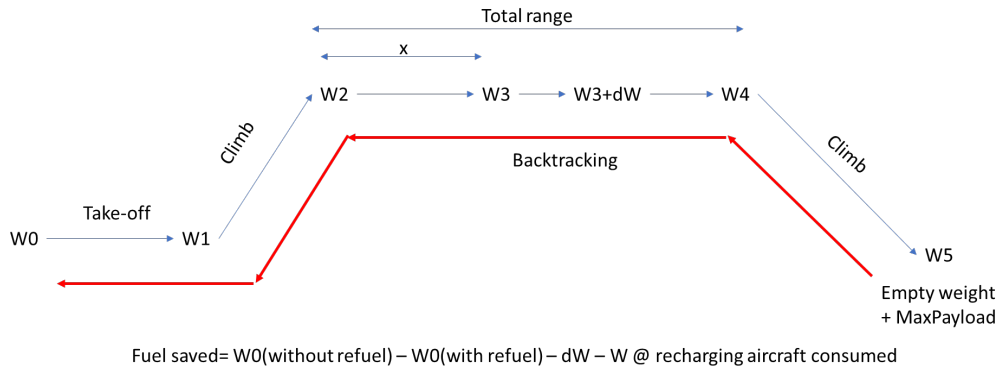

Figure 5-5: Mission profile of the receiver

Similar to the weight estimation of tankers, we estimate the weight of receivers as follow. We set the landing weight of the airplane and backtrack-calculate its take-off weight. The total range of the receiver airplane is estimated as total endurance times

cruise speed. At the position x, the receiver will be refueled with a fuel weight of dW.

The total fuel saved for the entire journey is calculated as *Take-off weight of the receiver without refueling - Take-off weight of the receiver with refueling – dW – fuel consumed by the tanker for itself.*

The fuel dW equals the maximum of refueling capacity of the tanker (how much fuel it can give) or refueled capacity of the receiver (how much fuel it can receive at a maximum given its own tank capacity).

Instead of numerical simulation, the weight calculation of the receiver aircraft is simplified. We apply an empirical formula from historical observation for all phases except for cruise as shown in Table 5.2.

Table 5.2: Receiver aircraft weight empirical formula from historical observations[41]

Mission segment	W_i/W_{i-1}
Warm-up and takeoff	0.970
Climb	0.985
Landing	0.995

With the mission profile now clearly defined, the next question is what the optimal refueling position x is, given refueling fuel weight dW. Intuitively one may think that the best refueling position is $x = 0.5$, that is exactly at the mid-point of the flight. However, this may not be true due to the non-linearity caused by the Bréguet range equation. The answer may therefore be more interesting. The best refueling position can be found analytically, the process is as follows,

Using the same convention as shown in Figure 5-5, We denote the weight of aircraft just after climb as W_2, the weight of the receiver aircraft just before landing as W_4.

Without refueling, the $W_{2,noRefuel}$ can be determined by $W_{4,noRefuel}$ using the Bréguet range equation as:

$$W_{2,noRefuel} = W_{4,noRefuel} e^{\frac{R}{VI_{sp}\left(\frac{L}{D}\right)_{\max}}} \tag{5.1}$$

Where R is the total range or flight distance of the flight (not accounting for

wind).

With refueling happening at the position x, we have W_3 just before refueling (amount of fuel refueled dW) as

$$W_3 = W_4 e^{\frac{R-x}{VI_{sp}\left(\frac{L}{D}\right)_{\max}}} - dW \tag{5.2}$$

Thus we have W_2 expressed as,

$$W_2 = W_3 e^{\frac{x}{VI_{sp}\left(\frac{L}{D}\right)_{\max}}} \tag{5.3}$$

Therefore, the amount of fuel saved for the receiver aircraft alone can be calculated as:

$$J = (W_2 - W_4)_{noRefueling} - (W_2 - W_4 + dW)_{Refueling} \tag{5.4}$$

We can find the optimal point using gradient-based optimization as the optimal refueling point satisfies the stationarity condition $\frac{dJ}{dx} = 0$:

$$dW + W_4 = W_4 e^{\frac{R-x}{VI_{sp}\left(\frac{L}{D}\right)_{\max}}} \tag{5.5}$$

The result satisfies the Karush-Kuhn-Tucker (KKT) optimality condition. Therefore, the optimal refueling position x is the position at which dW equals the fuel consumption for the remaining part of the flight.

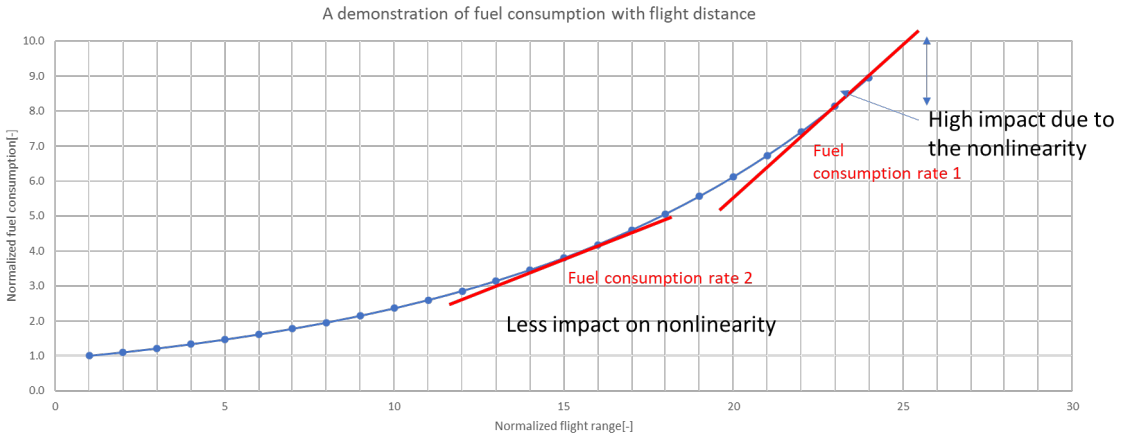

Figure 5-6: Schematic diagram of exponential growth of fuel consumption

The best refueling position can also be understood intuitively. Figure 5-6 shows a schematic diagram of the exponential growth of total fuel consumption as a function of range. As shown in the figure, the average fuel consumption rate per unit flight distance dW_{fuel}/dr will also increase exponentially as the flight distance increases. This is one of the reasons why particularly ultra-long-range flights such as 18-20 hours flights by projects such as 'Sunrise' by Qantas are so challenging. Due to this non-linearity, the fuel saved in the last part of the journey will have a greater impact, while the fuel saved in the early part of the flight will have little effect. Therefore, the optimal refueling position is the position where refueling is equal to the fuel used in the last part of the journey.

In the one-to-one strategy, we need to optimize the refueling amount dW. On the one hand, a large amount of refueling for the receiver will greatly reduce the amount of non-linear fuel consumed. On the other hand, if the amount of fuel refueled by the tanker is too large, the optimal refueling point x will move to a position where the nonlinear fuel consumption rate is still small, so the impact is small. In the worst case, if x is poorly chosen, there will be negative fuel gain when taking into account the fuel burned by the tanker. In addition, the amount of fuel refueled by the tanker itself will increase the weight of the aircraft, causing another nonlinear fuel loss curve (an extreme case is to refuel the receiver immediately after its take-off).

5.3 Multiple to One Refueling Strategy

In the multiple to one refueling strategy, the mission profile of the receiver airplane is shown in Figure 5-7. After the receiver cruises for a distance x, the refueling processes start. We denote the total number of refueling operations as n. The amount of fuel refueled at the i-th process is denoted as dW^i and the aircraft weight just before the refueling is denoted as W_3^i .

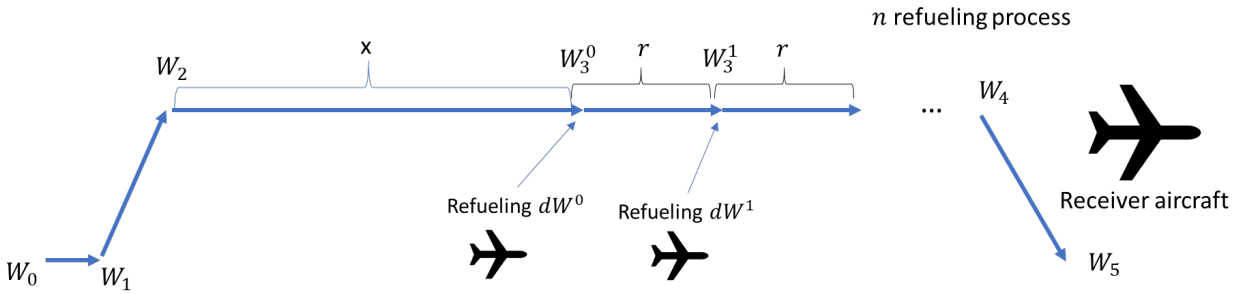

Figure 5-7: The mission profile for the multiple to one refueling strategy

Similar to the one-to-one strategy, we assume that the landing weight W_5 of the receiver equals its maximum payload plus operations empty weight and we use the backtracking method to calculate the aircraft's weight before landing.

Through one-to-one refueling strategy analysis, we know that the best refueling position refers to the position where the fuel refueled is equal to the fuel consumed by the rest of the flight. We adopt this conclusion here. Therefore, in our backtracking calculation, the distance between two consecutive refueling points is set equal to the projected distance of the fuel refueled at the previous refueling point to maximize its effect. In the optimal refueling strategy, the aircraft weight at each refueling point $n = 1, 2, ...$ should be equal, expressed as

$$W_3^{i+1} = W_3^i \tag{5.6}$$

$$W_3^i e^{\frac{\Delta x}{VI_{sp}\left(\frac{L}{D}\right)_{\max}}} = W_3^i + dW^i \tag{5.7}$$

Where Δx is the flight distance between the i-th refueling point and the i+1 th

refueling point.

To simplify the multi-to-one refueling strategy, we assume that each amount of refueling fuel at each refueling operation of the single receiver aircraft dW^i is equal, denoted as r, therefore:

$$W_3^0 = W_3^2 = \ldots = W_3^i = W_4 \tag{5.8}$$

$$r = V I_{sp} \left(\frac{L}{D}\right)_{\max} \ln \frac{W_4 + dW}{W_4} \tag{5.9}$$

Compared with the one-to-one strategy, the multi-step refueling strategy is not constrained by the tanker aircraft's capacity. Besides, instead of refueling a large amount of fuel all at one time, we can distribute the refueling at different stages with smaller amount of fuel, thereby avoiding the additional non-linear fuel consumption caused by supplementary fuel.

There are trade-offs in the number of refueling operations. On the one hand, more refueling processes will reduce the amount of fuel consumed due to non-linearity. On the other hand, the greater the number of refueling operations, the greater the amount of fuel consumed by the operation of the tankers, and the less impact on fuel savings due to the reduced non-linearity. There is an optimal number of refueling operations that can be found and this depends on the relative size and fuel efficiency of the receiver versus tanker aircraft.

5.4 One to Multiple Refueling Strategy

Compared with other refueling strategies, the one-to-multiple refueling strategy has natural advantages. According to this strategy, the refueling volume of each receiver aircraft will be reduced, so the optimal refueling point will be shifted towards the landing side $x > x_{opt}$. When the optimal refueling point of the receivers moves to the landing side, each unit refueled will have a greater impact due to the exponential non-linearity. By allocating fueling capacity to multiple receivers, the average fuel

consumption rate may not decline as in the other refueling strategies, so the total fuel savings is higher. Therefore, given the same tanker refueling capacity, the fuel savings using the one-to-multiple fueling strategy will be higher than other strategies. This is one of the reasons why, for example in military refueling operations, a single tanker will refuel multiple receiver aircraft in practice.

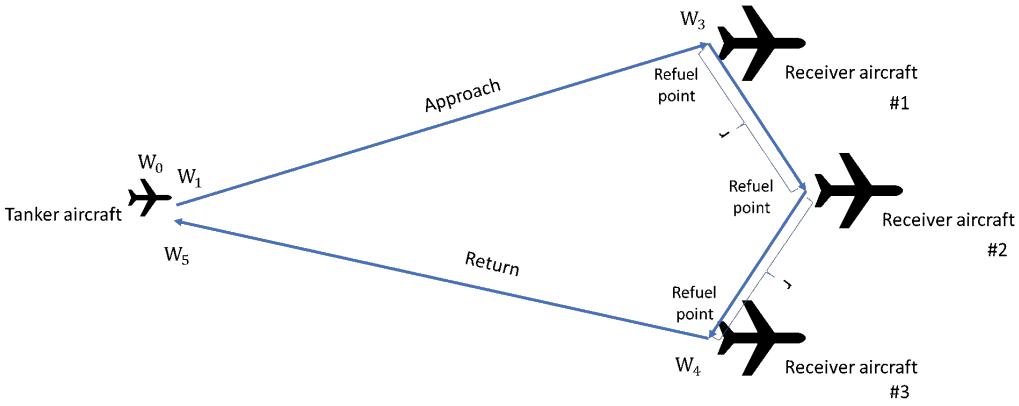

Figure 5-8: The mission profile of the one-to-multiple refueling strategy

We model the one-to-multiple strategy as follows. The mission profile of the receivers will be same as the profile for the one-to-one strategy, while the mission profile of tankers is modelled as shown in Figure 5-8. In the tanker's simulation, the take-off, climb, and landing phase simulation will be aligned with the method mentioned in last chapter. To account for the transient flight between successive receivers, we extend the flight distance in the approaching phase to approximate the extra fuel consumption due to the increased number of refuelings, expressed as

$$R_{approach} = R_{service} + (n-1)r \tag{5.10}$$

Where $R_{approach}$ is the flight distance of tanker aircraft in approaching phase. $R_{service}$ is the designed service range of tanker aircraft. r is the intermediate distance between successive refueling (we assumed they are equal in this study). In our research, we set r to 10 miles, which is twice the recommended distance (5 miles) [38].

However, the one-to-many refueling strategy is not without its shortcomings. First, the number of receivers available for each fueling operation is limited. For

example, in one operation, it is not practical for one tanker to refuel 100 receivers. Second, tanker aircraft need to pass through each receiver to refuel the next receiver. The flight between receivers consumes fuel. Therefore, increasing the number of refueling operations per tanker on the same mission will in turn consume more fuel.

5.5 Mixed Strategy and Design Inputs

The Multiple-to-Multiple refueling strategy is a mixture of the strategies mentioned above. In this strategy, each receiver airplane will be refueled at the different stages of the flight, while each tanker airplane will be refueling multiple receiver airplanes on the same mission, as shown in Figure 5-9.

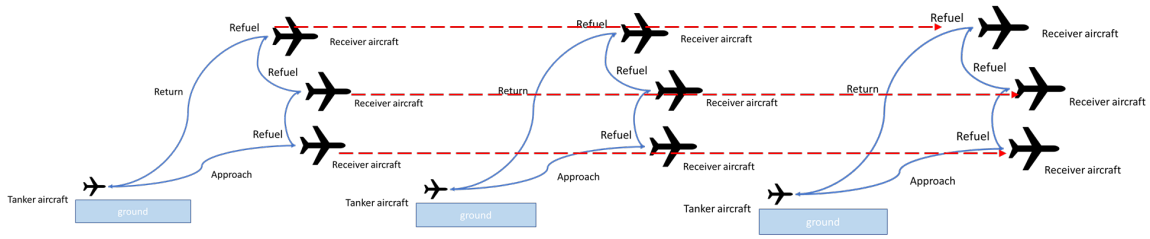

Figure 5-9: Schematic diagram of multiple-to-multiple refueling strategy

We select the mixed strategy as our baseline, because the mixed strategy can be converted into the other three strategies by selecting different design configurations. Table 5.3 shows the design variables of the mixed refueling strategy.

Table 5.3: Design variables of Mixed Refueling Strategy

Input variables	Unit	Initial values	Lower bound	Upper bound
Number of refueling per tanker	[-]	2	1	5
Number of refueling per receiver	[-]	2	1	10

5.6 Chapter Summary

This chapter introduces different fueling strategies between tankers and receivers. Generally, we consider four strategies: one-to-one strategy, multiple-to-one strategy, one-to-multiple strategy and multiple-to-multiple strategy. We start with a mathematical analysis of one-to-one strategy and then extend our findings to other strategies. Each strategy requires a trade-off between refueling impact and operating costs, so more intensive refueling operations are not always better.

The impact of the refueling strategy depends not only on the configuration of its design variables, but also on the overall design of FARS and the flight of the receivers. We will discuss further in following chapters.

Chapter 6

Mother Ship

6.1 System Overview

As discussed earlier, the mother ship is an important element of the FARS architecture. The reason for this is that the mother ship can be positioned near or ideally directly under the flight path of any receiver aircraft.

Figure 6-1 shows the form decomposition of the FARS Mother Ship.

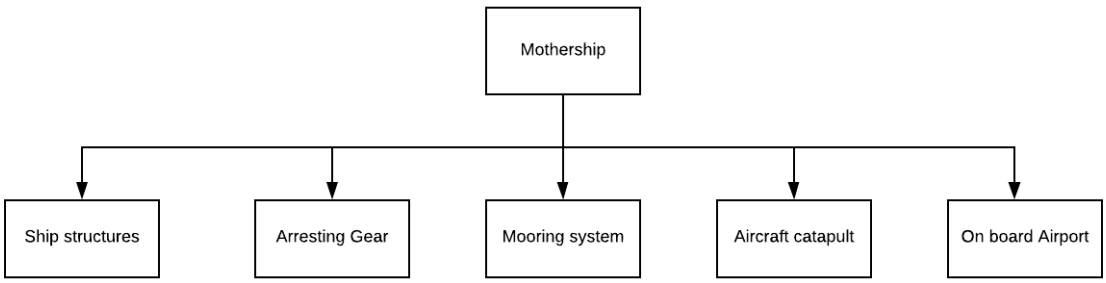

Figure 6-1: Decomposition of the mother ship

As shown in Figure 6-1, the mother ship consists of:

1. **Ship structures**, including the ship hull, cranes & outfits and kerosene tank. The size of the hull limits the storage capacity and the maximum runway length. In addition, the shape of the hull also determines the hydrodynamic performance of the mother ship, which in turn determines the FARS's operation window.

2. **Aircraft catapult** is a mechanical system used to rapidly accelerate the tanker aircraft during its take-off. Aircraft catapult allows the tanker aircraft to take-off from the mother ship within the limited length of runway.

3. **Arresting gear** is a mechanical system used to rapidly decelerate the tanker aircraft during its landing. The arresting gear allows the tanker aircraft to land on the mother ship within the limited length of ship-based runway.

4. **Mooring system** is a collection of connected devices to anchor the mother ship on the seafloor.

5. **On-board airport** refers to the system that allows the tanker aircraft to refuel onboard, storage, take-off and landing on the mother ship, and provides communications and scheduling of refueling operations. The biggest design factor is the runway length. Due to the limitation of the ship's hull, the runway length shall be no more than the length of the mother ship.

6.2 Ship Structure

As a feasible solution, we assume that we are going to convert second-hand oil tankers into mother ships. The conversion of second-hand oil tankers is common in the offshore oil & gas industry. SBM offshore N.V., one of the biggest offshore contractors, constructs their Floating Production Storage and Offloading (FPSO) ships by converting second-hand oil tankers [7]. In addition, the operating history of second-hand tankers also proves their reliability and feasibility (Sometimes a good second-hand oil tanker costs more than a new one). Building a complete new mother ship will cost more, take longer and face higher risks such as manufacturing errors.

Oil tankers are catalogued by class, as shown in Figure 6-2. The size of the tanker is limited for several reasons. First of all, as the length of the ship increases, the bending moment suffered by the ship in high seas will be higher, therefore, the critical stress of the ship's keel will increase. To prevent yielding and fatigue, the internal frame should also be strengthened. Second, the maneuverability of the ship

is limited by the size of the canal, such as the Panama Canal, so the tankers limit their size to pass these thresholds. In addition, the size of the available dock also limits the possible size of the ship. The largest ship that ever exist in the world is the Pioneering Spirit with 477 m length and 127m width. Pioneering spirit couldn't dock at any port in the world, so the Rotterdam Port Authority created a lake to accommodate it.

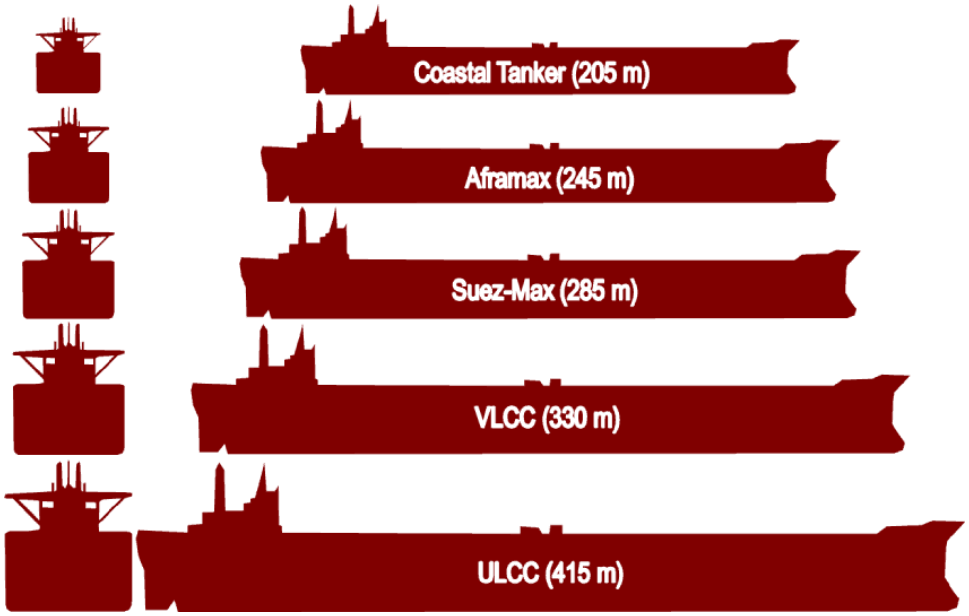

Figure 6-2: Tanker Sizes and Classes from Ref [42]

In this study, we consider five types of ship hulls based on the classification of oil tankers, as shown in Table 6.1.

Table 6.1: Potential selection of ship hull based on Ref [42]

Possible ship hull	Length	Beam	Height
Coastal	205 m	29 m	16 m
Afra-max	245 m	34 m	20 m
Suez-max	285 m	45 m	23 m
VLCC	330 m	55 m	28 m
ULCC	415 m	63 m	35 m

In addition, to increase the width of the mother ship in order to be stable, it is

possible to merge two ships in parallel. For instance, SBM offshore designed a twin-hull FLNG ship by merging two ships together side-by-side to contain their large equipment [10], as shown in Figure 6-3. Through proper design and construction, the risk of hull merger can be controlled. In our research, we use a variable "hull number" to represent single hull (1) or double hull (2).

Figure 6-3: Twin-hull FLNG by SBM offshore, from ref[35]

6.3 Mooring System

The mooring system is essential to maintain the position of the mother ship. First, the tanker aircraft requires a stable platform for take-off and landing. Second, the mooring system will prevent the mother ship from drifting due to environmental forces.

There are three types of mooring systems considered in this study: a spread mooring system, single point mooring system and turret system.

The spread mooring system connects the mother ship to the seafloor via several strong points and thus allows the mother ship to be moored at a fixed heading, as shown in Figure 6-4.

The single-point mooring buoy consists of a buoy, which is permanently fixed to the seabed by multiple mooring cables, as shown in Figure 6-5. The buoy contains a bearing system that allows a part of the buoy to rotate around the moored static pressure part of the buoy. When moored to the rotating part of the buoy through a mooring connection, the ship is able to change its heading to a favorable heading (generally into the wind). As the mooring ship rotates itself into the dominant

environment, the system will minimize the load on the buoy mooring system. The mooring system can also be used in conjunction with a fluid delivery system that can connect (subsea) pipelines to tankers. In addition, there are different types of buoys.

Under more severe environmental conditions, the turret mooring system is more suitable. The turret mooring system consists of a fixed turret column, which is supported by an internal or external vessel structure through bearing devices (see Figure 6-6). Therefore, the components bound to the vessel can freely rotate around the wind vane around the turret, which is fixed on the seabed by multiple anchor lines. This turret arrangement allows the FPSO to adopt the direction of least resistance to waves, wind, etc.

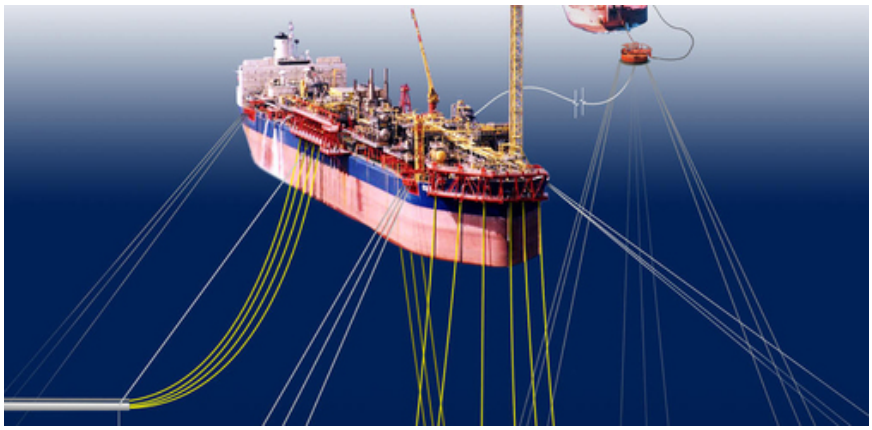

Figure 6-4: Spread mooring system, from ref[11]

Figure 6-5: Single point mooring system (SPM), from ref[11]

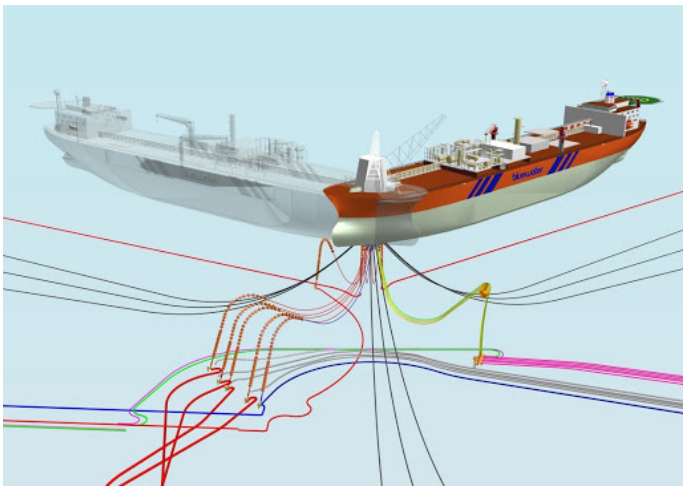

Figure 6-6: Turret mooring, from ref[11]

We consider spread mooring and single point mooring options in this study, since the turret is only necessary for more severe locations such as the North Sea and it is more expensive.

6.4 Aircraft-Mother ship Interfaces

The connections between the tanker aircraft and the mother ship are critical. Carrier-based take-off/landing depends on the hull shape of the mother ship and the environmental conditions.

The take-off distance of tanker aircraft shall not exceed the length of the mother ship. This may be a challenge for large airplanes such as the C-130 or B-737. However, we may integrate a carrier catapult to the FARS system. A Steam-powered catapult C-13-1 can accelerate 80,000 pounds at 140 knot within 310 feet[16]. As mentioned in the previous chapter, we model the catapult as extra thrust within the stroke distance during the take-off phase. Using energy conservation theory (not accounting for friction losses), the equivalent catapult thrust is

$$T_{catapult} = \frac{\frac{1}{2}mv^2}{L_{stroke}} = \frac{0.5 * 80000lb * 140knot^2}{310feet} \approx 221,854lbf \tag{6.1}$$

Here we assume that the tanker aircraft have been designed or redesigned to

tolerate the horizontal catapult thrust forces. Similarly, landing of refueling aircraft also poses a challenge. Arresting gear can be used in the landing phase to assist with the landing. The arresting system used on modern aircraft carriers is the Mark 7 Mod3, which can halt a 50,000lb aircraft with a 130 knot landing speed within 344 feet[16]. Similar to the catapult, we treat arresting as an extra decelerating thrust as

$$T_{arrest} = -\frac{\frac{1}{2}mv^2}{L_{stroke}} = -\frac{0.5 * 50000lb * 130knot^2}{3} 44feet \approx -107,741lbf \tag{6.2}$$

In addition to being restricted by the runway length, the landing of the tanker aircraft also faces more challenges. First, the mother ship is disturbed by hydrodynamic forces, which leads to tracking errors between the mother ship and the aircraft. Second, the air wake on the deck caused by the wind can interfere with the tanker aircraft, making it difficult for the aircraft to control its motions[45]. Usually, the naval landing requires every experienced pilots.

Recent development of autonomous landing/take-off may change this situations. Boeing is developing the Boeing MQ-25, which can perform Naval-based landing, takeoff and autonomous aerial refueling[49]. Autonomous landing and takeoff will significantly reduce the cost and risk of refueling operations. Therefore, we assume in this thesis that there will be commercial autonomous landing, takeoff and aerial refueling systems available in the future. Airbus for example just demonstrated the first fully autonomous refueling with large aircraft using an A330-MRTT.

The numerical simulation of naval landings given wind and wave conditions is very complex. A PID-based autonomous landing systems has been provided by previous research and shows robust performance even under relative severe sea states[45]. However, we do not have enough information to know what the best autonomous landing algorithm is. In this study, we will skip the detailed simulation of the landing process and take the maximum allowable ship motion as the landing criterion.

6.5 Design Variables

The most important output of the mother ship is availability, that is, the percentage of total operating time. The availability of the mother ship depends on the maximum ship motion given environmental conditions. Considering the importance of different factors, the design variables of ship sizing are given in Table 6.2.

Table 6.2: Design variables of Mother ship

Input variables	**Unit**	**Possible values**	**Notes**
Ship size	[-]	Coastal(205m) Afra-Max(245m) Suez-Max(285m) VLCC(330m) ULCC(415m)	Oil tanker classification
Hull number	[-]	1:Single-hull 2:Double-hull	Explained previously
Mooring configuration	[-]	Spread mooring Single point mooring	Explained previously

6.6 Numerical Modelling

With the ship's design variables defined, it is time to investigate how the ship moves given environmental conditions. Wind gusts have little impact on the ship motion given its large inertia. Constant wind forces and currents will only create a constant offset of the ship and are thus ignored in the motion study. More discussion of environmental conditions is attached in the appendices.

The characteristics of ship motion are dominated by its hydrostatic and hydrodynamic properties[26]. Hydrostatic force is caused by interaction between gravity and buoyancy. The hydrostatic force acts as the restoring force proportional to the ship's heave, roll and pitch motion. To be stable, the hydrostatic restoring force must be positive. Hydrodynamic forces are caused by the interaction between ship's

wetted surface with dynamic pressure difference of the water surrounding it. The hydrodynamics will contribute both inertia (added mass) and damping(diffraction force) terms to the ship's equations of motion. Finally, a dynamic pressure difference due to the waves will result in external forces acting the on ship and thus cause the ship's motion. Added mass, damping and external force vary with different frequency of the motion. In summary, the total motion of the ship can be treated as a frequency-dependent transfer function, expressed as

$$TF(\omega) \approx \frac{F_e(\omega)}{(-\omega^2(M + A(\omega))) - i\omega(B(\omega)) + K_{hyd})} \tag{6.3}$$

Where $TF(\omega)$ represents the transfer function of ship's 6-dof motion in the frequency domain, M is the inertia matrix of the ship, $A(\omega)$ is the added frequency-dependent mass, $B(\omega)$ is the diffraction damping, and K_{hyd} is hydrostatic matrix, $F_e(\omega)$ represents the external forces caused by wave motion.

Thus the ship's motion can be expressed in the frequency domain as,

$$X(\omega) \approx TF(\omega)s(\omega) \tag{6.4}$$

Or in term of the power spectral desnsity (PSD) as:

$$S_X(\omega) \approx |TF(\omega)|^2 S(\omega) \tag{6.5}$$

Where $X(\omega)$ and $S_X(\omega)$ represent the ship' frequency-domain motion and its spectrum in 6-dof and $s\,(\omega)$ represents the wave motion in the frequency domain, its spectrum is specified in the environmental modelling section.

We use the open source MATLAB library NEMOH to calculate A,B, F_e and K_{hyd}[39]. NEMOH is based on 3D fluid diffraction theory and validated with industry common practice. To simplify the model, we model the mother ship as a rectangular box with length A, width B and draft D. As a rule of thumb, the center of gravity of the ship is assumed to be 60% of draft above the ship's keel[5]. Table 6.3 shows a demonstration of mesh model we created.

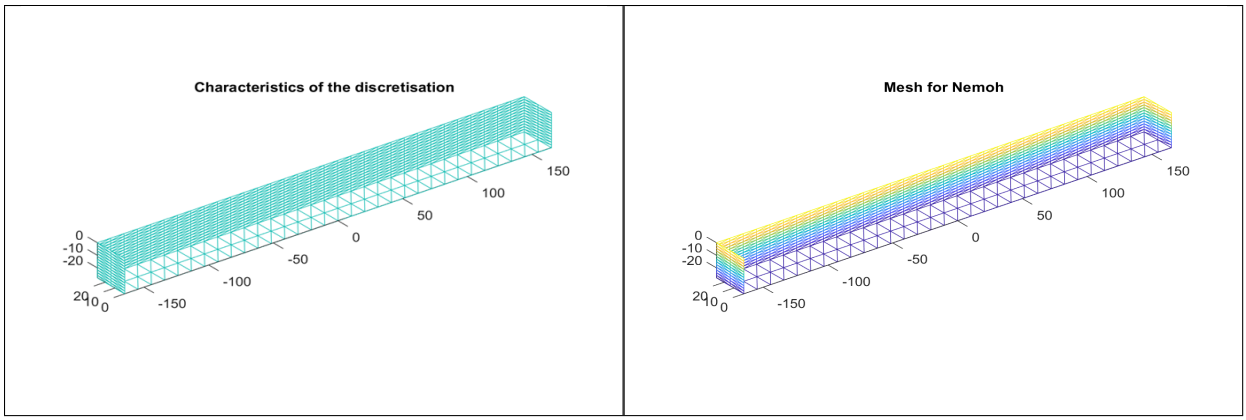

Table 6.3: A demonstration of the mesh model of the mother ship used for hydrostatic and hydrodynamic calculations (VLCC 330m, 1 single-hull)

Hydrostatic forces acting on the ship do not constrain the horizontal motion of the ship. As a common practice, we treat the mooring as a horizontal stiffness with a natural period of 180 sec, based on equation of $k = m^2\omega$.

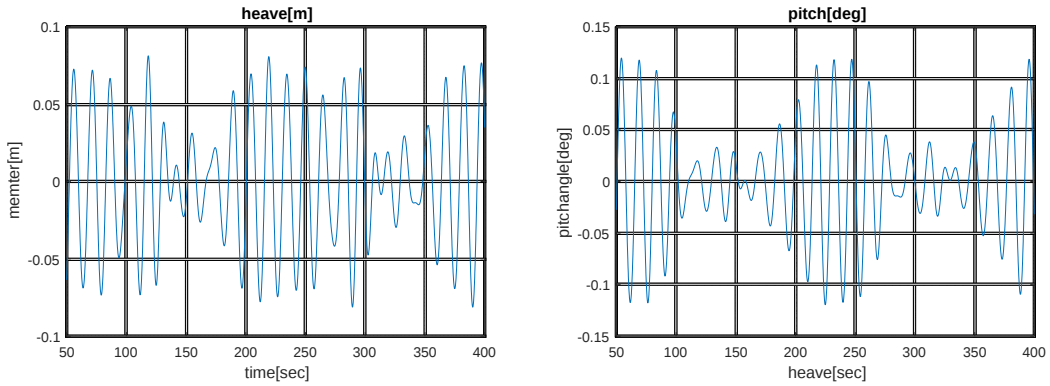

Figure 6-7: Ship motion at center of gravity (heave and pitch) under Hs=2.5m ,Tz =7.5sec, incoming waves with direction 45 deg(starboard side)

Combined with environmental conditions, we simulate the ship's motion at its center of gravity under Hs=2.5m, Tz=7.5 sec, waves with an incoming direction of 45 deg. The following figures show the heaving motion of the ship (up and down) and the center of gravity, as well as the pitching motion of the hull around the center of gravity. The peak-to-peak heave under the simulated sea state is about +/- 10 cm, while the simulated pitch motion is about =/- 0.15 degrees. In the demonstration simulation, the movement of the vessel seems to be relatively small, but it can be justified for the

following reasons: 1. The VLCC tanker is very large and therefore tends to be stable, especially in the pitch direction. 2. We only demonstrated the vessel motion of the incident wave at 45 degrees, not the vessel motion of all wave directions. 3.When the pitching motion is 0.15 degrees, considering the captain (330m), the heave motion at the bow is about +/- 0.5m.

Mother ship operation is limited by its maximum allowable motion. Once the maximum allowable motion is reached, the mother ship is facing the risk of losing its stability and damaging its equipment on board. Table 6.4 shows the maximum allowable ship motion from regulations. In our study, we will adopt the criteria for container carriers which are stricter than for tankers, because this is a similar situation to the mother ship with storage sensitive facilities in her container blocks. We determine the statistical maximum ship motion based on a Rayleigh distribution[48] with 3 hours simulations, expressed as

$$f(x) = \frac{x}{m_{0x}} \exp\{-\frac{x^2}{2m_{ox}}\} : X_{\max 3hr} \approx 1.86 * 2 * \sqrt{m_{ox}} \tag{6.6}$$

Where m_{ox} is the zeroth moment of the x motion spectrum, expressed as

$$m_{ox} = \int_0^\infty S_x(\omega)\, d\omega \tag{6.7}$$

Figure 6-8 shows the availability of the mother ship based on maximum allowable ship criteria, equivalent to 228 days of operations.

The operation feasibility is different for different vessel's heading as well as regions of the world due to different sea states. Therefore, different mooring configurations will lead to different heading preferences of the ship and thus different availability. In single point mooring or turret mooring systems, the mother ship will rotate to the favorable heading while taking into account the waves, while the mother ship with spread mooring will not. Therefore, to simulate the heading effect, we assume that the availability of the mother ship with single point mooring will be 80 percent of the availability in all directions, while the availability of the mother ship with spread mooring will be 50 percent of the availability in all directions .

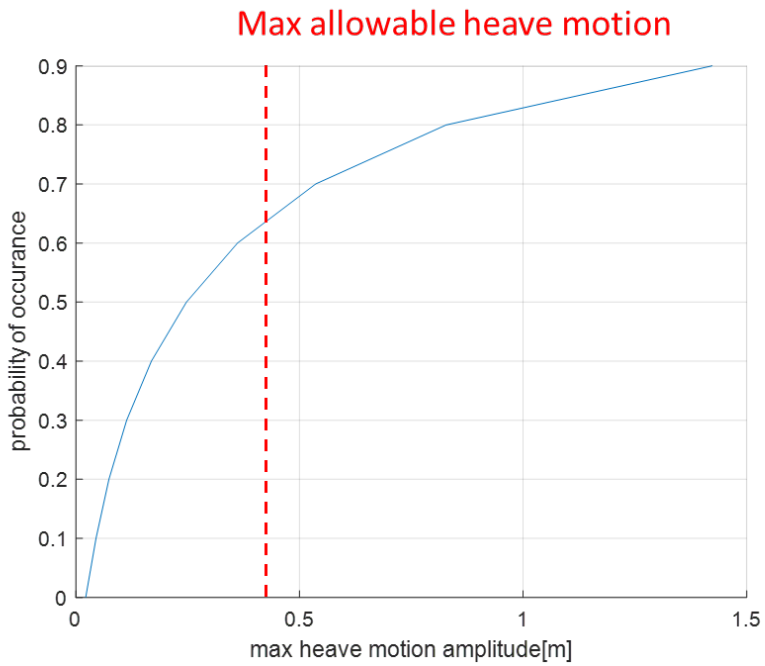

Figure 6-8: Max heave motion versus availability

Table 6.4: Maximum allowable ship motion from Ref[24]

Ship type	heave[m]	roll[deg]
Tanker	1.5	4
Container carrier	0.4	1.5
General cargo ship	0.5	3

6.7 Chapter Summary

In this chapter, we discuss the design of the mother ship. The mother ship affects the FARS system design in two main ways: First, the length of the mother ship limits the takeoff and landing capabilities of the tanker. Second, the size of the mother ship limits the capabilities of FARS, which determines the refueling operation window. The FARS model includes fluid dynamics simulation and stochastic analysis based on a long-term statistical environment model.

Chapter 7

FARS Design Optimization

7.1 Problem Formulation

While the overall FARS architecture and its constituent elements have been discussed in earlier chapters, there needs to be a concerted effort to optimize and synchronize all the elements of this system-of-systems (SoS) such that the overall benefit in terms of fuel savings and net present value (NPV) are optimzied. This chapter focuses on the design optimization of FARS in order to maximize the annual fuel savings. Figure 7-1 shows a block diagram of the FARS system's model implementation.

As shown in the figure, there are three major elements in the model implementation. First, FARS is designed to refuel the receivers and thus the refueling strategy is critical to the model implementation. Second, the amount of fuel saved is determined by the design of tankers (aircraft), because the amount of fuel saved depends on the refueling capacity and fuel consumption of the tankers. Finally, as the platform for the tankers take-off/landing, the design of the mother ship is critical to determine the landing/take-off's availability of tankers. We have introduced the design of all three players individually in the previous chapters. However we have not yet synchronized them as a functioning system.

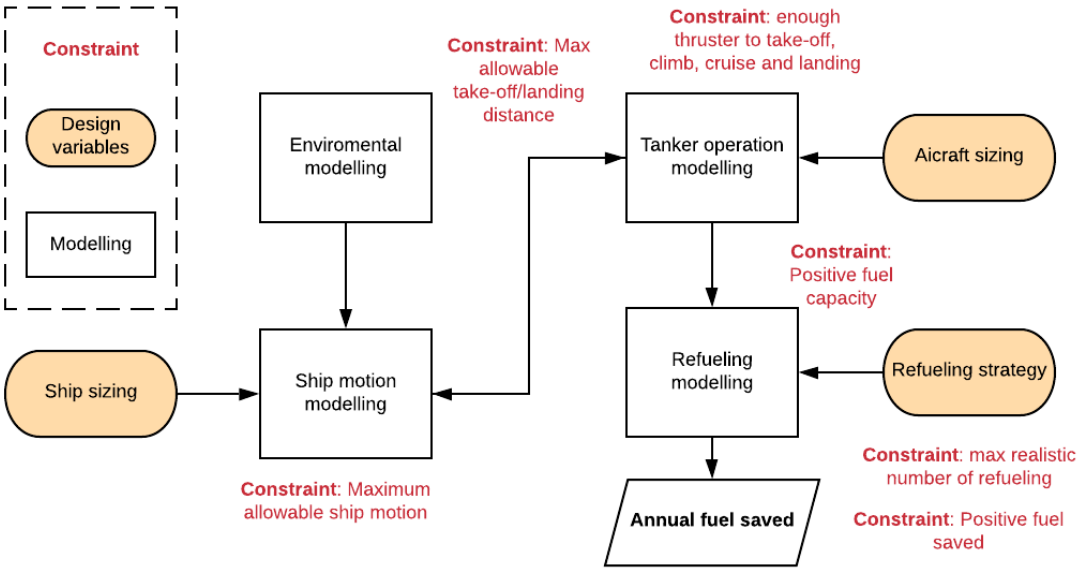

Figure 7-1: Overview of the FARS's design model implementation

In summary, the final objective function of the FARS's design that we need to maximize is,

J = total annual fuel saved = 365 days $*$ availability $*$ fuel saved per refueling operation $*$ number of operations per day

The total annual fuel savings is constrained by

1. Stability of the mother ship, characterized by its hydrostatic stability and maximum allowable ship motion
2. Maximum allowable take-off and landing distance
3. Physical limits (size, engine performance and aerodynamic performance) of refueling aircraft.
4. Maximum realistic refueling strategy
5. Fuel saved per operation must be positive.
6. Upper and lower bounds of input design variables, as stated in previous chapters.

The cruise speed of the tanker aircraft is set to be identical to the cruise speed of the receiver aircraft (e.g. 800km/h). This is done so that there is minimal or no disruption of the receiver aircraft flight. Ideally, in the future, the refueling operations would be autonomous and so smooth that they would go unnoticed by all or most of the passengers. Therefore, it takes about 1.25 hours for the tanker aircraft to approach and return (service range 500 km) based on the mother ship and it takes 2.5 hours for a tanker to approach and return (service range 1000 km) based on a flight from the base island. Therefore, we set assume 9 refueling operations per day per tanker if the tanker is taking off from the mother ship, and 6 refueling operations per day if the tanker is taking off from the base island.

In summary, the design variables of FARS are shown in Table 7.1, including initial values as well as lower and upper bounds.

Table 7.1: Design Variables of FARS for Optimization

Component	Input variables	Unit	Initial values	Lower bound	Higher bound
Tanker aircraft	Wing-span	[ft]	132	65	135
	Aspect Ratio	[-]	10.1	5.5	10.1
	Sweep angle	[deg]	25	0	25
	Max take-off weight	[lb]	42,000	40,000	250,000
	Thrust to Weight Ratio	[-]	0.35	0.2	0.35
Refueling strategy	Number of refueling operations per tanker	[-]	2	1	5
	Number of refueling operations per receiver	[-]	2	1	10
mother ship	Class of ship	[-]	Coastal(285m)	Coastal(285m)	ULCC(415m)
	Hull number	[-]	1:single-hull	1:single-hull	2:twin-hull
	Mooring configuration	[-]	Single point mooring	Spread mooring or single point mooring	

The important fixed parameters assumed in the FARS's design is shown as Table 7.2.

Table 7.2: Design parameters of FARS

Component	Parameters	Unit	Value	Note
Tanker aircraft	Airfoil type	[-]	BOEING BACXXX AIRFOIL	Airfoil used for Boeing 747
	Wing position	[-]	Middle of the aircraft	Similar to S-3 Viking
	SFC	lb/(h· lbf)	0.32 (sea level) 0.53 (cruise)	Based on engine LEAP-1C used in COMAC C919
	Weight distribution	[-]	Be scaled by empirical data, see Appendix	
	Drag at zero lift	[-]	0.0751 at 0.198 Mach, 0.0164 at 0.65 Mach, 0.0305 at 0.9 Mach	Based on Boeing 747-200 data. Spline interpolation for different values.
	Ground effect	[-]	Regression based on historical data with full flaps	
	Flying Boom Refueling ratio	[lb/min]	6000	Based on the military report to U.S. Congress
	Service range	[km]	500 km for mother-ship; 1000 km for island	Expert consultant
Receiver aircraft	Max take-off weight	[lb]	395,000	Based on Boeing 767-200ER
	Max L/D	[-]	16.1	
	Max payload	[lb]	78,390	
	Operating empty weight (OEW)	[lb]	181,610	

continued on next page

continued from previous page

	Cruise speed	Mach	0.8	
	Cruise altitude	[ft]	35,000	
	Mission endurance	[hours]	13.5	
	Transient distance between two receiver aircraft	[miles]	10	Double minimum distance requested by AIAA
Mother ship	Hull shape	[-]	box	Simplification
	Hydrodynamic theory	[-]	3D panel diffraction theory	Open-source hydrodynamic software "Nemoh"
	Site met-ocean data	[-]	DNV world wave scatter data	Based on DNV guidance DNV-RP-C205 [48]
	Wave extreme model	[-]	Rayleigh distribution	Based on DNV guidance DNV-RP-C205 [48]
	Frequency of refueling operations	[time/day]	9 (from mother ship) 6(from base island)	estimated based on service range and cruise speed

7.2 Distributed Optimization

The design optimization for FARS is very complex, involving mixed integer optimization, gradient search and complex constraints boundary. A full-scale optimization requires massive computational power. Besides, it is also difficult to track the rationale behind the full-scale optimization. Thus, in this study, we attempt to explore the design space step by step, rather than through full-scale optimization in one step. Figure 7-2 shows the optimization procedure of FAR's design optimization.

As discussed above, the design of the mother ship is a separate entity than the design and refueling strategy of the tanker aircraft, because the only design input from the mother ship to the design of the tanker aircraft is the runway length.

We can separate the tanker aircraft design and refueling strategy for three rea-

sons. First, the influence of refueling capacity and refueling strategy are different regarding the final output. Therefore, it is feasible to optimize refueling capacity without the refueling strategy. Second, the refueling strategy is a discrete optimization problem with a narrow design space. The refueling strategy alone can be easily analyzed using a brute force method (full enumeration). But it will greatly increase the computational complexity if we include the refueling strategy into the heuristic optimization. Third, the optimal refueling strategy is sensitive to the specific type of receiver aircraft and its mission profile (range, SFC, fuel capacity etc...), while the design of tanker aircraft shall be robust. Considering different factors, we decide to separate refueling capacity from the refueling strategy optimization.

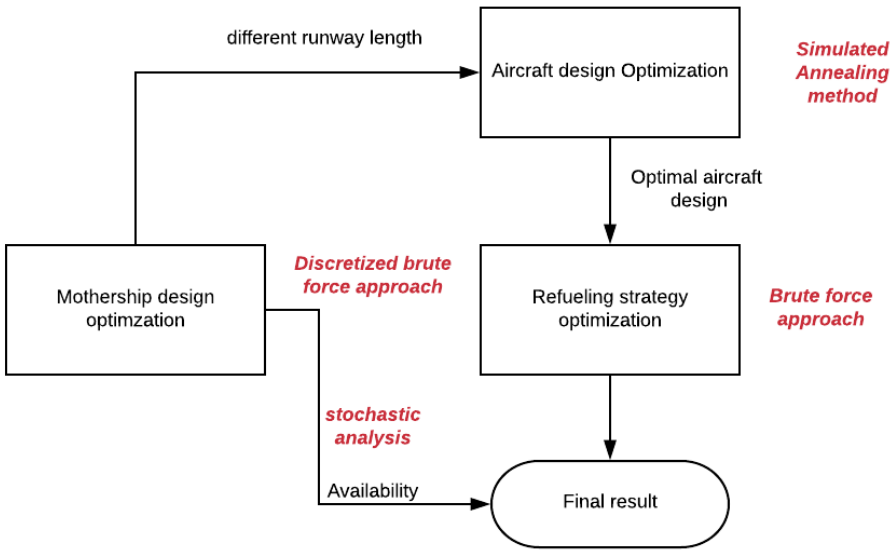

Figure 7-2: Optimization procedure for the FARS system

Therefore, the procedure of the FARS design optimization consists of:

1. Tanker aircraft design: We use the simulated annealing (SA) method to find the optimal design of tanker aircraft. However, the optimal design of tanker aicraft depends on the runway length of the mother ship. Therefore, we will calculate optimal tanker aicraft designs for all possible motership runway lengths.

2. Mother ship design: For the design of the mother ship, it is difficult to apply gradient-based optimization: the hydrodynamic properties of the mother ship are determined by the hull size of the mother ship. However, as shown in the previous chapter, the modelling of ship hydrodynamic force involves an iterative computational fluid dynamics (CFD) calculation, which is very complex and time-consuming. Instead, we discretized the ship's hull size into Coastal(205m), Afra-Max(245m), Suez-Max(285m), VLCC(330m) and ULCC(415m). We calculate all possible design configurations. The design of the mother ship is within the range of calculation(5 discretized ship sizes $*$ 2 ship numbers $*$ 2 mooring options), while maintaining its accuracy and fidelity.

3. Refueling strategy: The design optimization of the refueling strategy is a combinatorial problem. Combinatorial optimization is difficult to solve. Fortunately, the design space of the refueling strategy is within computable levels (maximum 5 refueling operations per tanker aircraft $*$ 10 refueling operations per receiver aircraft) Therefore, we adopted a brute force approach in optimizing the refueling strategy: We calculated all possible designs through full factorial enumeration and thus find the best one.

7.3 Tanker Aircraft Design Optimization

We use the SA method to optimize the design of tanker aircraft.

The Simulated Annealing method is a heuristic optimization method used to find the global optimal design (without guarantees) under complex objective function and constraint situations[15][61][22]. Simulated Annealing imitates the physical process of heating a material and then slowly lowering the temperature to decrease defects, thus minimizing the system energy globally.

In each iteration of the Simulated Annealing algorithm, a new design point is randomly generated through perturbation of an earlier design. The distance from the new point to the current point, or search range, is based on a probability distribution proportional to temperature. The algorithm accepts all new points that lower the

objective function, but also accepts points that increase the target with a certain probability which is temperature dependent. By accepting the point of view of the proposed goal, the algorithm avoids falling into local minima and can explore more possible solutions on a global scale. We select the annealing schedule to systematically lower the temperature as the algorithm progresses. As the temperature decreases, the algorithm naturally reduces the search range to a local region.

However, although SA helps us avoiding local optima, the SA algorithm does not guarantee that the algorithm converges to the global optimal. Therefore, to increase the chance of finding a global optimum, we run Simulated Annealing 15 times with random initial designs. We select the design that gave us the lowest (best) objective function value.

The runway length of the mother ship depends on the design of the mother ship, which in turn depends on the design of tanker aircraft. As discussed later, we use a discretized full enumeration approach to explore the optimal design of the mother ship. Thus, in the tanker design, we perform the optimization based on all possible ship sizes, e.g.205m(Coastal), 245 m(Afra-Max), 285m(Suez-Max), 300m(VLCC), 415m(ULCC).

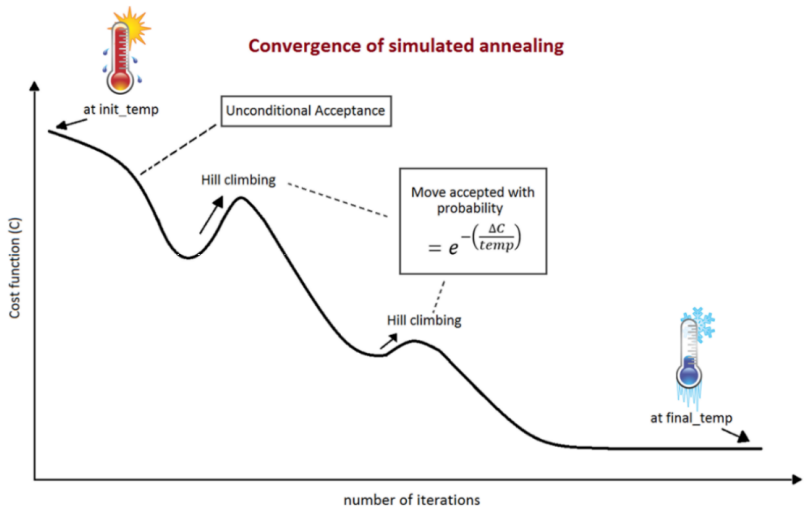

Figure 7-3: A schematic diagram of convergence of Simulated Annealing from Ref [8]

To implement the constraints of the tanker design, we define a minimum objective using the exterior penalty method, expressed as

$$f(x) = -\phi(x) + \sum_{i=1}^{N_{con}} r_i(\max[0, -g_i])^2 \tag{7.1}$$

Where $\phi(x)$ is the refueling utility of the tanker aircraft, e.g. the difference between refueling capacity available to receiver aircraft and fuel consumed for each refueling operation. g_i is the constraints of the optimization problem mentioned in the previous section, the design is valid if $g_i \geq 0$.

We define the following constraints:

1. The tanker's take-off distance with assistance of an aircraft catapult is less than the mother ship's length (varied with settings).

2. The tanker's take-off distance without assistance of an aircraft catapult is less than the standard runway length (the runway length of the base island is set to be 9000 ft).

3. The tanker aircraft shall have enough fuel to take off from and return to the ship (service range: 500km) e.g the weight at each step (take-off, climb, approach, return, landing) is larger than the empty weight of tanker aircraft

4. The tanker aircraft shall have enough fuel to take off and return from the base island (service range:1000km) e.g weight at each step (take-off, climb, approach, return, landing) is larger than the empty weight of tanker aircraft.

5. There shall be more fuel that is available to refuel than the fuel consumed for each tanker's operation.

The optimal tanker aircraft design for different ship runway limits is shown as Table 7.3. In addition, we have attached the case with no ship runway limits as a comparison. Interestingly the wing span and thrust-to-weight ratio are not too different and the expected trend that larger ship runways lead to larger refueling capacity is confirmed.

Table 7.3: Optimal Design of Tanker Aircraft with different runway limits

Ship runway limits [ft]	Wing span [ft]	Thr to weight ratio [-]	Aspect ratio [-]	Sweep angle [deg]	Max take-off weight [lb]	$W_{capacity} - W_{consume}$ **@ island [lb]**	$W_{capacity} - W_{consume}$ **@ships [lb]**
Coastal (205m)	132.0	0.35	7.6	0.0	124,379	28,177	38,604
Afra-Max (245m)	132.0	0.35	7.53	0.0	128,209	29,154	40,127
Suez-Max (285m)	132.0	0.35	7.18	0.0	134,310	30,919	42,113
VLCC (330m)	132.0	0.35	6.67	0.0	142,826	32,602	44,720
ULCC (415m)	132.0	0.35	6.01	0.0	158,304	36,093	49,738
None	112.0	0.35	10.10	0.46	250,000	81,830	94,889

In order to be confident in the global optimal method we discovered, we also used Particle Swarm Optimization (PSO) with a swarm size of 1,000 to optimize the tanker aircraft again. We did not find any new design that can bring better optimized performance. Therefore, we are confident in having found the global optimal value within the design space that was defined.

We can observe some patterns from the table:

1. When the takeoff distance is limited by the ship's runway, the aspect ratio is relatively small. This can be explained by the relationship between stall speed and aspect ratio. In the case of finite wing spans, high aspect ratio aircraft have a smaller projected wing area. Given the same airfoil, an airplane with a smaller wing area requires a longer take-off distance.

2. The refueling capacity of tankers is sensitive to the service range. When the tanker takes off from the ship, it has a higher refueling capacity than when it

takes off from the island, because the tankers taking off from the ship need a shorter service range than the tankers taking off from the base island.

3. Refueling capacity is positively related to the maximum takeoff weight of the tanker. The higher the takeoff weight of the aircraft, the greater the potential weight of the refueling capability. However, higher aircraft takeoff weights require higher lift, which in turn leads to higher drag. Therefore, the maximum takeoff weight of an aircraft is not always proportional to the refueling aircraft, because the flights of heavier tankers consume more fuel.

4. The sweep angle of all tankers is close to zero to reduce the stall velocity and thus take-off distance.

7.4 Mother ship Design Optimization

This section describes the way in which the mother ship design was optimized. Table 7.4 shows the availability [-] versus wave heading [deg] for the single-hull configuration versus the double-hull configuration.

Table 7.4: Operation Availability[-] versus wave heading [deg]

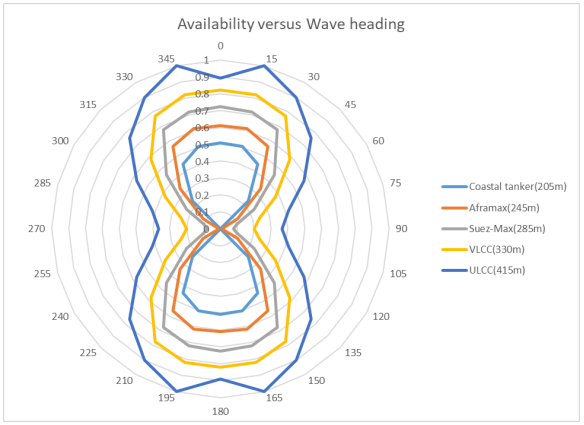

Single-hull option

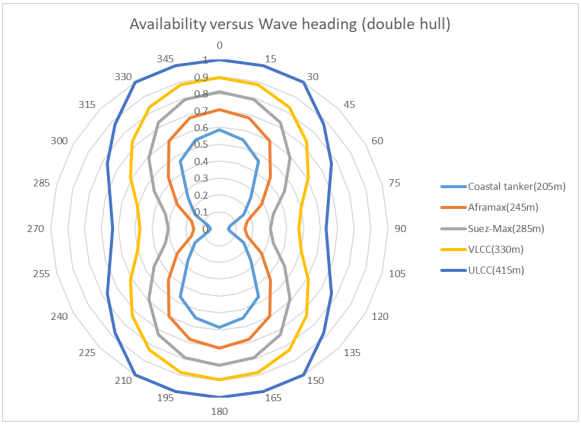

Double-hull option

Table 7.5: Operational availability for different design configurations

Ship size		**Mooring option**	
		single point mooring	**spread mooring**
Coastal tanker (205m)	**single hull**	50.3%	23.3%
	double hull	54.6%	26.4%
Afra-Max (245m)	**single hull**	61.1%	33.9%
	double hull	67.8%	42.8%
Suez-Max (285m)	**single hull**	71.7%	45.3%
	double hull	79.0%	59.0%
VLCC (330m)	**single hull**	82.1%	58.0%
	double hull	88.3%	72.9%
ULCC (415m)	**single hull**	89.7%	75.9%
	double hull	100.0%	87.3%

Table 7.5 shows the operational availability of different mother ship design configurations. As shown, we can observe and conclude that

1. The difference in availability between a favorable heading (about 0 degrees) and an unfavorable heading (about 90 degrees) is very obvious. Spread mooring is not recommended.

2. The availability of single-hull mother ships is less than that of double-hull mother ships. However, the difference in the favorable direction (about 0 degrees) is not very large, and the construction cost of the single-hull mother ship is much lower than that of the twin-hull mother ship.

Considering cost and benefits, it is recommended to design the mother ship with single point mooring and single-hull, which will give an availability of 50% - 90% (depends on ship size). The optimal design of the mother ship size depends on the design of tanker aircraft and refueling strategies and thus will be determined in the integrated optimization section below.

7.5 Refueling Strategy Design Optimization

As mentioned earlier, we use a brute force approach to calculate the optimal refueling strategy. This is implemented as a full factorial enumeration. Table 7.6 shows the total amount of fuel saved for different refueling strategies for a single tanker mission (not annually). In each strategy we use the optimal tanker aircraft design determined in the previous section. In the table, we fixed the number of refueling operations per tanker on a single sortie mission and iterate different number of refuelings per receiver.

As discussed in the last section, we postpone part of the mother ship design to the final integration step. Therefore, we have calculated the optimal refueling strategies for different mother ship sizes.

As shown in the table, there are several patterns can be observed:

1. The amount of fuel saved per each refueling operation is sensitive to service range. For the same design of tanker aircraft and mother ship, the refueling operations from the mother ship can save more fuel than the operations from the base island because of the different service range.

2. Within the maximum allowable number of refueling operations, the one-to-multiple refueling strategy does not reach its critical point at which the fuel consumed by the tanker round trip flight dominates. In contrast, the multiply-to-one refueling strategy is more sensitive to the number of refuelings, because of the non-linearity of the receivers' fuel consumption. As the number of mid-air refuelings for a single receiver aircraft increases the benefit quickly declines with the number of refuelings due to the progress in aircraft fuel efficiency improvement. As a rule of thumb, the optimal number of refuelings per receiver airplane is usually less than the optimal number of refuelings per tanker airplane. This is a positive trend as it makes the real world implementation of a FARS system more likely.

3. The trend we observed is aligned with our discussion in the refueling strategies

chapter.

The optimal refueling strategy can save 60,813 lb of fuel per refueling operation (5 number of refueling per tanker aircraft, 7 number of refueling per receiver aircraft service from a Ara-max mother ship). In practice the total number of refuelings per receiver would probably be kept lower than 7, but the optimization shows that when multiple tankers can refuel multiple receivers more than once that there is an amortization effect whereby the "overhead" fuel cost of getting the tankers into position can be spread across multiple receiver aircraft. This shows the importance that more than one airline would likely have to participate to make the FARS service viable.

Table 7.6: Optimal refueling strategies for different FARS configurations

Design configuration	**service from ship**		**service from island**	
Number of refueling per tanker:1	No of refuel per receiver [-]	Total fuel saved [lb]	No of refuel per receiver [-]	Total fuel saved [lb]
Coastal tanker (205m)	1	7,175	1	931
Afra-max (245m)	1	7,220	1	928
Suez-max (285m)	1	6,991	1	450
VLCC (330m)	1	6,498	1	(449)
ULCC (415m)	1	5,529	1	(2,021)
Number of refueling per tanker : 2				
Coastal tanker (205m)	3	20,360	2	5,878
Afra-max (245m)	3	20,410	2	6,144
Suez-max (285m)	2	19,622	1	5,642
VLCC (330m)	2	19,270	1	5,344
ULCC (415m)	2	18,566	1	4,977

continued on next page

continued from previous page

Number of refueling per tanker : 3				
Coastal tanker (205m)	4	33,833	3	10,702
Afra-max (245m)	4	34,334	3	11,246
Suez-max (285m)	4	33,879	2	10,911
VLCC (330m)	4	32,533	2	10,276
ULCC (415m)	3	31,612	2	9,466
Number of refueling per tanker : 4				
Coastal tanker (205m)	6	46,961	4	15,309
Afra-max (245m)	6	47,497	4	16,131
Suez-max (285m)	5	47,089	3	15,883
VLCC (330m)	5	45,989	3	14,886
ULCC (415m)	4	44,433	3	13,591
Number of refueling per tanker : 5				
Coastal tanker (205m)	7	59,828	4	19,716
Afra-max (245m)	7	60,813	4	20,878
Suez-max (285m)	7	60,135	4	20,575
VLCC (330m)	6	58,781	4	19,193
ULCC (415m)	6	56,989	3	17,929

7.6 Integrated FARS Optimization

As discussed above, we integrate the design optimization of tanker aircraft, mother ship and refueling strategies, based on the total annual fuel saved, expressed as:

$$J = availability * 365 days * number\ of\ refueling\ operation\ per\ day * fuel\ saved\ per\ operation$$

Table 7.7 shows the fuel and equivalent CO_2 emissions saved based on different

FARS's design configurations. According to ICAO, one pound of fuel saved is equivalent to 3.16 pounds of CO_2 emission saved in the fuel production life cycle[23]. As shown in the table, the optimal design of a single FARS system can save 83,576 imperial tons of jet fuel and reduce 264,100 imperial tons of CO_2 emission associated with it. The saving is equivalent to 20% of fuel consumption of flights without refueling. This is for a ULCC mother ship, 6 refuelings per flight and a double hull ship.

Table 7.7: The amount of fuel saved when servicing from mother ship

	Service from ship				
Number of refueling per tanker :1	**Number of refueling per receiver**	**Fuel saved**		**Emission saved**	
		single [ton]	**double [ton]**	**single [ton]**	**double [ton]**
Coastal (205m)	1	5,298	5,748	16,741	18,165
Aframax(245m)	1	6,468	7,182	20,439	22,696
Suez-Max(285m)	1	7,353	8,104	23,236	25,609
VLCC(330m)	1	7,827	8,416	24,733	26,594
ULCC(415m)	1	7,273	8,108	22,984	25,620
Number of refueling per tanker: 2					
Coastal (205m)	3	15,033	16,312	47,505	51,544
Aframax(245m)	3	18,285	20,304	57,782	64,161
Suez-Max(285m)	2	20,637	22,745	65,214	71,873
VLCC(330m)	2	23,210	24,957	73,344	78,863
ULCC(415m)	2	24,425	27,227	77,184	86,036
Number of refueling per tanker: 3					
Coastal (205m)	4	24,981	27,105	78,940	85,652

continued on next page

continued from previous page

Aframax(245m)	4	30,761	34,157	97,203	107,935
Suez-Max(285m)	4	35,633	39,271	112,599	124,097
VLCC(330m)	4	39,186	42,134	123,827	133,144
ULCC(415m)	3	41,590	46,360	131,424	146,498
Number of refueling per tanker: 4					
Coastal (205m)	6	34,675	37,623	109,572	118,888
Aframax(245m)	6	42,553	47,251	134,467	149,313
Suez-Max(285m)	5	49,527	54,584	156,504	172,485
VLCC(330m)	5	55,393	59,561	175,042	188,213
ULCC(415m)	4	58,456	65,161	184,722	205,909
Number of refueling per tanker: 5					
Coastal (205m)	7	44,175	47,931	139,593	151,462
Aframax(245m)	7	54,483	60,499	172,167	191,176
Suez-Max(285m)	7	63,248	69,706	199,863	220,271
VLCC(330m)	6	70,800	76,127	223,729	240,563
ULCC(415m)	6	74,976	83,576	236,925	264,100

As can be seen below the fuel savings achievable from the base island alone are significantly less due to the longer round trip tanker flights (max 17,529 tons annual savings). This is about a factor of 5 less savings than without the mother ship.

Table 7.8: The amount of fuel saved when servicing from base island

	Service from island				
Number of refueling per tanker :1	**Number of refueling per receiver**	**Fuel saved**		**Emission saved**	
		single [ton]	**double [ton]**	**single [ton]**	**double [ton]**

continued on next page

continued from previous page

Coastal (205m)	1	458	497	1,448	1,571
Aframax(245m)	1	554	616	1,752	1,945
Suez-Max(285m)	1	315	348	997	1,098
VLCC(330m)	1	(361)	(388)	(1,139)	(1,225)
ULCC(415m)	1	(1,773)	(1,976)	(5,602)	(6,245)
Number of refueling per tanker: 2					
Coastal (205m)	2	2,893	3,139	9,143	9,920
Aframax(245m)	2	3,670	4,075	11,596	12,876
Suez-Max(285m)	1	3,956	4,360	12,502	13,778
VLCC(330m)	1	4,291	4,614	13,561	14,581
ULCC(415m)	1	4,365	4,866	13,794	15,376
Number of refueling per tanker: 3					
Coastal (205m)	3	5,268	5,716	16,647	18,063
Aframax(245m)	3	6,717	7,459	21,226	23,570
Suez-Max(285m)	2	7,650	8,432	24,175	26,644
VLCC(330m)	2	8,251	8,872	26,074	28,036
ULCC(415m)	2	8,303	9,255	26,237	29,246
Number of refueling per tanker: 4					
Coastal (205m)	4	7,536	8,177	23,813	25,838
Aframax(245m)	4	9,635	10,699	30,446	33,807
Suez-Max(285m)	3	11,137	12,274	35,192	38,786
VLCC(330m)	3	11,953	12,852	37,771	40,613
ULCC(415m)	3	11,920	13,288	37,669	41,989
Number of refueling per tanker: 5					

continued on next page

continued from previous page

Coastal (205m)	4	9,705	10,531	30,669	33,276
Aframax(245m)	4	12,470	13,846	39,404	43,755
Suez-Max(285m)	4	14,426	15,900	45,588	50,243
VLCC(330m)	4	15,412	16,572	48,702	52,367
ULCC(415m)	3	15,725	17,529	49,691	55,391

7.7 Sensitivity Study

It is necessary to conduct a sensitivity study of our design to see how changes in assumptions can affect the recommended design. First, some misalignment will inevitably occur during manufacturing. Secondly, our preliminary design involves a lot of simplifications and assumptions. These assumptions are only valid within a certain tolerance range, such as aero-elastic effects and variations in payload. Third, during the operation of the FARS, due to maintenance and natural aging, the design of our system may be different. Therefore, it is important to guarantee the performance of aircraft within certain tolerances.

The sensitivity study will be focused on the tanker aircraft design, because we have used a brute force approach to calculate all possible mother ship designs and refueling strategies and a sensitivity analysis for the mother ship and refueling strategies would therefore not be as meaningful.

The sensitivity study is conducted as follows. We increase or reduce one specific design variable at a time and check its impacts on the performance or constraints, holding all else constant. In such way, we can determine how 'sensitive' the performance is to a certain design variable. The variation of each design variable is within a reasonable assumption: +/- 2ft for wing span, +/- 0.02 for thrust to weight ratio, +/- 0.3 for aspect ratio, +/- 1 deg for sweep angle, +/- 1000 lbs for max take-off weight.

We check the sensitivity for three types of performance objectives: 1. Refuel-

ing capacity – fuel consumption from the mother ship 2. Refueling capacity – fuel consumption from the base island 3. Take-off distance from the mother ship. The landing distance is not included in the sensitivity analysis because the take-off distance is basically longer than the landing distance and landing distance will not be an active constraint assuming the tankers take-off and land from the same ship.

Table 7.9 shows the sensitivity study of the optimal tanker aircraft design.

Table 7.9: Sensitivity study of optimal tanker design

Ship runway limits[ft]	**wing-span + 2ft**			**wing-span - 2ft**		
	ship	**island**	**take-off distance**	**ship**	**island**	**take-off distance**
Coastal (205m)	-1.9%	-0.9%	-12.2%	1.9%	0.8%	13.8%
Afra-max(245m)	-1.8%	-0.8%	-10.9%	1.8%	0.8%	14.0%
Suez-Max(285m)	-1.8%	-0.8%	-9.0%	1.7%	0.8%	10.1%
VLCC(330m)	-1.8%	-0.8%	-8.2%	1.8%	0.8%	8.3%
ULCC(415m)	-1.8%	-0.8%	-6.3%	1.8%	0.8%	8.5%
Ship runway limits[ft]	**thr to weight ratio + 0.02**			**thr to weight ratio - 0.02**		
	ship	**island**	**take-off distance**	**ship**	**island**	**take-off distance**
Coastal (205m)	1.0%	0.7%	-5.7%	-1.2%	-0.9%	11.8%
Afra-max(245m)	0.9%	0.7%	-6.9%	-1.1%	-0.8%	10.8%
Suez-Max(285m)	0.9%	0.7%	-6.2%	-1.1%	-0.8%	11.0%
VLCC(330m)	1.0%	0.7%	-7.2%	-1.2%	-0.9%	10.0%
ULCC(415m)	1.0%	0.7%	-7.1%	-1.3%	-0.9%	9.9%
Ship runway limits[ft]	**aspect ratio + 0.3**			**aspect ratio - 0.3**		
	ship	**island**	**take-off distance**	**ship**	**island**	**take-off distance**

continued on next page

continued from previous page

Coastal (205m)	2.8%	1.2%	12.5%	-3.0%	-1.4%	-11.6%
Afra-max(245m)	2.7%	1.2%	12.9%	-2.9%	-1.3%	-10.4%
Suez-Max(285m)	2.8%	1.3%	9.2%	-3.1%	-1.4%	-9.0%
VLCC(330m)	3.1%	1.4%	8.0%	-3.4%	-1.5%	-8.2%
ULCC(415m)	3.4%	1.5%	8.5%	-3.9%	-1.7%	-6.7%
Ship runway limits[ft]	**sweep ratio + 1 deg**			**sweep ratio -> 0 deg**		
	ship	**island**	**take-off distance**	**ship**	**island**	**take-off distance**
Coastal (205m)	0.0%	0.0%	0.6%	0.0%	0.0%	0.0%
Afra-max(245m)	0.0%	0.0%	0.0%	0.0%	0.0%	0.0%
Suez-Max(285m)	0.0%	0.0%	0.5%	0.0%	0.0%	0.0%
VLCC(330m)	0.0%	0.0%	0.0%	0.0%	0.0%	0.0%
ULCC(415m)	0.0%	0.0%	0.3%	0.0%	0.0%	0.0%
Ship runway limits[ft]	**max take-off weight + 1000lb**			**max take-off weight - 1000lb**		
	ship	**island**	**take-off distance**	**ship**	**island**	**take-off distance**
Coastal (205m)	1.4%	1.1%	8.4%	-1.4%	-1.1%	-3.5%
Afra-max(245m)	1.3%	1.1%	5.9%	-1.3%	-1.1%	-3.5%
Suez-Max(285m)	1.3%	1.0%	5.1%	-1.3%	-1.0%	-2.1%
VLCC(330m)	1.2%	1.0%	3.6%	-1.2%	-1.0%	-2.3%
ULCC(415m)	1.1%	0.9%	2.9%	-1.1%	-0.9%	-1.2%

As shown in the table, the take-off distance is sensitive to the perturbation of the design variables, while refueling capacities are more robust to the perturbation. This characteristic will impose a significant challenge on the construction of tanker aircraft, since a small manufacturing misalignment will result in a large change in the

aircraft's naval take-off and landing performance.

To overcome this drawback, we update our tanker design by increasing by 3ft the tanker aircraft's wing-span, as shown in Table 7.10. By increasing the wing span of the aircraft, we shifted the variation of takeoff distance to a safer area: the takeoff distance of the tanker will not exceed the runway limit, and the change in refueling capacity will not exceed 4.5% under the same kind of sensitivity test. In this way, we make our design both optimized and more robust. Table 7.11 shows the sensitivity study of the updated tanker aircraft design with larger wing span.

Table 7.10: The optimal design of tanker aircraft (Updated)

Ship runway limits [ft]	**Wing span[ft]**	**thr to weight ratio [-]**	**aspect ratio [-]**	**sweep angle [deg]**	**max takeoff weight [lb]**	$W_{capacity} - W_{consume}$ **@ island [lb]**	$W_{capacity} - W_{consume}$ **@ships [lb]**	**Naval take-off distance[m]**
205	135.0	0.35	7.60	0.00	124,379	27,357	38,094	167
245	135.0	0.35	7.53	0.00	128,209	28,703	39,624	206
285	135.0	0.35	7.18	0.00	134,310	30,074	41,588	246
330	135.0	0.35	6.67	0.00	142,826	31,691	44,151	291
415	135.0	0.35	6.01	0.01	158,304	35,098	49,114	374

Table 7.11: The sensitivity study of tanker aircraft (Updated)

Ship runway limits[m]	**wing-span + 2ft**			**wing-span - 2ft**		
	ship	**island**	**take-off distance**	**ship**	**island**	**take-off distance**
Coastal tanker(205m)	-2.1%	-0.9%	144m	2.0%	0.9%	193m
Afra-max(245m)	-2.0%	-0.9%	181m	1.9%	0.9%	233m
Suez-Max(285m)	-2.0%	-0.9%	221m	1.9%	0.9%	273m
VLCC(330m)	-2.0%	-0.9%	266m	1.9%	0.9%	318m

continued on next page

continued from previous page

ULCC(415m)	-2.0%	-0.9%	349m	1.9%	0.9%	402m
Ship runway limits[m]	**thr 2 weight ratio + 0.02**			**thr 2 weight ratio - 0.02**		
	ship	**island**	**take-off distance**	**ship**	**island**	**take-off distance**
Coastal tanker(205m)	1.1%	0.8%	158m	-1.4%	-1.0%	188m
Afra-max(245m)	1.0%	0.7%	193m	-1.3%	-0.9%	230m
Suez-Max(285m)	1.0%	0.8%	230m	-1.3%	-0.9%	273m
VLCC(330m)	1.1%	0.8%	271m	-1.4%	-1.0%	323m
ULCC(415m)	1.1%	0.8%	348m	-1.4%	-1.0%	413m
Ship runway limits[m]	**aspect ratio + 0.3**			**aspect ratio - 0.3**		
	ship	**island**	**take-off distance**	**ship**	**island**	**take-off distance**
Coastal tanker(205m)	3.0%	1.3%	190m	-3.3%	-1.5%	144m
Afra-max(245m)	2.9%	1.3%	230m	-3.2%	-1.4%	183m
Suez-Max(285m)	3.1%	1.4%	272m	-3.4%	-1.5%	221m
VLCC(330m)	3.4%	1.5%	318m	-3.8%	-1.7%	266m
ULCC(415m)	3.8%	1.7%	408m	-4.3%	-1.9%	347m
Ship runway limits[m]	**sweep ratio + 1 deg**			**sweep ratio -> 0 deg**		
	ship	**island**	**take-off distance**	**ship**	**island**	**take-off distance**
Coastal tanker(205m)	1.0%	0.5%	180m	1.0%	0.5%	180m
Afra-max(245m)	1.0%	0.4%	220m	1.0%	0.4%	220m
Suez-Max(285m)	1.0%	0.4%	259m	1.0%	0.4%	259m
VLCC(330m)	1.0%	0.4%	304m	1.0%	0.4%	304m
ULCC(415m)	1.0%	0.4%	388m	1.0%	0.4%	388m
Ship runway limits[m]	**max take-off weight + 1000lb**			**max take-off weight - 1000lb**		
	ship	**island**	**take-off distance**	**ship**	**island**	**take-off distance**

continued on next page

continued from previous page

Coastal tanker(205m)	1.5%	1.1%	184m	-1.5%	-1.1%	160m
Afra-max(245m)	1.4%	1.1%	222m	-1.4%	-1.1%	199m
Suez-Max(285m)	1.3%	1.0%	260m	-1.3%	-1.0%	240m
VLCC(330m)	1.3%	1.0%	304m	-1.3%	-1.0%	285m
ULCC(415m)	1.1%	0.9%	386m	-1.1%	-0.9%	369m

7.8 Chapter Summary

In this chapter, we introduce the design optimization of FARS based on the models defined in the previous chapters. We have adopted a distributed optimization strategy to optimize the tanker, mother ship and refueling strategies step by step. The optimization is based on one reference flight route of the receiver aircraft. The optimal FARS design can save up to 20% of the total fuel consumption.

The optimization in this chapter is based on one single objective: maximum fuel savings. However, single-objective optimization may not be realistic: first, the FARS design optimized for maximizing fuel saved may not be economically feasible; second, the optimization is based on a single flight route, so it may not be robust enough for broader operations. Therefore, the optimization strategy described in this chapter will be further improved along with economic analysis and case studies in subsequent chapters.

Chapter 8

FARS Economic Analysis

8.1 Overview

As a civilian project that requires a significant upfront investment, economic feasibility analysis is critical to the FARS design. There are trade-offs between the fuel saving performance and economic feasibility of FARS. For example, in the refueling strategy part of the design, the more refuelings per receiver, the higher the total fuel savings per operation. However, due to the reduced non-linearity linked to the Breguet equation, the increase in the number of refuelings per receiver will also result in a reduction in the unit fuel savings rate, thereby decreasing the unit revenue of each operation. Therefore, the optimal design of FARS shall be a balance between fuel performance and economic feasibility depending on the preference of the stakeholders.

The financial analysis is all about revenues and costs. The operation of FARS is not an exception. The revenue of FARS mainly comes from the jet fuel saved from the receiver airplanes' operations and extra seats that can be provided due to the receivers' weight reduction. In a multi-stakeholder world the airlines would pay the FARS operator(s) for each successful mid-air refueling operation. The cost of FARS comes from the construction and operation of the elements of the FARS system. In addition, the capital has its own cost due to the inflation rate and loan interest rate. In this study, we consider FARS as an economically viable system when it is profitable considering revenues, costs and interests.

There are two different views on evaluating the economic viability of FARS, depending on the preference of stakeholders:

1. V1: We take financial income as a priority. In this strategy, we will maximize the capital returns of the FARS system while meeting the minimum emissions reduction goal.

2. V2: We view financial benefits as a constraint. In this strategy, while meeting the minimum financial requirements, we will minimize aircraft emissions through the FARS system.

In order to merge these two perspectives, we evaluated the economic feasibility of FARS as follows. First, we calculated all possible FARS design configurations as shown in prior chapters. For each design configuration, we calculate two utilities: financial benefits and fuel saved. The financial benefits are represented by the net present value (NPV) of the FARS system with given discount factors. The discount factor shall reflect the minimum expectation of FARS's profitability. Any design with a negative NPV means that we have to pay extra money for reducing emission, while a positive NPV means we can profit from saving fuels. With the NPV and total fuel savings calculated, we present the utilities of all viable designs into one tradespace and determine all non-dominated design cases using the Pareto front analysis method. The non-dominated designs on the Pareto front represent the optimal designs for different preferences of stakeholders.

In this study, we only enumerate the different configurations of ship sizes and refueling strategies. The tanker optimal design is already pre-determined for different ship sizes and will not be re-calculated when evaluating FARS's financial feasibility. This arrangement can be justified for two reasons. First, the objective function used in tanker aircraft design optimization is the difference between tanker refueling capacity and fuel consumption. Therefore, the design optimization of tanker aircraft has already reflected the optimization between economic benefits and emission reductions. In addition, as mentioned earlier, the difference in FARS capacity can be reflected by selecting the ship type, and recalculating the optimization of the tanker aircraft

which is less valuable and time-consuming. Second, the fuel savings and economic feasibility are sensitive to the fueling strategy and the type of receiver aircraft. However, the design of the tankers should be robust and independent of receiver aircraft fleets (of course the refueling receptacle has to be compatible). Therefore, we decided to exclude the physical design of the tanker aircraft as a free variable in the economic analysis. On the contrary, as mentioned in the previous chapter, the optimal design of the tanker aircraft depends on the size of the mother ship. Therefore choosing a mother ship architecture also implicitely selects the corresponding optimal tanker aircraft design.

We assume a discount rate of 6.5% for FARS's NPV analysis, which is consistent with the discount rate for commercial aircraft leasing projects proposed by D. Kelly[27]. As argued by D. Kelly[27], this rate is at a 1.8% premium compared to the corporate BBB yield of 4.7% as measured by Deutsche Bank or Bank of America Merrill Lynch and compares to a 10-year U.S. treasury yield of 3.0%. The corporate tax rate on profits is assumed to be 35% .

First, we will introduce the revenue and cost of FARS, respectively. Second, we will present the economic analysis of different benchmark flights to explore trade-offs between FARS's performance and cost. Finally, we present several conclusions from the trade-off study and a recommended final design.

8.2 Revenue Estimation

The revenues generated by FARS mainly come from the jet fuel saved from the receiver aircraft and extra seats or cargo of receivers due to weight reduction of not having to take off with a full fuel load at the airport of origin. To be conservative, we ignore the revenue of receivers due to weight reduction in this study.

The saved jet fuel can generate revenue in two ways: market price and carbon tax.

First, the saved jet fuel can generate revenue directly from its equivalent market price. Figure 8-1 shows the spot price of Kerosene-Type Jet Fuel (e.g. Jet A, Jet

A-1) from 1990 to 2018[42]. As shown in the figure, the spot price of jet fuel is highly fluctuating, but quasi stationary in long term. Therefore, we assume that the spot price used in this study equals to $ 2.2. per gallon, an average price from 2016 to 2018. (Note: this does not include price reductions or fluctuations that may be caused by the global COVID-19 crisis).

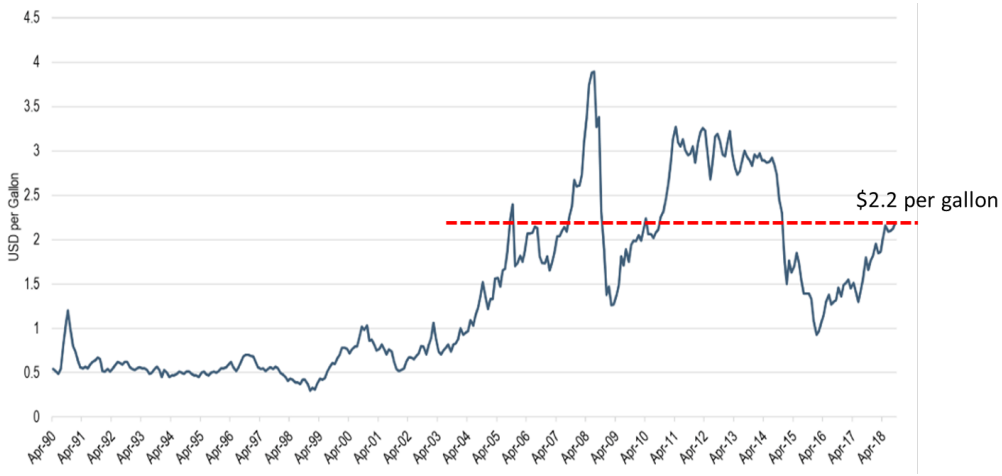

Figure 8-1: U.S. Gulf Coast Kerosene-Type Jet Fuel Spot Price FOB

Second, the savings in jet fuel can avoid (current or future) carbon taxes, thereby reducing airline costs and generating more revenue. A carbon tax is a pollution tax. It charges fees for the production, distribution, or use of fossil fuels based on the amount of carbon produced by combustion. The government sets the price per ton of carbon and then converts it to an aviation fuel tax. According to the World Bank[40], the explicit price of carbon needs to be at least in the range of $ 40-$ 80 per mt CO2 by 2020, $ 50-$100 per ton of CO2 by 2030 to meet the Paris Agreement. The international panel on climate change(IPCC) report[40] provides a more progressive price: US$ 130-6,050/tCO2e in 2030, US$ 690-30,100/tCO2 in 2100 to keep peak temperatures below 1.5 degree in the 21st century with 50-66% probability. In order to meet the requirements of the Paris Agreement, in our research, we assume that the carbon tax for the first year of FARS operations is US $ 50 per metric ton of carbon dioxide, and the annual growth rate in the carbon tax is 2.2%. This carbon tax level is consistent with current carbon taxes in countries such as France and Finland but

lower than the carbon tax of Switzerland (the highest in the world).

Therefore, the revenue R generated by FARS can be expressed as,

$$R = \frac{W_{fuel}}{\rho} * \frac{\$2.2}{gallon} + \frac{W_{fuel}}{\rho} e_{co_2} * \frac{\$50\,(1+2.2\%)^{year}}{2205\frac{lb}{ton}}$$

Where W_{fuel} is the weight of the total amount of fuel saved. ρ is the density of jet fuel, e.g 6.71 lb/US gal. e_{co_2} is the amount of CO_2 [lb] generated by jet fuel per unit. According to EIA, e_{co_2} = 21.1 lb/gallon. Thus, the first part of the revenue comes from saving on fuel expenditures and the second part comes from avoiding carbon taxes.

8.3 Cost Estimation

The cost estimation of FARS is more difficult. FARS is an innovative system and thus does not have similar civilian systems to compare to. In the military domain, FARS is similar to aircraft carrier systems. However, aircraft carriers are not a good reference for financial analysis. First, the cost breakdown of aircraft carriers is confidential, so we cannot know its cost structure exactly. For example, there is no public reference describing the cost structure of an aircraft steam catapult or arresting system. Second, the cost of military systems is usually much higher than similar civilian systems, because military products have more stringent and special requirements than civilian products, and the defense sector has no strong price pressure. For example, a Nimitz-class aircraft carrier costs $ 8.5 billion in FY 12 dollars, while the Ultra Large Crude Carrier (ULCC) Seaways Laura Lynn, which is much bigger than a Nimitz-class aircraft, is priced at 'only' $ 32.5 million[18]. Therefore, in this study, we estimate the cost structure of FARS based on comparable components and reasonable estimations.

In this study, we did not include the initial R & D costs of aircraft and systems, because we believe that the initial R & D costs will be depreciated due to the mass production of FARS products, government sponsorship, and a long time span of operations.

Therefore, the cost structure of FARS consists of:

1. Capital expenditures (CapEx) for tanker aircraft, which occurs at year 0
2. Capital expenditures (CapEx) for mother ship, which occurs at year 0
3. Operating expenditures (OpEx) of tanker aircraft, which occurs from year 1 to the end of life-span(e.g. year 25).
4. Operating expenditures (OpEx) of the mother ship, which occurs from year 1 to the end of life-span(e.g. year 25).

We do not calculate any operating costs for the base island and consider those to be out-of-scope.

8.3.1 Cost estimation of tanker aircraft

To begin with, we will estimate the CapEx of tanker aircraft. According to Roskam[43], the price of a commercial jet with take-off weight between 60,000 lb and 1,000,000 lb can be expressed as,

$$AMP_{1989} = 10^{3.3191+0.8043 \log W_{TO}} \tag{8.1}$$

Where AMP_{1989} is the price of aircraft in 1989 US dollar. W_{TO} is the take-off weight of the aircraft.

To estimate the aircraft price in 2020, we applied an adjustment factor of 2.08 due to the declined purchase power due to inflation. The adjustment factor is determined based on the U.S. CPI data from 1989 to 2020.

Therefore, the Capex of the tanker aircraft C_{tanker} is estimated as,

$$C_{tanker} = 2.08 * 10^{3.3191+0.8043 \log W_{TO}} \tag{8.2}$$

The Opex of tanker aircraft is estimated based on the guidance of FAA[20]. Figure 8-2 shows the recommended operating and fixed costs of different categories of aircraft by FAA (in 2003 USD)

In this study, we assume our cost structure is aligned with FAA's recommended cost structure for turbofan aircraft above 65,000 lb with an inflation correction factor of 1.4 (2003- 2020). There are three modifications in the Opex estimation. The first difference is that we will reduce the cost of crews ($ 200 per hour) as the tanker aircraft will be autonomous. The second difference is that we will use the depreciation directly calculated from our Capex, rather than the number cited by the FAA (see column 7 in the table below). The number of operational hours will be adjusted to the real operational hours of the FARS refueling operation. The fuel consumption of tanker aircraft has accounted for fuel savings from refueling and thus it is irrelevant here.

			1	2	3	4	5	6	7	8
	Economic Values Category	Certification	Crew	Fuel & Oil	Maintenance	Variable Operating Costs (Including Crew)	Variable Operating Costs (Excluding Crew)	Annual Fixed Cost Other (Without Depreciation)	Annual Depreciation	Fixed Cost Per Hour
1	Piston Engine Airplanes 1 to 3 seats (<=200hp)	Part 23	$45	$12	$30	$87	$42	$2,251	$1,338	$34
2	Piston Engine Airplanes 1 to 3 seats (>200hp)	Part 23	$45	$42	$56	$143	$98	$21,147	$4,855	$215
3	Piston Engine Airplanes 4 to 9 seats One-Engine (<=200hp)	Part 23	$45	$30	$40	$116	$71	$15,198	$2,897	$139
4	Piston Engine Airplanes 4 to 9 Seats One-Engine (>200hp)	Part 23	$45	$43	$61	$150	$105	$20,024	$6,310	$235
5	Piston Engine Airplanes 4 to 9 Seats Multi-Engine	Part 23	$45	$94	$118	$257	$212	$27,761	$8,770	$256
6	Piston Engine Airplanes 10 or more Seats	Part 23	$112	$118	$141	$372	$259	$32,130	$8,816	$107
7	Turboprop Airplanes 1 to 9 seats One-Engine	Part 23	$181	$139	$142	$462	$281	$83,021	$59,166	$340
8	Turboprop Airplanes 1 to 9 seats Multi-Engine	Part 23	$238	$214	$410	$862	$623	$65,408	$36,501	$479
9	Turboprop Airplanes 10 to 19 seats	Part 23	$244	$271	$396	$911	$667	$86,486	$65,555	$543
10	Turboprop Airplanes 20 or more seats	Part 25	$433	$323	$357	$1,113	$681	$92,475	$56,876	$532
11	Turbojet/Turbofan Airplanes <=12,500 lbs	Part 23/25	$475	$445	$433	$1,353	$878	$139,144	$167,669	$1,058
12	Turbojet/Turbofan Airplanes >12,500 lbs and <=65,000 lbs	Part 25	$559	$631	$677	$1,868	$1,309	$325,350	$324,828	$1,737
13	Turbojet/Turbofan Airplanes >65,000 lbs	Part 25	$713	$1,217	$807	$2,737	$2,024	$473,248	$978,930	$3,419
14	Rotorcraft Piston <=6,000 lbs	Part 27	$45	$34	$97	$176	$131	$78,113	$7,936	$381
15	Rotorcraft Turbine <=6,000 lbs	Part 27	$188	$94	$259	$539	$353	$159,656	$35,783	$561
16	Rotorcraft Piston >6,000 lbs	Part 29	NR	NR	NR	NR	NR	NR	NR	NR
17	Rotorcraft Turbine >6,000 lbs	Part 29	$233	$231	$596	$1,060	$827	$254,891	$94,957	$1,075
18	Other	NR	NR	NR	NR	NR	NR	NR	NR	NR
All Aircraft			**$109**	**$114**	**$138**	**$362**	**$253**	**$54,587**	**$46,503**	**$728**

Sources of cost data: GRA analysis of 2002 GA Survey and 1) Conklin and de Decker, Aircraft Cost Evaluator, Spring 2003; 2) http://www.planequest.com/; 3)Aircraft Bluebook, Summer 2003; 4) Ai Guidelines 2002-2003; 5) GRA estimate of aircraft prices.
Note: Class 8 Turboprops also included Cessna 421 which is a piston aircraft. For this reason we have not included this aircraft type in our calculations. Class 11 Turbojets also included PC-12 whi reason we have not included this aircraft type in our calculations.
NR = Not Reported
Col 1: Crew: for GRA groups 1-5, 14 and 16, crew cost = value of time = $45 and assumes a single pilot; for other categories, crew cost includes salaries and benefits reported by Conklin and de De flight hours (based on 2002 NBAA salary survey, p. 136).
Col 2: Fuel, oil and additives used per hour, with fuel at $2.51 per gallon for pistons and $2.41 per gallon for all other economic values groups.
Col 3: Total Maintenance cost, including labor, parts, engine allowances, propeller/thrust reverser overhaul, and APU overhaul* if applicable.
Col 4: Variable Operating Cost Total. Addition of columns 1, 2 and 3.
Col 5: Maintenance and Fuel only (Column 2 plus Column 3).
Col 6: Annual fixed cost including hangar cost, insurance cost, training cost, services* typically used by air taxi and commercial operators (e.g., Weather service, maintenance programs, etc.).
Col 7: Average annual aircraft depreciation assuming that aircraft retain 95% of their value from year to year.
Col 8: Fixed Cost per hour, assuming hours of utilization reported in Column 10 = (Column 6 + Column 7)/Column 10.
Col 9: Total Cost per Hour: Column 4 plus Column 8.
Col 10: Average (weighted) hours of utilization for each economic values group for all aircraft with both operating cost data and price data used in calculating annual depreciation.
* Conklin and de Decker only

Figure 8-2: Snapshot of operating cost estimation for various aircraft from Ref[20]

Thus, the variable Opex of tanker aircraft is estimated as,

$$O_{tanker} \approx (\$200 + \$807 + \$2024) * 1.4 * T_{op} \tag{8.3}$$

Where T_{op} is the tanker's operating time, depending on the service range and cruise speed of tanker aircraft In the future a more refined cost model for tankers can

be developed that is more sensitive to tanker design variables.

Besides the variable Opex, the annual fixed Opex of tanker aircraft is estimated as $ 473,248 ∗ 1.4

per aircraft in the tanker fleet.

8.3.2 Cost estimation of mother ship

As discussed earlier, we will convert second-hand oil tankers to mother ships. Therefore, the Capex of a mother ship is estimated based on the price of oil tankers and their associated conversion fee.

As a common practice, the price of a second hand oil tanker is estimated based on its deadweight tonnage. The deadweight tonnage (DWT) is a measurement of how much an oil tanker can carry. To estimate the relationship between price and DWT, we extract actual sales information from Horizon Ship Brokers and apply a regression analysis between the DWT and price of oil tankers, as shown in Figure 8-3.

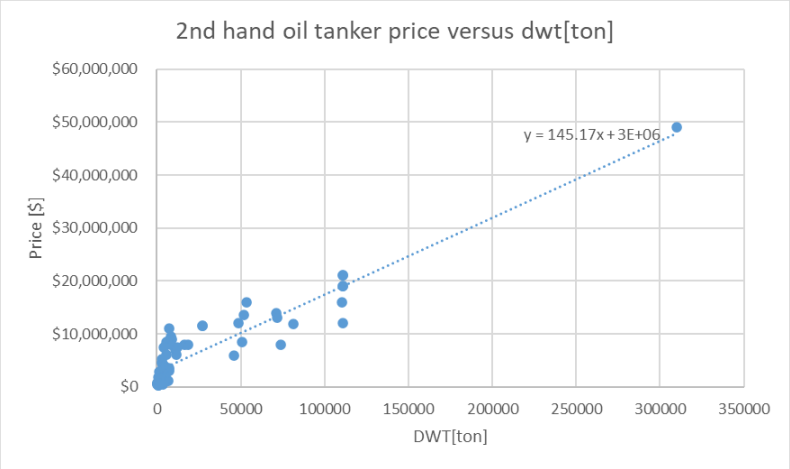

Figure 8-3: The price versus displacement in DWT[ton] of second hand oil tankers [extracted from Horizon Ship Brokers access: February 2020]

The DWT of the mother ship can also be estimated from an unbiased linear relationship between DWT and ship's geometry (length ∗ width ∗ draft). The data shows the regression factor $R^2$is 0.48. Therefore, for the mother ship design, we can estimate DWT and price as:

Class	Length	Beam	Draft	Est. DWT [ton]	Est. price [$]
Coastal Tanker	205	29	16	46,772	9,952,671
Aframax	245	34	20	80,000	14,892,000
Suezmax	285	45	23	141,645	24,055,478
VLCC	330	55	28	244,034	39,275,597
ULCC	415	63	35	439,412	68,318,559

It is interesting to note that a single second hand oil tanker may be cheaper to acquire than a single new long-range receiver commercial aircraft from a manufacturer like Boeing or Airbus. With the price of 2$^{\text{nd}}$ hand oil tankers estimated, the next task is to estimate the conversion cost. We estimate the conversion cost based on the reference to FPSOs in linear form, expressed as

$$c_{converison} = \alpha c_{oiltanker} + \beta \tag{8.4}$$

Where α is the coefficient proportional to the oil tanker cost (such as hull modification, runway) and β is the coefficient for the fixed cost such as adding an aircraft catapult system and arresting gear.

To estimate the conversion cost, we use the conversion cost of FPSOs as a reference. First, the FPSO have similar mooring systems and conversion process as FARS, therefore the cost is comparable to the hull modification. Second, the conversion cost of FPSOs includes the installation of fixed cost facilities such as oil processing units. This is similar to the installation of catapult and arresting system in the mother ship. S. McClure et al. estimated that the FPSO conversion cost per unit in 1993 was $ 26 million ($ 46.54 million in 2020). Therefore, we assume $\beta = \$46.54 million$.

There is no good reference for estimating α . We assume α is 1.3 first in this study based on industry common practice. This assumption can be refined in future work.

Therefore, considering different factors, the Capex for different ship sizes are estimated as shown in Table 8.1.

Table 8.1: Capex of mother ship based on Oil Tanker conversion

Ship Size	**Capex [million$]**
Coastal	58.89
Aframax	65.36
Suezmax	76.99
VLCC	96.31
ULCC	133.18

The Opex for the mother ship is assumed to be identical to the Opex of an FPSO. H. Kruniawati et al[29] conducted a survey on the operating costs of FPSOs and suggested that the annual operating expenses of a typical FPSO in 2016 be U.S. $ 982,000 ($ 1.04 million in 2020), as shown in Table 8.2.

Table 8.2: Cost breakdown of FPSO's annual Opex[29]

Crew	$ 201,196
Maintenance & Repairs	$ 100,000
Admin and charges	$ 25,000
Lub Oil	$ 6,000
Insurance	$ 600,000
Provision and stores	$ 50,000
Total	$ 982,196

8.3.3 Depreciation

In this study, we assume that the Capex of the mother ship and tanker aircraft is depreciated into the life cycle of 25 year. The depreciation each year is assumed to be equal in terms of absolute USD value per year.

8.4 Chapter Summary

In this chapter, we introduce the economic analysis method of FARS. Economic analysis includes two parts: cost and revenue. Revenues mainly come from jet fuel savings from refueling operations, including jet aircraft spot costs and carbon taxes. These costs take into account the capital and operating costs of tankers and mother ships. The estimate is based on relative guidances and observations of historical data. In next chapter, we will apply the FARS economic analysis method together with FARS architectural design to several practical flight cases.

Chapter 9

Case Studies and Conclusion

In this final chapter we apply the FARS concept to a number of real world situations and evaluate the outcomes. The real world situations correspond to actual long range flights by potential receiver aircraft that are on the market today. We conclude the chapter by summarizing our findings and making recommendations for future work.

9.1 Benchmark Flights

In order to understand the potential impact of FARS on the real world, we selected several long-distance cross-continental flights as our analysis benchmark[58], as shown in Table 9.1. All the flights shown here are transcontinental flights across significant stretches of open ocean. The model of the receiving aircraft is based on the specifications of commercial aircraft, as shown in Table 9.2. The benchmark flights cover the longest and some very long transcontinental flights.

These long-haul flights do not represent FARS 'maximum fuel-saving capabilities. According to the Breguet range equation, the cost of jet fuel depends not only on the range, but also on the specifications of the commercial aircraft, such as the maximum lift-to-drag ratio, aircraft weight and SFC. The aircraft used in these benchmark flights (Airbus A350, Boeing 777/787) are highly optimized and represent the current state of the art. Through FARS, shorter flights using less optimized (or older) and cheaper aircraft (such as Boeing's 767) may save more fuel than our baseline flights

here.

In addition, the long-haul flights are highly concentrated as several airports such as Singapore Changi Airport, Dubai International Airport, Newark Liberty International Airport and Hong Kong International Airport. Therefore, it is feasible for one tanker aircraft to refuel multiple receiver aircraft in one operation as long as it is positioned properly along these flight routes.

Table 9.1: Specification of benchmark flights from ref[58]

Case	From	To	Flight	Distance [km]	Aircraft
1	Newark	Singapore	Singapore Airlines SQ 21	15,344	A350-900
2	Los Angeles	Singapore	Singapore Airlines SQ 37, SQ 35	14,114	A350-900
3	Johannesburg	Atlanta	Delta Air Lines DL 201	13,581	777-200LR
4	Toronto	Manila	Philippine Airlines PR 119	13,230	A350-900
50	Dallas/Fort Worth	Hong Kong	American Airlines AA 125	13,072	777-300ER

Table 9.2: The specification of commercial aircraft [52][55][56]

Aircraft	Cruising speed [km/h]	Cruising Altitude [ft]	Max drag to lift ratio [-]	Thrust SFC∗ [lb/hr/lbf]	OEW [lb]	Max Payload [lb]
A350-900	903	35000	21	0.565	314000	243662
777-200LR	892	35000	19.3	0.565	320000	446000
787-9	902	35000	20	0.565	284000	116000

∗ based on Rolls-Royce Trent[60]

9.2 Analysis and Result

In this section, we will first present one particular benchmark case to demonstrate the design and sensitivity study of FARS regarding the trade-off between performance and economic feasibility. Then, we will present the trade-off analysis for all benchmark flights presented in Table 9.1 .

Singapore Airline SQ 21[59] is the longest regularly scheduled non-stop flight in the world. The flight is between Newark Liberty International Airport (EWR) and Singapore Changi Airport (SIN). The flight distance and time is 15,344 km (or 16,600 km SIN-EWR) in about 18 hours. Figure 9-1 shows the flight route of flight SQ21 on a world map. As shown in the figure, the flight path of SQ21 covers both oceans and land. Especially SQ21's route to EWR Airport from Singapore is the best place to deploy FARS.

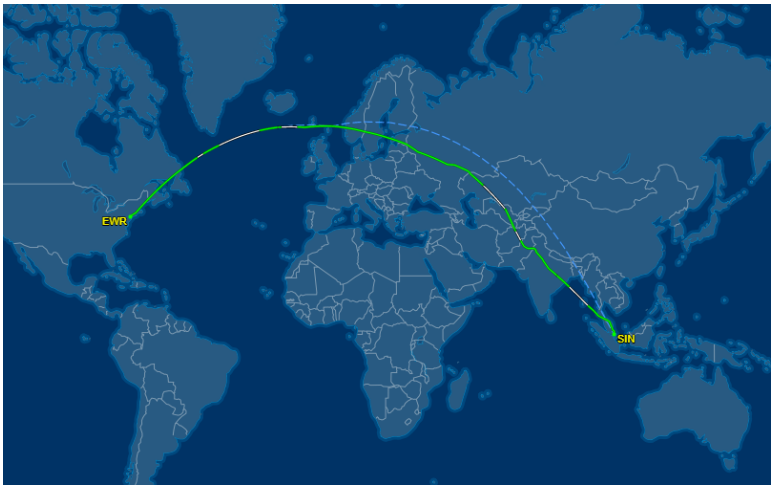

Figure 9-1: The flight route of Singapore Airline SQ21

We simulate all possible designs of FARS and obtain the tradespace plot as shown in Figure 9-2. The Utopia point is the design with higher NPV and higher annual fuel saved (blue star in upper right corner). To make a better comparison, we also include the optimal tanker aircraft with standard runway limit (9000 ft) in the tradespace plot. The optimal tanker aircraft design with standard runway limit does not include the cost of a mother ship. As shown in the table, there is an obvious convex Pareto

frontier of non-dominated design cases. However, none of non-dominated design cases of FARS achieved a positive NPV, while design cases without mother ship showed excellent profitability. Therefore, it can be concluded that aerial refueling from islands is economically feasible, while FARS based on mother ships is not (mainly due to the cost of the maritime infrastructure.

However, as discussed in the earlier chapter, the aerial refueling from land doesn't have the flexibility and mobility as the FARS system. Therefore, the next question is how to improve the profitability of FARS.

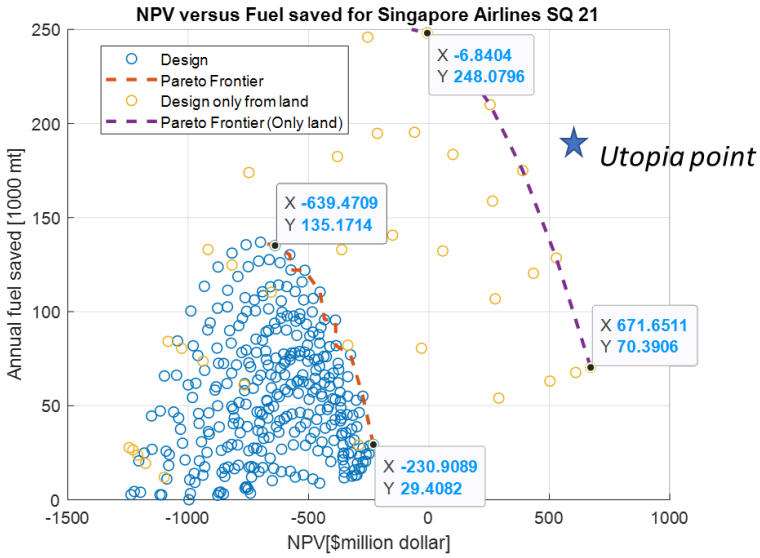

Figure 9-2: NPV versus Annual fuel saved

It is possible to cover the capital and operations costs of mother ship. There are two strategies to achieve it. The first strategy is to increase the number of tankers on one mother ship. To increase the number of tankers does not increase the cost of the mother ship (up to a maximum limit). Therefore, if there are enough tankers on one mother ship, the profits from each tanker can cover the cost of the mother ship. The second strategy is to add more functionality to mother ships. In the mother ship design, we only use the surface area of the ship as an airport and a relatively small portion of its storage capacity for jet fuels. For instance, the storage capacity of a ULCC is above 320,000ton. The monthly fuel consumption of one tanker aircraft only

occupies around 10% of ULCC's storage capacity. Thus, there is enough space in the mother ship for other functionalities. The possible additional functionalities include serving as a refueling center for other ships passing by or as an electrical hub for solar/offshore wind powerplants. Each option may be feasible and profitable enough to cover the capital cost and operating cost of the mother ship.

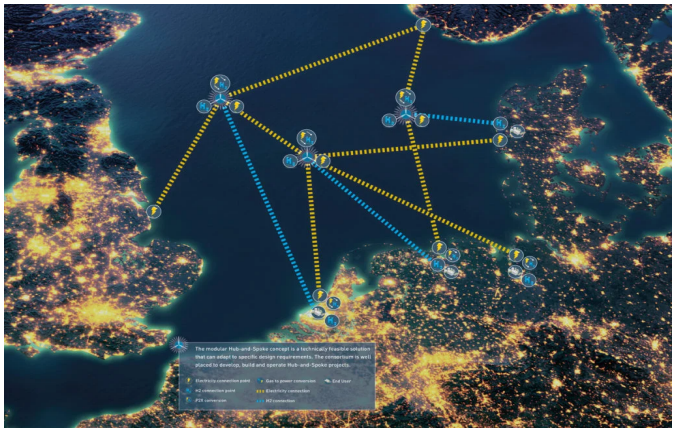

Figure 9-3: A demonstration of offshore wind powerplant hub, from ref[13]

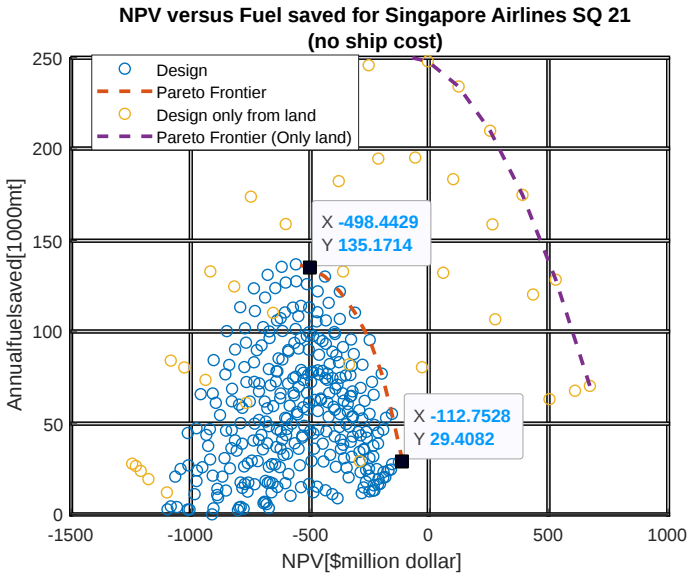

Figure 9-4: NPV versus Annual fuel saved (excluding ship cost)

With strategies to cover the ship cost, it is important to examine the profitability of tankers, because tankers cannot easily be modified for extra functionalities. Therefore,

we will first examine the tradespace of FARS design without ship cost. This moves everything to the right, closer to a positive NPV. Figure 9-4 shows the trade-space of NPV versus annual fuel saved excluding ship cost with flight SQ21 as a reference. As shown in the figure, the financial performance of FARS is significantly improved. However, the NPV of all FARS designs is still negative, indicating that we still need to pay more to cover the cost of reducing aircraft emission (under the assumptions of a $2.2 per gallon price of jet fuel and $50 carbon tax).

We now rearrange the axis of the trade-space plot: We replace the x-axis with the unit cost of fuel saved, as shown in Figure 9-5. As shown, the unit NPV cost of fuel of the optimal FARS design is around $ 0.059/lb - $ 0.1/lb, which is equivalent to a 23% -30% increase in the jet fuel price. This price may be already profitable for some airlines by selling more seats due to the weight reduction of aircraft that don't need to be fully fueled at takeoff. For example ,the design cases labelled in the Figure 9-5 can save 61,000 mt every year, equivalent to 500,000 more seats if we assume each seat and passenger weight is 200 kg (440lbs). In addition, the cash flow analysis in this study is based on a discount rate of 6.5% . Therefore, we can further improve the profitability of FARS if the we can obtain a loan with lower than current interest rate.

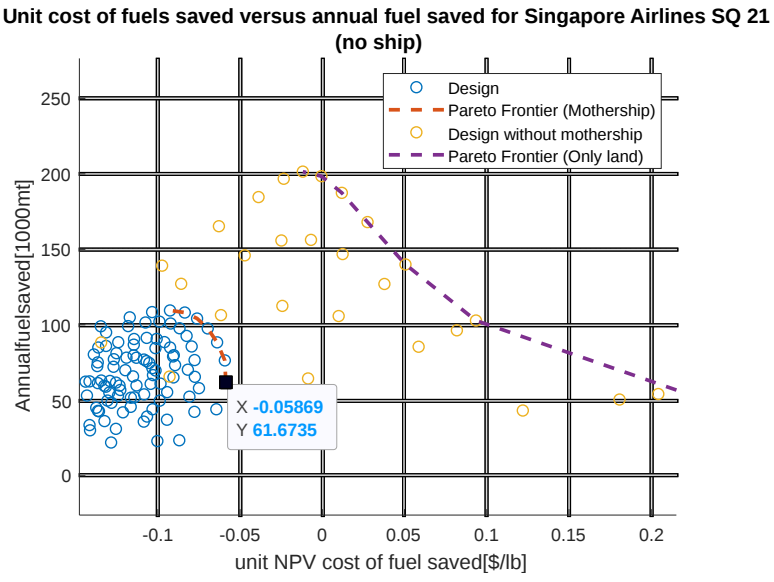

Figure 9-5: Unit cost of fuel saved versus annual fuel saved (excluding fuel cost)

As shown in the previous chapter, the refueling capacities of tankers is sensitive to the FARS's service range. In the current setting, we set the serving range to be 500km. If we reduce the service range, we can further improve the profitability of FARS. Figure 9-6 shows the NPV versus Annual fuel saved for a service range of 400km. As shown, there are already design cases with positive NPV, stating the profitability of FARS system based on jet fuel alone. This shows that careful and strategic placement of the FARS system with respect to the inter-continental flight routes is very important.

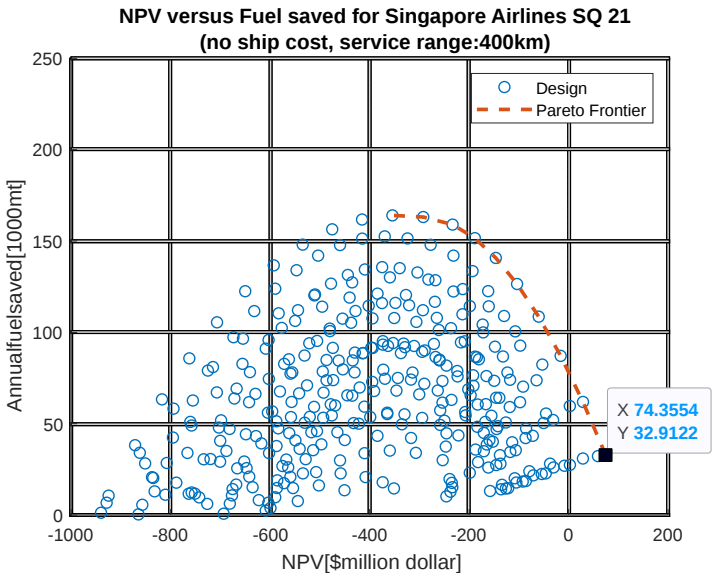

Figure 9-6: NPV versus Annual fuel saved (excluding ship cost, serving range: 400km)

If we further decrease the service range from 400km to 300km, we have a major shift of NPV of designs toward the positive region. Figure 9-7 shows the trade-space of NPV versus annual fuel saved with a service range of 300km. As shown in the table, 60% of design cases on the Pareto front are now showing a positive NPV. However, a service range of 300km may be a challenge for FARS, as reducing service range also will reduce the availability of FARS or may force airlines to choose a sub-optimal trajectory in order to cross the FARS service range.

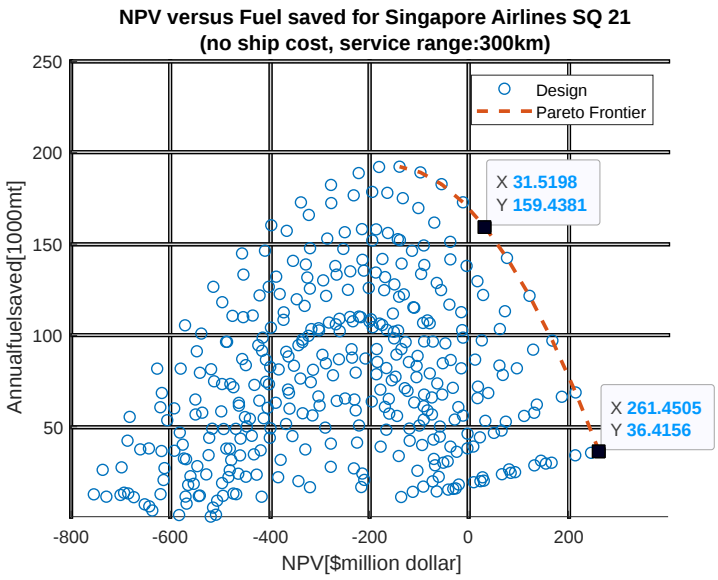

Figure 9-7: NPV versus Annual fuel saved (excluding ship cost, serving range: 300km)

By further improving the aerodynamic characteristics of the tanker aircraft, the same benefits of reducing the scope of FARS services can also be obtained. In our research, the airplane wing is assumed to be a uniform wing, and the optimization is based on a simple geometric arrangement. The max lift to drag ratio of our optimal tanker aircraft is around 15, while the studies show the max lift to drag ratio of aircraft can be further optimized to around 21 using more complex optimization methods[28]. Such an improvement of aircraft aerodynamics is equivalent to reducing service range from 500km to 350km (or from 400km to 286km), which makes most of FARS design cases profitable.

In addition, we can further improve the weight efficiency of tanker aircraft. First of all, in our research, the weight estimation of tankers is based on regression analysis of historical data, which is based on aircraft designed in the last century, not specifically designed for jet tankers. Second, since the tanker aircraft is designed as a drone, it should not include the weight of the crew and the cockpit. Research shows that if the F-111F is switched to a drone, the F-111F can reduce its empty weight by 3000 pounds[34]. The weight of 3000 pounds is 5% -6% of the FARS tanker's empty weight. Kenway et al[28] also show that the weight of modern aircraft can easily be reduced by

10% using advanced optimization approaches and an increase in composite materials. Therefore, if we assume that the no-load weight of the aircraft is reduced by 10% , the net present value of the design will be positive, even at a 500 km service range, as shown in Figure 9-8.

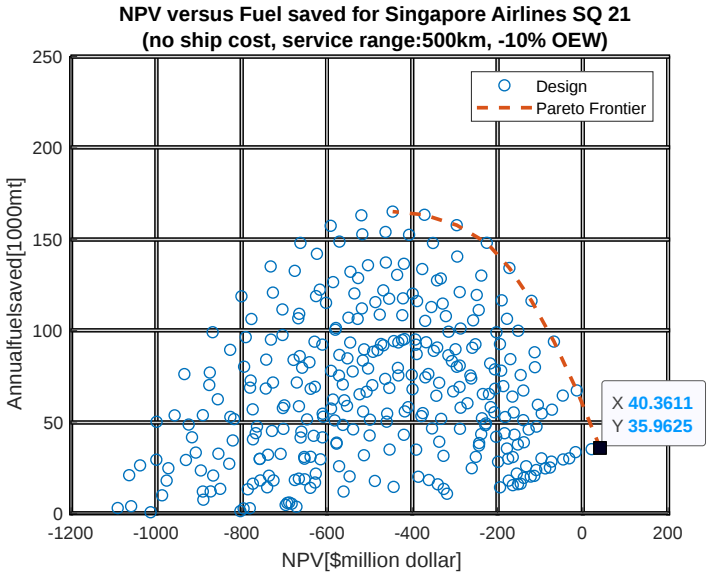

Figure 9-8: NPV versus annual fuel saved with 10% reduction on aircraft's OEW.

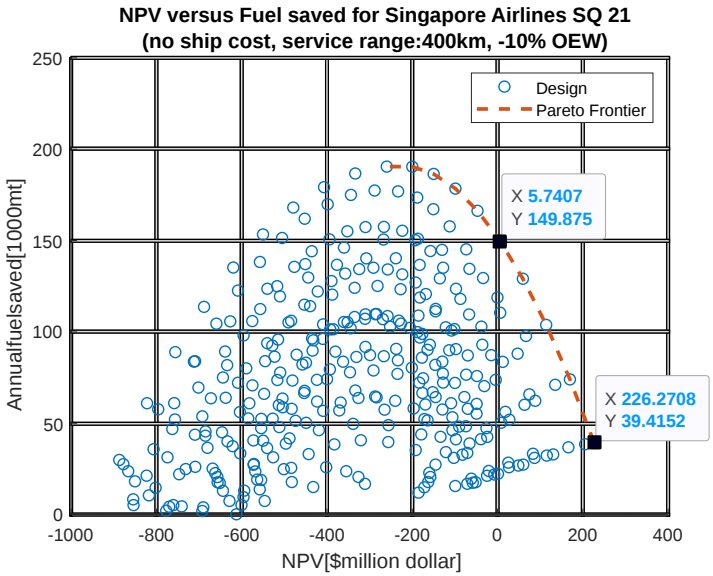

Figure 9-9: NPV versus annual fuel saved with 10% reduction on aircraft's OEW and service range of 400km.

Combined with a reasonable reduction of service range (400 km), we can shift the majority of non-dominated designs toward the positive NPV region, as shown in Figure 9-9. The maximum positive NPV that FARS can achieve using our revised assumptions is USD 226 million, while the maximum fuel savings that can be achieved at zero NPV is 149,875 mt per year.

Table 9.3: The profitable FARS designs with maximize NPV for different benchmark cases

#	Flight	ship size	refueling per tanker	refueling per receiver	NPV value [million USD]	Annual fuel saved [1000mt]
1	Singapore Airlines SQ 21	ULCC	5	1	226	39
2	Singapore Airlines SQ 37, SQ 35	ULCC	5	1	138	35
3	Delta Air Lines DL 201	ULCC	5	1	128	34
4	Philippine Airlines PR 119	ULCC	5	1	88	32
5	American Airlines AA 125	ULCC	5	1	70	32

Therefore, the FARS system may be economically feasible if we reduce the service range from 500 km to 400 km and achieve a 10% reduction of tankers' OEW. To extend this conclusion to all benchmark cases, we have analyzed the profitable designs which maximize NPV and the profitable designs with maximum emissions reduction, as shown in Table 9.3 and Table 9.4. As shown the design with maximum NPV is the same for all benchmark cases, while the design with maximize emission reduction is highly influenced by the particular flights of the receiver aircraft. This is an important conclusion.

Therefore, we recommend the design selection criteria should be the design with maximum NPV, while at the same time maintaining a positive emission reduction, which is robust to different types of intercontinental flights. Such an architecture would not to be externally subsidized but could be self-sustaining. One advantage

of the maximum NPV FARS architecture from an operational perspective is that it only requires one mid-air refueling per flight.

Table 9.4: The profitable FARS designs with maximize emission reduction for different benchmark cases

#	Flight	ship size	refueling per tanker	refueling per receiver	NPV value [million USD]	Annual fuel saved [1000mt]
1	Singapore Airlines SQ 21	ULCC	5	5	5.7	150
2	Singapore Airlines SQ 37, SQ 35	ULCC	5	3	25	89
3	Delta Air Lines DL 201	ULCC	5	4	4	115
4	Philippine Airlines PR 119	ULCC	5	3	6	87
5	American Airlines AA 125	ULCC	5	2	29	60

9.3 Thesis Summary and Recommendation

To sum up, the analysis of benchmark flights has pointed us towards several major updates of FARS in order to be economically feasible:

1. The design selection criteria shall be the design with maximum NPV in order to obtain a robust design

2. The refueling from land is more profitable than the refueling from a mother ship given same service range. However, due to the lack of facilities of FARS's deployment, the deployment of refueling on land shall be further examined. FARS may lead to the revival of several island-based or peripheral airports that were used in the 1950s and 1960s when aircraft did not have full intercontinental range. An example would be the Azores in the mid-Atlantic, or Iceland or Greenland for North Atlantic flights.

3. A reduction of service range from 500km to 400km has the potential to significantly improve the profitability of FARS.

4. Further improvements of unmanned tanker aircraft weight optimization and aerodynamic properties is necessary for the economic feasibility of FARS to be established.

Considering both performance and economic benefits, we recommend an optimal design of FARS based on the analysis so far, as shown in Table 9.5.

Table 9.5: The recommended design for FARS

Wing span[ft]	135
thrust to weight ratio[-]	0.35
aspect ratio[-]	6.01
sweep angle[deg]	0.01
max takeoff weight[lb]	158,304
Ship size	ULCC(415m)
Ship hull number	Single-hull
Mooring	Single point mooring
No refueling per tanker	5
No refueling per receiver	1

9.4 Future Work

Several areas are recommended for future work in order to further explore the potential of refueling architectures for commercial aircraft:

1. Monte-Carlo simulations with variations in the future fuel price of Jet-A as well as a future carbon tax for aviation

2. Systematic analysis of all trans-continental flights for major airlines around the world, including those using older and less efficient long range aircraft, to find which routes and airlines may benefit the most from mid-air refueling

3. Do a geographic analysis of existing airlines, airports and FPSO/mooring locations around the world that might be top candidates to host a FARS system in the future

4. Refine tanker aircraft design optimization, mother ship design and refueling operations to remove inefficiencies

5. Perform a risk and failure mode analysis (e.g. using the STAMP/STPA framework) and evaluate potential certification requirements

6. Establish modifications (retrofits) and future design requirements for receiver aircraft to be able to be refueled in mid-air (this is not a requirement for current airlines)

7. Perform a survey of existing airlines to gauge their interest and requirements for a potential FARS system

8. Develop a detailed agent based model (ABM) or discrete event simulation (DES) of a FARS architecture as a potential basis for a FARS mission control center

9. Repeat the analysis of this thesis that was done for Jet-A kerosene for a potential future liquid hydrogen based LH2 aviation fuel economy with mid-air refueling

Appendix A

Environment modelling

There are two levels of environment model in this study: Long-term environment model and short-term environment model. The long-term environment model is based on the statistical observations to determine probability of occurrence of different short-term environmental conditions. The short-term environmental model is based on the physical modelling of waves and wind in a shorter period (approximately 3 hours). Under the short-term environment model, the physical behavior of the ship is tested.

A.1 Long-term environment modelling

The long term environment model is about the probability of occurrence given specific wind/wave characteristics. Industry-recognized regulation DNV-RP-C205[48] recommends the CMA joint model for modelling of occurrence of different wave heights (Bitner -Gregersen and Hagen, 1999)

$$f_{H_s}(h) = \frac{\beta_{H_s}}{\alpha_{H_s}}(\frac{h-\gamma_{H_s}}{\alpha_{H_s}})^{\beta_{H_s}-1}\exp\{-(\frac{h-\gamma_{H_s}}{\alpha_{H_s}})^{\beta_{H_s}}\} \tag{A.1}$$

Where Hs is the significant wave height of the wave (explained later), and the wave's zero crossing wave period conditional on Hs is modelled by a lognormal distribution

$$f_{T_z|H_s}(t|h) = \frac{1}{\sigma t\sqrt{2\pi}} \exp\{-\frac{(\ln t - \mu)^2}{2\sigma^2}\} \tag{A.2}$$

Where $\mu = E[\ln T_z] = a_0 + a_1 h^{a_2}$, $\mu = std[\ln T_z] = b_0 + b_1 e^{b_2 h}$. a_0, a_1 , a_2, b_0, b_1, b_2 are statistical values estimated by DNV for different oceanic regions. By deploying the mothership in different regions, the long-term statistics vary. In this study, we use the generic 'world' data for the environment modelling.

To simplify the calculation, we adopted a maximum likelihood value of the Tz for given Hs.

For the generic estimation recommended by DNV, we have a cumulative probability distribution of waves, as shown in Figure A.1.

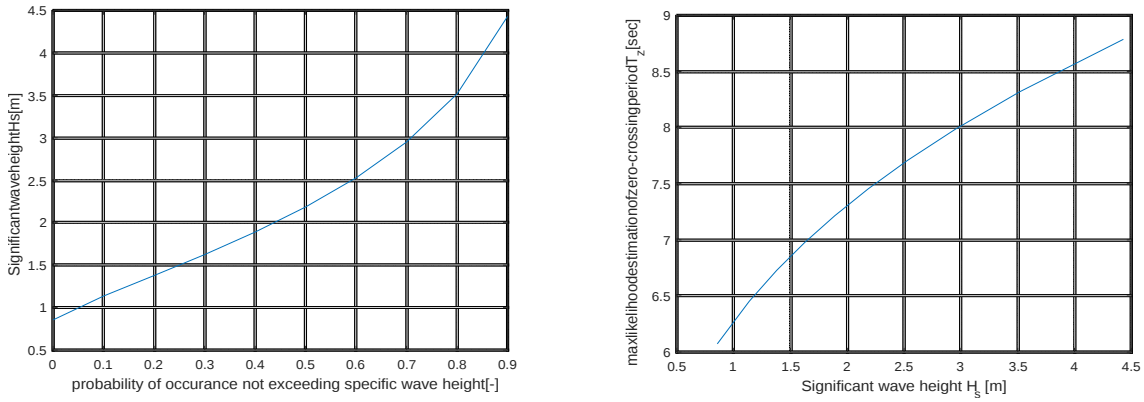

Table A.1: Long-term statistics of wave (significant wave height Hs [m] and zero-crossing period Tz[sec])

A.2 Short-term environment modelling

In this section, we will discuss the short term environmental model of ocean waves.

Ocean waves are a stochastic process, characterized by their significant wave height[m] H_s and zero-crossing period T_z [sec] as shown in Figure A-1. In this study, we adopted the Pierson–Moskowitz (PM) spectrum for the ocean modelling,

$$S_{PM}(\omega) = \frac{5}{16} H_s^2 \omega_p^4 \omega^{-5} \exp\left(-\frac{5}{4}\left(\frac{\omega}{\omega_p}\right)^{-4}\right) \tag{A.3}$$

Where ω is the angular frequency [rad/sec], ω_p is the angular spectral peak frequency $\omega_p = 1.4049 * 2\pi/Tz$. Figure A.2 shows the Pierson-Moskowitz spectrum with Hs=2.5m, Tz=7.5sec.

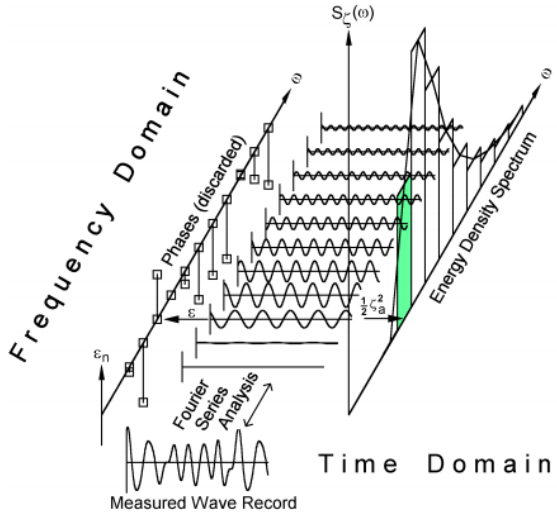

Figure A-1: A demonstration of the ocean wave's stochastic model from Ref [26]

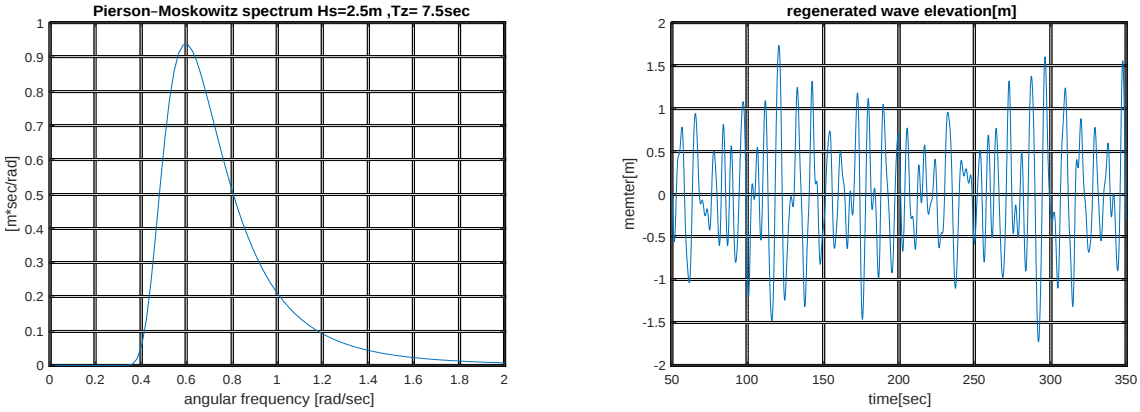

Table A.2: Pierson-Moskowitz spectrum with regenerated wave elevation (Hs=2.5 m, Tz = 7.5sec)

Appendix B

Weight estimation and Aerodynamic model

Studies have shown the empty-weight fraction for current aircraft [34], as shown in Figure B-1. As shown in the figure, there is a linear relationship between the weight fraction and the logarithm of the take-off weight. Larger aircraft tend to have a smaller empty weight fraction which makes them more efficient on a per unit of passenger or per unit of cargo basis.

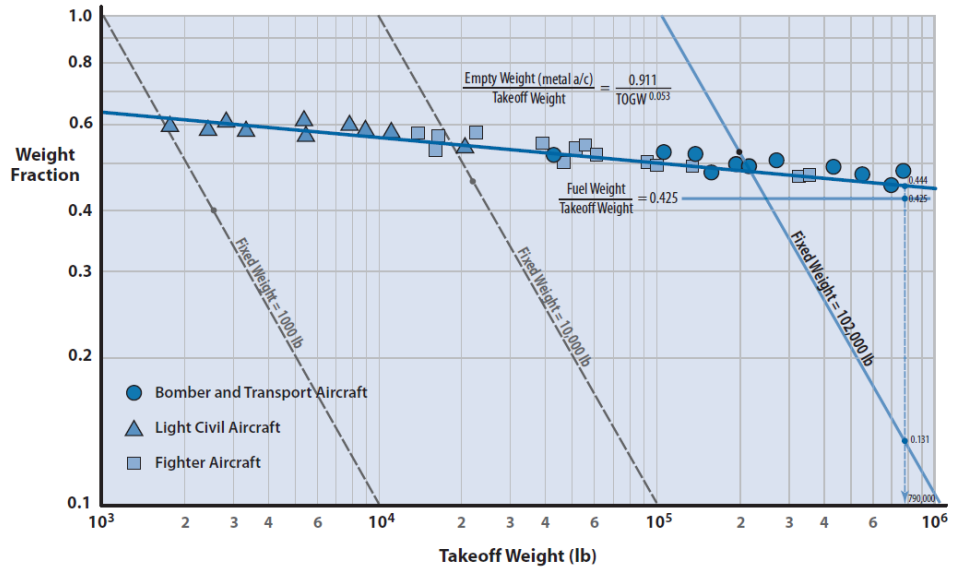

Figure B-1: Empty weight fraction of Current aircraft[34],

Therefore, we can estimate the aircraft empty weight W_{empty} based on the regression estimation, expressed as

$$\frac{W_{empty}}{W_{takeoff}} = -0.0656 \log_{10} W_{takeoff} + 0.8267 \tag{B.1}$$

In this study, we assume a unique airfoil profile and sample aircraft geometry model as shown in Figure B-2.

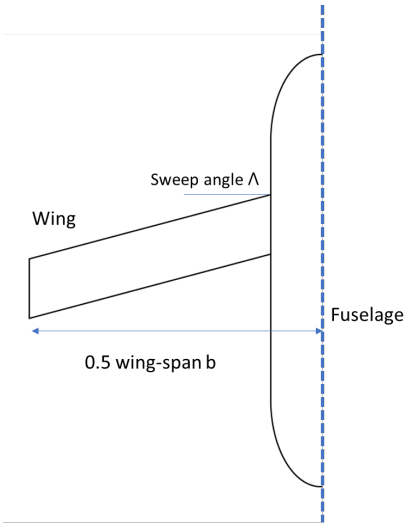

Figure B-2: The geometry of tanker aircraft

The relationship between the drag and lift coefficient can be described by polar drag theory, expressed as

$$C_d = C_{d0} + K_{eff}\ C_l^2 \tag{B.2}$$

Where C_d is drag coefficient, C_{d0} is drag at zero lift coefficient, K_{eff} is the effective drag due to lift coefficient, C_l is the lift coefficient.

The lift is mainly generated by the aircraft wing. In this study, we assume the airfoil of the tanker aircraft to be BAC-XXX Energy Efficient Transport Program airfoil[21]. BAC-XXX is the airfoil used for Boeing 747 and its profile is shown in Figure B-3.

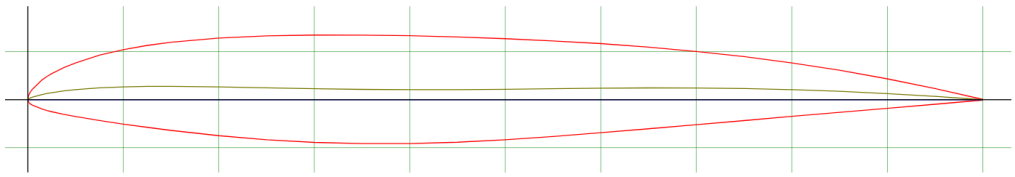

Figure B-3: Airfoil profile of BAC-XXX

Using the open software Xfoil, we can determine the aerodynamic properties of BAC XXX, as shown in Figure B-4.

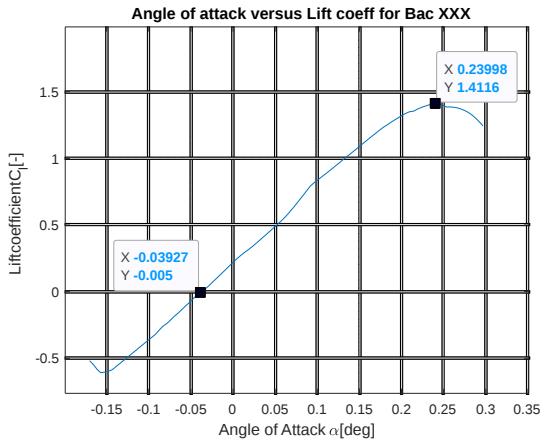

Figure B-4: BAC-XX Angle of Attack versus Lift Coefficient (Re = 1,000,000)

As shown in the figure, we can approximate the lift of the BAC-xxx airfoil in linear form. From the analysis, we determine that the linear angle of attack efficiency factor is $a_0 = 6.4047 \approx 2\pi$. The angle of attack at highest lift coefficient $\alpha_{\max}$ is 0.24rad($\sim$ 13.8 degree) and the angle of attack at zero lift α_0 is -0.03927rad($\sim$ -2.25 degree),

However, due to the finite wing-span, the lift performance of the airfoil is discounted, thus a discounted linear lift relationship can be expressed as

$$C_l = a(\alpha - \alpha_0) \tag{B.3}$$

Where, a is the corrected linear coefficient, expressed as

$$a = \frac{\pi AR}{1 + \sqrt{1 + \left(\frac{\pi AR}{a_0 \cos \Lambda_{c/4}}\right)^2 \left(1 - M^2(\cos \Lambda_{c/4})^2\right)}} \tag{B.4}$$

Where AR is the aspect ratio, $\Lambda_{c/4}$ is the sweep angle at a quarter of chord, in our aircraft geometry, $\Lambda_{c/4} = \Lambda$ M is the flight Mach number

Thus the max lift coefficient $C_{l,max}$ is determined as

$$C_{l,max} = a\left(\alpha_{\max} - \alpha_0\right) \tag{B.5}$$

K_{eff} is the effective drag due to lift coefficient, determined based on Oswald span efficiency method[34], express as

$$K_{eff} = \frac{1}{\pi e AR} \tag{B.6}$$

Where e is determined as

$$e = \{ \begin{array}{c} 4.61(1 - 0.045AR^{0.68})(\cos 1.03\Lambda)^{0.15} - 31 \quad if \Lambda > 30deg \\ 1.78(1 - 0.045AR^{0.68}) - 0.64 \quad if \Lambda \leq 30deg \end{array} \tag{B.7}$$

The direct estimation of zero-lift drag coefficient C_{d0} is difficult for system design. Therefore, we use C_{d0} coefficient from Boeing 747-200. However, the C_{d0} of Boeing 747 depends on Mach number[32]. Thus, we interpolate the data in between sample points, as shown in Figure B-5.

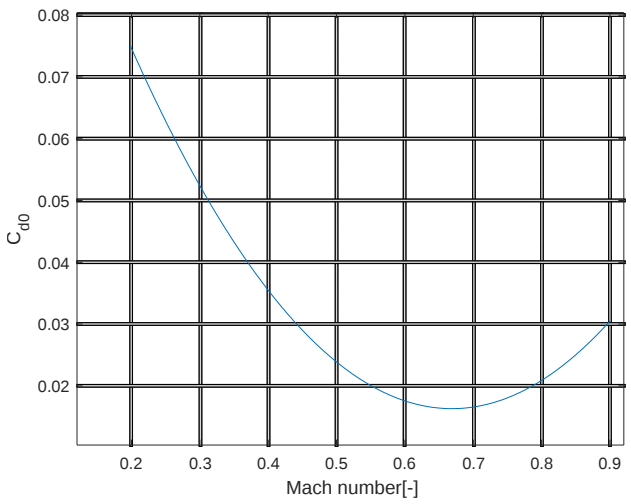

Figure B-5: Cdo versus Mach number

During the take-off phase, the drag polar relationship is different than those during crusing phase[30], express as

$$C_{dgrd} = C_{d0} + \Delta C_{d0} + K_g C_{lgrd}^2 \tag{B.8}$$

C_{lgrd} is the ground lift coefficient. To take-off in a short distance, aircraft usually install some kind of high-lift device to increase the lift during take-off. However, the detailed modelling of a high-lift device is complex and not necessary for system design. Therefore, studies have shown a linear relationship between ground lift coefficient and aspect ratio. Therefore we applied regression to the ground lift coefficient and aspect ratio of historical aircraft from reference [34], as shown in Figure B-6 and applied the relationship here.

ΔC_{d0} is the extra drag at zero lift due to the ground effect, express as

$$\Delta C_{d0} = \frac{W}{S} K_{uc} m^{-0.215} \tag{B.9}$$

Where $\frac{W}{S}$ is the wing load at N/m2, m is aircraft in kg. K_{uc} is set to be 3.16$*$ 10^{-5} for full flap deflection.

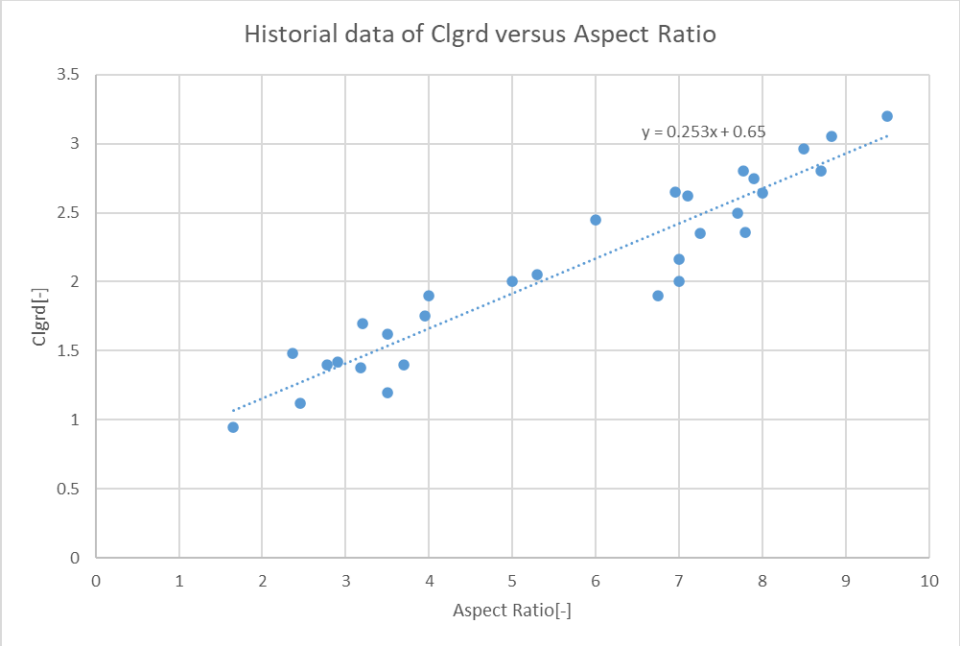

Figure B-6: Historical data of Clgrd versus aspect ratio based on ref[34]

K_g is the in-ground-effect induced drag parameter [30], expressed as

$$K_g = \phi K \tag{B.10}$$

$$\phi = 1 - \frac{2e}{\pi} \ln \left[1 + (\frac{\pi b}{8h}) \right] \tag{B.11}$$

Where $\frac{b}{h}$ is set to be 0.5 for middle-wing configuration.

Bibliography

[1] NAVAIR 00-110AS3-1. Standard aircraft characteristics model s-3a aircraft. Technical report, Naval Air Systems command, 1973.

[2] Airbus. Pioneering bionic 3d printing. `https://www.airbus.com/newsroom/news/en/2016/03/Pioneering-bionic-3D-printing.html`, Sep 2018.

[3] Gustafson Andrew. Carrier catapult tests once a common sight at brooklyn navy yard. `https://turnstiletours.com/carrier-catapult-tests-once-a-common-sight-at-brooklyn-navy-yard/`, June 2015.

[4] *atmosfair Flight Emissions Calculator: Documentation of the Method and Data*, September 2019.

[5] Bryan Barrass and Capt DR Derrett. *Ship stability for masters and mates*. Elsevier, 2011.

[6] Christopher Bolkcom and Jon D Klaus. Air force aerial refueling methods: flying boom versus hose-and-drogue. LIBRARY OF CONGRESS WASHINGTON DC CONGRESSIONAL RESEARCH SERVICE, 2005.

[7] Pam Boschee et al. Tanker conversions to fpso: Design and integrity management challenges. *Oil and Gas Facilities*, 2(05):16–21, 2013.

[8] Marloes Boxelaar. Shift scheduling in a nursing home using simulated annealing. 2017.

[9] Guy P Brasseur, Mohan Gupta, Bruce E Anderson, Sathya Balasubramanian, Steven Barrett, David Duda, Gregg Fleming, Piers M Forster, Jan Fuglestvedt, Andrew Gettelman, et al. Impact of aviation on climate: Faa's aviation climate change research initiative (accri) phase ii. *Bulletin of the American Meteorological Society*, 97(4):561–583, 2016.

[10] Maneenapang Bunnag, Nunthachai Amarutanon, Saranee Nitayaphan, and Manit Aimcharoenchaiyakul. Flng development: strategic approaches to new growth challenges. In *IPTC 2012: International Petroleum Technology Conference*, pages cp–280. European Association of Geoscientists & Engineers, 2012.

[11] Bluewater B.V. Mooring systems. https://www.bluewater.com/products-technology/mooring-systems/, 2020.

[12] Lockheed Martin Co. *C-130J Pocket Guide*.

[13] Leigh Collins. Energy islands plan for north sea 'feasible', says consortium. https://www.rechargenews.com/wind/energy-islands-plan-for-north-sea-feasible-says-consortium/2-1-635620, July 2018.

[14] Oliver de Weck. Case study 2: Aircraft. *Lecture note on MIT 16.887 Technology Roadmapping and Development*, 2019.

[15] Olivier de Weck and Cyrus Jilla. Simulated annealing: a basic introduction. *Online document*, 2007.

[16] Johnny Eggleston. Aviation boatswain's mate e. *Naval education and training program development and technology center*, 2001.

[17] Lillian E.Nolan Daniel R.Simmons Jeffrey S. Michalke John W.Leland Ellery D. Wallwork, Mark L.Morgan. *Air refueling: Without Tankers, We Cannot...* Office of History, Air Mobility Command, Scott Air Force Base, Illinois, October 2009.

[18] EURONAV. Euronav purchases ulcc laura lynn from international seaways. https://www.euronav.com/media/65479/20180629-euronav-purchases-seaways-laura-lynn.pdf, June 2018.

[19] GA Ganley. Concorde propulsion-did we get it right? the rolls-royce/snecma olympus 593 engine reviewed. Technical report, SAE Technical Paper, 1991.

[20] Incorporated GRA. Economic values for evaluation of federal aviation administration investment aand regulatory decisions. Technical report, 2007.

[21] UIUC Applied Aerodynamic Group. Uiuc airfoil coordinate database, 2020. data retrieved from, https://m-selig.ae.illinois.edu/ads/coord_database.html.

[22] Darrall Henderson, Sheldon H Jacobson, and Alan W Johnson. The theory and practice of simulated annealing. In *Handbook of metaheuristics*, pages 287–319. Springer, 2003.

[23] ICAO ICAO. Environmental report 2016. *Aviation and climate change*, 2016.

[24] Permanent Int. Association of navigation congresses (pianc)," criteria for movements of moored ships in harbours: A practical guide,". *Rept. Working Group No. 24, Permanent Technical*.

[25] CFM International. Type-certificate data sheet for engine leap-1a & leap-1c series engines. certificate, European Aviation Safety Agency(EASA), 2, boulevard du Général Martial Valin 75015 Paris France, May 2018.

[26] Johan MJ Journee and JA Pinkster. Offshore hydromechanics. *TUDelft, Faculty of Marine Technology, Ship Hydromechanics Laboratory, Report No. 1112-K, Lecture Notes*, 1997.

[27] Douglas B. Kelly. Valuing aircraft with a lease attached - an appraiser's perspective. Technical report, 2019.

[28] Gaetan Kenway, Graeme Kennedy, and Joaquim Martins. Aerostructural optimization of the common research model configuration. In *15th AIAA/ISSMO multidisciplinary analysis and optimization conference*, page 3274, 2014.

[29] Hesty A Kurniawati, Wasis D Aryawan, and Achmad Baidowi. Long-term fso/fpso charter rate estimation. *Kapal: Jurnal Ilmu Pengetahuan dan Teknologi Kelautan*, 13(1):7–12, 2016.

[30] Frederick H. Lutze. Lecture notes in aoe 3104 vehicle performance, February 2003.

[31] Rodrigo Martinez-Val, Emilio Perez, and Jose F Palacin. Historical evolution of air transport productivity and efficiency. In *43 rd AIAA Aerospace Sciences Meeting and Exhibit*, page 2005, 2005.

[32] Marcello Napolitano. *Aircraft Dynamics: From Modeling to Simulation: From Modeling to Simulation*. Wiley Global Education, 2011.

[33] Defense Media Network. The flying boom | video. `https://www.defensemedianetwork.com/videos/the-flying-boom/`, July 2015.

[34] Leland M Nicolai and Grant E Carichner. *Fundamentals of aircraft and airship design, Volume 1–Aircraft Design*. American Institute of Aeronautics and Astronautics, 2010.

[35] SBM Offshore N.V. Lng floating facilities. `https://www.sbmoffshore.com/what-we-do/our-products/lng-floating-facilities/`, 2020.

[36] U.S. Bureau of Transportation Statistics. U.s. international air passenger and freight statistics report (2016-2020). `https://www.transportation.gov/policy/aviation-policy/us-international-air-passenger-and-freight-statistics-report`.

[37] U.S. Bureau of Transportation Statistics. 2018 traffic data for u.s airlines and foreign airlines u.s. flights. `https://www.bts.dot.gov/newsroom/2018-traffic-data-us-airlines-and-foreign-airlines-us-flights`, October 2019.

[38] FAA Order. 7110.65 n: Air traffic control. *Change*, 2(2):4, 2002.

[39] Markel Penalba, Thomas Kelly, and John Ringwood. Using nemoh for modelling wave energy converters: A comparative study with wamit. 2017.

[40] Celine Ramstein, Goran Dominioni, Sanaz Ettehad, Long Lam, Maurice Quant, Jialiang Zhang, Louis Mark, Sam Nierop, Tom Berg, Paige Leuschner, et al. *State and Trends of Carbon Pricing 2019*. The World Bank, 2019.

[41] Daniel P Raymer. Aircraft design: a conceptual approach (aiaa education series). *Reston, Virginia*, 2012.

[42] Jean-Paul Rodrigue. *The geography of transport systems*. Taylor & Francis, 2016.

[43] Jan Roskam. *Airplane design*. DARcorporation, 1985.

[44] US Air Force Fact Sheet. Kc-135 stratotanker, 2001.

[45] Joseph Franklin Sweger. Design specifications development for unmanned aircraft carrier landings: A simulation approach. 2003.

[46] David Szondy. Airbus achieves first large-aircraft autonomous aerial refueling. `https://newatlas.com/airbus-raaf-large-aircraft-refueling/55463/`, Jul 2018.

[47] Defense Update. Lca completes first ski-jump takeoff. `https://defense-update.com/20141224_naval_lca.html`, Dec 2014.

[48] Det Norske Veritas. Dnv-rp-c205 environmental conditions and environmental loads. *Det Norske Veritas: Oslo, Norway*, 2010.

[49] Xiaohui Wang, Zhen Huang, Guangzhou Sui, Haishan Lian, et al. Analysis on the development trend of future uav equipment technology. *Academic Journal of Engineering and Technology Science*, 2(1), 2019.

[50] Wikipedia contributors. Jet blast deflector — Wikipedia, the free encyclopedia. `https://en.wikipedia.org/w/index.php?title=Jet_blast_deflector&oldid=928034825`, 2019. [Online; accessed 6-May-2020].

[51] Wikipedia contributors. Airbus a330 — Wikipedia, the free encyclopedia. `https://en.wikipedia.org/w/index.php?title=Airbus_A330&oldid=949814687`, 2020. [Online; accessed 21-April-2020].

[52] Wikipedia contributors. Airbus a350 xwb — Wikipedia, the free encyclopedia. `https://en.wikipedia.org/w/index.php?title=Airbus_A350_XWB&oldid=955434253`, 2020. [Online; accessed 8-May-2020].

[53] Wikipedia contributors. Arresting gear — Wikipedia, the free encyclopedia. `https://en.wikipedia.org/w/index.php?title=Arresting_gear&oldid=951170483`, 2020. [Online; accessed 6-May-2020].

[54] Wikipedia contributors. Boeing 767 — Wikipedia, the free encyclopedia. https://en.wikipedia.org/w/index.php?title=Boeing_767&oldid=951897806, 2020. [Online; accessed 19-April-2020].

[55] Wikipedia contributors. Boeing 777 — Wikipedia, the free encyclopedia. https://en.wikipedia.org/w/index.php?title=Boeing_777&oldid=954814271, 2020. [Online; accessed 8-May-2020].

[56] Wikipedia contributors. Boeing 787 dreamliner — Wikipedia, the free encyclopedia. https://en.wikipedia.org/w/index.php?title=Boeing_787_Dreamliner&oldid=955059272, 2020. [Online; accessed 8-May-2020].

[57] Wikipedia contributors. Boeing kc-46 pegasus — Wikipedia, the free encyclopedia. https://en.wikipedia.org/w/index.php?title=Boeing_KC-46_Pegasus&oldid=951596391, 2020. [Online; accessed 21-April-2020].

[58] Wikipedia contributors. Longest flights — Wikipedia, the free encyclopedia. https://en.wikipedia.org/w/index.php?title=Longest_flights&oldid=953726476, 2020. [Online; accessed 28-April-2020].

[59] Wikipedia contributors. Singapore airlines flights 21 and 22 — Wikipedia, the free encyclopedia. https://en.wikipedia.org/w/index.php?title=Singapore_Airlines_Flights_21_and_22&oldid=953724218, 2020. [Online; accessed 28-April-2020].

[60] Wikipedia contributors. Thrust-specific fuel consumption — Wikipedia, the free encyclopedia. https://en.wikipedia.org/w/index.php?title=Thrust-specific_fuel_consumption&oldid=954409939, 2020. [Online; accessed 8-May-2020].

[61] Bo Yang Yu, Olivier de Weck, and Maria C Yang. Parameter design strategies: a comparison between human designers and the simulated annealing algorithm. In *ASME 2015 International Design Engineering Technical Conferences and Computers and Information in Engineering Conference*. American Society of Mechanical Engineers Digital Collection, 2015.